Understanding the mechanisms utilised by *Coxiella burnetii* for intracellular replication within the host phagolysosome

Miku Kuba

B.Sc. (Hons)

ORCID ID: 0000-0002-1300-3855

Submitted in total fulfilment of the requirements of the degree of Doctor of Philosophy

March 2020

Department of Microbiology and Immunology

Peter Doherty Institute for Infection and Immunity

The University of Melbourne

Abstract

The human pathogen *Coxiella burnetii* is the causative agent of Q fever, a febrile illness which may lead to chronic disease in a small percentage of infected individuals. *C. burnetii* is a unique Gram-negative intracellular bacterium which replicates within a host cell lysosome-derived vacuole, termed the *Coxiella*-containing vacuole (CCV). Currently, the exact mechanisms which allow *C. burnetii* to replicate within this normally hostile compartment are unknown. In order to understand how *C. burnetii* survives within this intracellular niche, this research investigated carbon metabolism of both intracellular and axenically cultivated bacteria, using steady state metabolic profiling and ^{13}C-stable isotope labelling. Both *C. burnetii* populations were shown to assimilate exogenous [^{13}C]glutamate and [^{13}C]glucose, with concomitant labelling of intermediates in glycolysis and gluconeogenesis, and in the TCA cycle. Significantly, the two populations displayed metabolic pathway profiles reflective of the nutrient availabilities within their propagated environments. Disruption of the *C. burnetii* glucose transporter, CBU0265, by transposon mutagenesis led to a significant decrease in [^{13}C]glucose utilisation but did not abolish glucose usage, suggesting that *C. burnetii* express additional hexose transporters that may be able to compensate for the loss of CBU0265. This was supported by intracellular infection of human cells and *in vivo* studies in the *Galleria mellonella* insect model showing loss of CBU0265 had no impact on intracellular replication or virulence. Using this mutagenesis and [^{13}C]glucose labelling approach, this study identified a second glucose transporter, CBU0347, the disruption of which also showed significant decreases in ^{13}C-label incorporation. Despite maintaining a relatively small genome, *C. burnetii* have retained seemingly redundant strategies to obtain glucose. This suggests that glucose may be an important metabolite for *C. burnetii*. Together, these

analyses indicate that *C. burnetii* may use multiple carbon sources *in vivo* and exhibits greater metabolic flexibility than expected. In addition, this thesis also investigated the novel and unique *C. burnetii* protein CBU2072, a small, 18.3 kDa protein, which has subsequently been named essential for intracellular replication A (EirA), as loss of this protein prevents replication of *C. burnetii* within the CCV. Intracellular replication of the EirA mutant can be restored during co-infection of the same vacuole with *C. burnetii* wild type, which is analogous to the phenotype observed for mutants of the Dot/Icm type 4B secretion system in *C. burnetii*. EirA localises to the *C. burnetii* inner membrane, and absence of this protein leads to the loss of Dot/Icm effector translocation. These data together contribute important understanding of the unique mechanisms involved in *C. burnetii* pathogenesis within the host phagolysosome.

Declaration

This is to certify that:

1. The thesis comprises only my original work towards the Ph. D except where indicated in the text,
2. due acknowledgement has been made in the text to all other materials used, and
3. the thesis is less than 100,000 words in length, exclusive of tables, figures, bibliographies and appendices.

……

Miku Kuba

B.Sc. (Hons)

Department of Microbiology and Immunology

Peter Doherty Institute for Infection and Immunity

The University of Melbourne

Preface

In accordance with the regulation of The University of Melbourne, I acknowledge that some of the work presented in this thesis was collaborative. Specifically:

Chapter 3: Development of steady state profiling and ^{13}C-stable isotope labelling techniques in *C. burnetii* by Nitika Neha from the Asia-Pacific Centre for Animal Health, Melbourne Veterinary School, Faculty of Veterinary and Agricultural Sciences, The University of Melbourne, Parkville, Australia, and later Metabolomics Australia, The Bio21 Molecular Science and Biotechnology Institute, The University of Melbourne, Parkville, Australia, in collaboration with Dr. David P. De Souza from Metabolomics Australia, The Bio21 Molecular Science and Biotechnology Institute, The University of Melbourne, Parkville, Australia.

Chapter 3: Generation of steady state profiling data for both axenic and intracellularly cultivated *C. burnetii*, in addition to day 2 post-infection HeLa cell-derived *C. burnetii* and day 6 post-inoculation samples of axenically cultivated *C. burnetii* for ^{13}C-stable isotope labelling by Nitika Neha.

Chapter 3 and 5: Statistical analysis of GC/MS steady state profiling datasets by Dr. Saravanan Dayalan, from Metabolomics Australia, The Bio21 Molecular Science and Biotechnology Institute, The University of Melbourne, Parkville, Australia.

Chapter 3-5: Facilitating the running of GC/MS and LC/MS samples, in addition to data processing and assistance with data analysis by Dr. David P. De Souza and Dr. Dedreia Tull from Metabolomics Australia, The Bio21 Molecular Science and Biotechnology Institute, The University of Melbourne, Parkville, Australia.

Chapter 3-5: Contributions to data interpretation, as well as ongoing intellectual input for Metabolomics-based datasets by Professor Malcolm J. McConville from the Metabolomics Australia, The Bio21 Molecular Science and Biotechnology Institute, The University of Melbourne, Parkville, Victoria, Australia, and Department of Biochemistry and Molecular Biology, The Bio21 Molecular Science and Biotechnology Institute, The University of Melbourne, Parkville, Victoria, Australia.

Chapter 3-5: Contributions to designing studies, in addition to ongoing intellectual input by Dr. Hayley J. Newton from the Department of Microbiology and Immunology, University of Melbourne at the Peter Doherty Institute for Infection and Immunity, Melbourne, Victoria, Australia, and Dr. Fiona M. Sansom, from the Asia-Pacific Centre for Animal Health, Melbourne Veterinary School, Faculty of Veterinary and Agricultural Sciences, The University of Melbourne, Parkville, Australia.

Chapter 4: Assistance with *G. mellonella* infections using *C. burnetii* wild type, *0265*::Tn and *0265*::Tn pFLAG-0265 by Dr. Joshua P. M. Newson from the Department of Microbiology and Immunology, University of Melbourne at the Peter Doherty Institute for Infection and Immunity, Melbourne, Victoria, Australia.

Chapter 5: Initial intracellular replication assays in HeLa cells using *C. burnetii* wild type, *eirA*::Tn and *eirA*::Tn pFLAG-EirA by Dr. Patrice Newton from the Department of Microbiology and Immunology, University of Melbourne at the Peter Doherty Institute for Infection and Immunity, Melbourne, Victoria, Australia.

Chapter 5: Provision of bacterial subcellular fractionation protocol by Dr. Abderrahman Hachani from the Department of Microbiology and Immunology, University of Melbourne at the Peter Doherty Institute for Infection and Immunity, Melbourne, Victoria, Australia.

Chapter 5: Generation of steady state profiling data for wild type and *eirA*::Tn *C. burnetii* using GC/MS by Nitika Neha.

Chapter 5: Facilitating the running of LC/MS samples, in addition to data processing and assistance with data analysis by Dr. Brunda Nijagal from Metabolomics Australia, The Bio21 Molecular Science and Biotechnology Institute, The University of Melbourne, Parkville, Australia.

Chapter 5: Assistance with counting colonies for antibiotic treatment experiments in *C. burnetii* by Yi Wei Lee from the Department of Microbiology and Immunology,

University of Melbourne at the Peter Doherty Institute for Infection and Immunity, Melbourne, Victoria, Australia.

Chapter 5: Generation of transmission electron microscopy images by Vicki Bennett-Wood from the Department of Microbiology and Immunology, University of Melbourne at the Peter Doherty Institute for Infection and Immunity, Melbourne, Victoria, Australia.

The remainder of this thesis comprises only my original work.

This thesis contains material that has been published or is currently in preparation for publication:

Chapter 3 and 4: *Coxiella burnetii* utilizes both glutamate and glucose during infection with glucose uptake mediated by multiple transporters. (2019). **Miku Kuba**, Nitika Neha, David P. De Souza, Saravanan Dayalan, Joshua P. M. Newson, Dedreia Tull, Malcolm J. McConville, Fiona M. Sansom, and Hayley J. Newton. Biochemical Journal. **476**. 2851-2867.

Chapter 5: EirA is a membrane associated protein essential for intracellular replication of *Coxiella burnetii*. **Miku Kuba**, Nitika Neha, Patrice Newton, Yi Wei Lee, Vicki Bennett-Wood, Abderrahman Hachani, David P. De Souza, Brunda Nijagal, Saravanan Dayalan, Dedreia Tull, Malcolm J. McConville, Fiona M. Sansom, Hayley J. Newton. (Under revision following peer review by Infection and Immunity December 2019-).

Other publications during candidature

Coxiella burnetii: Hiding in plain sight. (2019). Patrice Newton, **Miku Kuba**, Bhavna Padmanabhan, Eleanor A. Latomanski, Hayley J. Newton. Defence against biological attacks. Sunit K. Singh and Jens H. Kuhn (eds). Springer, Cham.

Loss of *O*-linked protein glycosylation in *Burkholderia cenocepacia* impairs biofilm formation and siderophore activity and alters transcriptional regulators. (2019). Cameron

C. Oppy, Leila Jebeli, **Miku Kuba**, Clare V. Oates, Richard A. Strugnell, Laura E. Edgington-Mitchell, Miguel A. Valvano, Elizabeth L. Hartland, Hayley J. Newton, Nichollas E. Scott. mSphere. **4.** e00660-19.

Acknowledgements

Firstly, I would like to acknowledge and thank my primary supervisor, Dr. Hayley Newton, for her ongoing guidance throughout my degree. I will be forever grateful to you for taking me in as your Honours student, back in 2015. You have been a wonderful, supportive supervisor, and, although I am ready to move on, I will definitely miss being a part of your Lab. Thank you for looking after me, and investing your time on me for all these years.

I would also like to thank my co-supervisor, Dr. Fiona Sansom, for properly introducing me to the field of Metabolomics. Your expertise in this field was always greatly appreciated. Thank you for always extending a hand to support me, particularly during manuscript and thesis preparations.

Thank you to the other members of the Newton Lab, who have kept me company at various times throughout my degree. Thank you to all the Post-Docs, Patrice, Dave, Yilin, and Jen. Thank you to Chen Ai, for being the best person. Thank you to all the fellow students, Eleanor, Bec, Laura, Bhavna, Nicole, Robson, and Yi Wei in particular, alongside all the other people who have come through- thank you all for your friendship, and for keeping me well entertained. Thank you also to Dr. Nick Scott, for allowing me to collaborate with him and letting me use my *G. mellonella* skills so that I could be an author on his manuscript.

I would also like to acknowledge Nitika Neha, whose Metabolomics and CBU2072 projects I inherited. Thank you for teaching me everything, and I hope this thesis does justice to the story you started. In addition, I would not have been able to perform all of the Metabolomics related techniques without the facilities and people from Metabolomics Australia. Thank you in particular to Dr. David P. De Souza, Dr. Brunda Nijagal, Dr. Saravanan Dayalan, and Dr. Dedreia Tull.

Thank you to my Ph. D committee, Professor Richard Strugnell and Professor Malcolm McConville, for ongoing guidance with this project, in addition to career guidance and networking opportunities organised by Dick.

I would also like to acknowledge the Department of Microbiology and Immunology, as well as the overall Doherty Institute, for allowing me this amazing opportunity to

pursue my Ph. D. In particular, thank you to the past and present members of the level 6 west labs, SPASIM (particularly 2017 committee members), and DMI Admin staff.

Thank you to all the academic and non-academic friends for helping me get through this degree. It has been a massive undertaking, and every bit of support has helped me achieve my goals. My 'P Dubz' Honours 2015 cohort (CLUSTERATION), in particular to the current on-site members Cat, Keit, Will, and Rachel. It has been an amazing journey and I'm honoured to have shared it with you all.

Thank you to my Ballarat friends, who have supported me since I moved down to Melbourne at the beginning of Honours. It's nice to put things into perspective and be reminded of life outside of the lab. I will be forever grateful to the McGee/Rice family for taking me in and looking after me throughout my tertiary studies. You have all been very patient and kind towards me, even when I'm struggling. Thank you.

Thank you to my housemate and lab mate, Laura (soon to be Dr. Laura F. Fielden), for being awesome. It's been brilliant sharing this journey with you. I'll miss living with you, even when you let the 'food delivery guy' stay in the house- Hi Dan! I wish you all the best with all your future endeavours, starting with your first Post-Doc position!

おじいちゃん、おばあちゃん、博士論文書けました。卒業したらやっと久芳博士です。おじいちゃんも最後の最後まで応援してくれてありがとう。いつもおじいちゃんを思っています。おばあちゃん、結構立派な本でしょう（笑）。おばあちゃんもいつも応援してくれてありがとう。二人共長年難しい微生物学のお話をたくさん聞いてくれてありがとうございます。

お母さん、今まで本当にお世話になりました。多分、これで学生生活は終わります。病気になったり、つらくなった時にちゃんと駆けつけて、面倒見てくれてありがとう。まぁ、これからもお世話になりますので宜しくお願い致します。

Finally, thank you to Tim. My journey as a Uni student has taken a little longer than what I had initially planned, and the last few months have been particularly tough. Thank you for being there and supporting me throughout. I really appreciate the amount of effort you have put in to make those numerous Ballarat-Melbourne trips, just to spend time with me. You're the best. Here's to many more adventures.

Table of Contents

List of Abbreviations

The following abbreviations have been used throughout this thesis.

Abbreviation	
°C	Degrees Celsius
Δ	Deletion mutant
::Tn	Disruption of gene due to transposon insertion
%	Percent
±	Plus minus
0265	CBU0265
0347	CBU0347
2072	CBU2072
$2072_{24\text{-}165}$/$EirA_{24\text{-}165}$	CBU2072/EirA from amino acid residue 24-165
ABC	ATP-binding cassette
ACCM-2	Acidified citrate cysteine medium-2
ACCM-D	Defined acidified citrate cysteine medium
AGRF	Australian Genome Research Facility
Amp	Ampicillin
ATCC	American type culture collection
AX	Axenically cultivated
BH	Benjamini-Hochberg
BlaM	β-lactamase
BLAST	Basic local alignment search tool
BLASTp	Protein BLAST
bp	Base pairs
BSA	Bovine serum albumin
CCV	*Coxiella*-containing vacuole
CFU	Colony forming units
Cm	Chloramphenicol
cm	Centimetre

cm^3	Cubic centimetre
Cyto	Cytoplasm
DAPI	4′,6-diamidino-2-phenylindole
dH_2O	Deionised water
DMEM	Dulbecco's Modified Eagle Medium
DMSO	Dimethyl sulphoxide
DNA	Deoxyribonucleic acid
dNTP	Deoxyribonucleotide triphosphate
dsDNA	Double-stranded DNA
EDTA	Ethylenediaminetetraacetic acid
EirA	Essential for intracellular replication A (CBU2072)
ESI	Electrospray ionisation
FCS	Foetal calf serum
G	Gauge
g	Gram
GC	Gas chromatography
GC/MS	Gas chromatography/mass spectrometry
gDNA	Genomic DNA
GE	Genome equivalent
H^+	Proton
IB	Immunoblot
IC	Intracellularly cultivated
ID	Identification
IF	Immunofluorescence
IM	Inner membrane
in^2	Inch squared
IPTG	isopropyl-β-D-thiogalactoside
Kan	Kanamycin
kb	Kilobase
kDa	Kilodalton

KEGG	Kyoto Encyclopedia of Genes and Genomes
kV	Kilovolts
L	Litre
LAMP-1	Lysosomal associated membrane protein 1
LB	Luria-Bertani
lb	Pound
LC	Liquid chromatography
LC/MS	Liquid chromatography/mass spectrometry
LCV	Large cell variant
LPS	Lipopolysaccharide
M	Molar
MceA	Mitochondrial *Coxiella* effector protein A
MCS	Multiple cloning site
MES	2-(N-morpholino)ethanesulphonic acid
MFS	Major facilitator superfamily
µF	Microfarad
µg	Microgram
µL	Microlitre
µM	Micromolar
µm	Micrometre
mg	Milligram
mL	Millilitre
mM	Millimolar
mm	Millimetre
MOI	Multiplicity of infection
MS	Mass spectrometry
m/z	Mass/charge number of ions
NA	Not applicable
ng	Nanogram
nM	Nanomolar

nm	Nanometre
nmol	Nanomole
OD	Optical density
Ω	Ohm
OM	Outer membrane
PBS	Phosphate buffered saline
PCR	Polymerase chain reaction
PEPCK	Phosphoenolpyruvate carboxykinase
PIPES	Piperazine-1,2-bis(2-ethanesulphonic acid)
PMA	Phorbol 12-myristate 13-acetate
PMSF	Phenylmethylsulphonyl fluoride
ppm	Parts per million
PSI-BLAST	Position-specific iterative BLAST
PTS	Phosphotransferase system
Q fever	Query fever
qPCR	Quantitative PCR
®	Registered trademark
^{R}	(Antibiotic) resistant
RE	Restriction endonuclease
ROS	Reactive oxygen species
rpm	Revolutions per minute
RPMI	Roswell Park Memorial Institute
RT	Room temperature
SCV	Small cell variant
SD	Standard deviation
SDM	Site directed mutagenesis
SDS	Sodium dodecyl sulphate
SDS-PAGE	SDS-polyacrylamide gel electrophoresis
SOB	Super optimal broth
SOC	Super optimal broth with catabolite expression

T3SS	Type 3 secretion system
T4BSS	Dot/Icm type 4B secretion system
TAE	Tris acetate EDTA
TB	Transformation buffer
TBS	Tris-buffered saline
TBST	Tris-buffered saline + Tween-20
TCA	Tricarboxylic acid
TEM	Transmission electron microscopy
™	Trademark
TOF	Time-of-flight
TX-100	Triton X-100
V	Volt
VANTED	Visualization and Analysis of Networks conTaining Experimental Data
v/v	Volume by volume
W	Watts
WCL	Whole cell lysate
WEHI	Walter and Eliza Hall Institute
WT	Wild type
w/v	Weight by volume
x *g*	Times gravitational force

List of metabolite abbreviations in Appendix 2.

List of Figures

List of Tables

Chapter 1

Introduction

1.1 Historical relevance

Query (Q) fever was first reported in Queensland, Australia in 1935 during an outbreak of febrile illness amongst abattoir workers. (1). In collaboration with Edward Derrick, Frank MacFarlane Burnet and Mavis Freeman observed Rickettsial bodies in the spleens of mice infected with specimens from this outbreak. Subsequently this organism was named *Rickettsia burnetii* (1-3). Concurrently in the USA, Gordon Davis and Herald Cox were investigating a tick-borne pathogen which could cause febrile illness in guinea pigs (4). Davis and Cox attempted to isolate the causative agent from infected guinea pigs but were unsuccessful in doing so. The two groups discovered that they had isolated the same infectious agent when a researcher working on the Nine Mile agent in the Rocky Mountain Laboratories became infected with the laboratory isolate. Cross-protection studies in guinea pigs confirmed the agent was identical to the Q fever organism. The bacterium was renamed *Coxiella burnetii* in 1948, after the two prominent researchers involved in the identification process (2, 4-6).

1.2 Q fever

1.2.1 Epidemiology and transmission

C. burnetii has been detected almost worldwide, with the exception of New Zealand and French Polynesia (7). The natural reservoir of *C. burnetii* are ruminants (3). Infection in these animals is generally subclinical (8). However, *C. burnetii* can cause abortion in pregnant animals (8). The bacteria are shed into the environment in milk, faeces, urine, and also in particularly high titres in reproductive products such as the placenta and the amniotic fluid (9-11). Once excreted, environmental *C. burnetii* are resistant to UV radiation, osmotic pressure, and desiccation (12). The environmental stability of this

pathogen means *C. burnetii* are difficult to eradicate once established in a given area. *C. burnetii* are transmitted primarily through aerosol inhalation (13, 14), where less than ten bacteria are required to cause disease in humans (15). This means infection may not require the host to be near infected animals, as the bacteria may be carried in the air to new locations. Studies have shown seroprevalence of *C. burnetii* in those who had never lived in rural areas, whose contact with ruminants were minimal (16, 17). This high infectivity, coupled with environmental stability and aerosol spread, has resulted in *C. burnetii* being classified as a "category B critical biological agent" by the Centers for Diseases Control and Prevention (18).

Many Q fever outbreaks have occurred across the world (19-21), with the largest outbreak in the Netherlands between 2007 and 2010 (22, 23). In this outbreak, transmission to humans occurred through infected goats (24). Over 4000 patients were confirmed to have been infected, with many more assumed undiagnosed (24). Conditions were exacerbated by the presence of numerous small-scale farms located in close proximity to residential areas (24). The total cost of containing this outbreak was calculated to be in excess of 300 million euro (25), and over 50,000 goats and sheep were culled between December 2009 to June 2010, in an attempt to minimise the spread of disease (22). In addition, there are debilitating long-term health consequences to those who were infected (26). This outbreak highlights the substantial risk that *C. burnetii* could pose, as evidenced by the severe economic and public health burden experienced in the Netherlands.

The environmental stability of this pathogen means *C. burnetii* infection rates may also rise in the current global climate, where incidents of severe weather events, such as drought and strong winds, will become more common place (27).

1.2.2 Clinical features

In humans, 40% of Q fever patients will typically present with an acute, flu-like illness or pneumonia (10, 28). Symptoms of acute Q fever can take 2-3 weeks to arise, and can last from a couple of days to several weeks (29-31). Symptoms of chronic Q fever may not arise until months or years after initial exposure, with patients typically presenting with endocarditis and other vascular infections (26). The mechanisms underlying the progression from acute to chronic Q fever are currently not well understood, although it does not appear to be strain related (28). These symptoms, alongside factors such as underlying vascular or cardiac pathologies, increased age and inadequate treatment, raise the risk of mortality significantly (26). Chronic fatigue is also known to be a major symptom in those with Q fever, with one study finding 37% of their patients suffered from reduced health status 24 months after the onset of illness (32). Costs arising from the management of these long-term symptoms can pose a significant health and economic burden to affected countries (25).

1.2.3 Diagnosis and treatment

Definitive acute Q fever diagnosis requires serological testing coupled with polymerase chain reaction (PCR), due to the symptoms being indistinguishable from influenza and other febrile illnesses (33). Chronic Q fever detection is more difficult, and new

guidelines implemented after the Netherlands outbreak recommend a combination of serological testing against phase I antibodies and PCR, coupled with a diagnosis for endocarditis with detection of visible infection using an imaging platform (34).

Standard treatment of Q fever requires administration of doxycycline with or without hydroxychloroquine (12, 35). Co-trimoxazole is used as an alternative long-term treatment, as doxycycline usage is contraindicated during pregnancy. For chronic Q fever, treatment lasts for a minimum of 18 months with doxycycline taken twice-daily. Side effects to this treatment and long-term compliance issues mean an alternative therapeutic approach is required (12). Currently the only commercially available human vaccine against *C. burnetii* is Q-Vax, a formalin-inactivated whole cell vaccine containing the phase I Henzerling strain, licensed for use in Australia (36, 37). This vaccine is recommended for at risk individuals including farmers and abattoir workers (38). Q-Vax is effective at preventing infection in those that are at high risk of exposure (17). However, a two-step screening process is required before administration. This screening process involves identifying antibodies against Q fever, as well as conducting an intradermal skin test using diluted vaccine (17). Screening for sensitisation is an important process, as it was found that individuals who have pre-existing immunity can have adverse side effects to the vaccine, such as abscess formation at the site of injection (39-41).

There are also ongoing efforts to develop cheap vaccines for use on agricultural animals, thus reducing potential loss of livestock and exposure of *C. burnetii* to humans. Coxevac is a livestock specific vaccine consisting of inactivated *C. burnetii* phase I Nine Mile,

which is currently the most effective at preventing shedding of bacteria in infected animals (42, 43).This vaccine, although widely used in Europe, is not available in all countries, particularly in Australia where importation of inactivated, whole cell *C. burnetii* is a quarantine risk (20). Thus, there is a need to identify *C. burnetii* components that are essential for pathogenesis, which could be developed as vaccine candidates.

1.3 *C. burnetii*: the bacterium

C. burnetii is a Gram-negative intracellular bacterium, of the order *Legionellales* (3, 44). 16S RNA sequence alignment shows *C. burnetii* have 91.3% sequence similarity to the *Legionella* species 16S RNA, particularly to the human pathogen *Legionella pneumophila* (45, 46). The genome of the phase I Nine Mile strain RSA493 is 1,995,275 base pairs long, with a G + C content of 42.6% and 29 insertion sequences (47). This strain is also predicted to have 2094 protein-coding genes and 83 pseudogenes. many of which are only disrupted by a single frameshift mutation (47). Genome reduction is a common phenotype of obligate intracellular bacteria. However, a high percentage (89.1%) of the *C. burnetii* genome still encode coding regions (47). Coupled with the minimal mutations present in the pseudogenes, it is likely the genome reduction is either at the early stages or is not as extensive in *C. burnetii*, compared to other intracellular bacteria. Some Nine Mile strains may also contain a 36-54 kb plasmid, although the exact function of this plasmid is yet to be determined (44, 48, 49).

Advances in sequencing strategies have led to the number of sequenced *C. burnetii* genomes to rapidly increase, allowing the comparison of multiple strains (50). For instance, genomes of *C. burnetii* strains K (Q154) and G (Q212), both isolated from chronic Q fever patients, as well as the naturally attenuated Dugway (5J108-111) rodent isolate, were compared against the Nine Mile RSA493 genome (50). These comparisons suggest that the acquisition of multiple pseudogenes over time in pathogenic strains of *C. burnetii* are consistent with the evolutionary progression observed in other bacterial pathogens that have evolved from once non-pathogenic strains (50). This demonstrates that naturally attenuated strains such as the Dugway rodent isolate, may be from earlier lineages in the process of pathoadaptation in *C. burnetii*.

1.3.1 Lipopolysaccharide

C. burnetii display antigenic variation on the surface lipopolysaccharide (LPS). *C. burnetii* phase I are pathogenic, as they express full length LPS (51), and can be isolated from naturally infected humans or from naturally and laboratory infected animals (52). *C. burnetii* phase II have a truncated form of LPS, due to spontaneous mutations that can arise when *C. burnetii* are cultured in eggs or cells (50, 51, 53). These strains are avirulent in mammalian hosts, but are still able to infect cultured cells and some insect hosts (51, 54). The phase II Nine Mile Strain RSA439 is a well characterised and utilised phase II variant in research settings. This strain has a 35 kb deletion within the chromosome, which affects the ability of the bacteria to synthesise components of the LPS and alters metabolic functions (55). Mutations in the predicted LPS biosynthesis enzyme CBU0678 was common across multiple phase II strains, and the enzyme was shown to be essential in the transition of phase II *C. burnetii* to phase I (56). In addition

to *cbu0678*, disruptions of predicted LPS biosynthesis genes *cbu0533*, *cbu0845*, and *cbu1657* were present in phase II strains.

It is important to note that, despite losing virulence in mammalian models of infection, comparative studies have demonstrated that phase II strains are able to infect macrophages with the same kinetics as phase I *C. burnetii* (57). This indicates that phase II strains are a safe and effective model for exploration of molecular mechanisms involved in host-pathogen interactions in *C. burnetii*.

1.4 The *C. burnetii* life cycle

1.4.1 Morphological forms

As with many intracellular bacteria, *C. burnetii* has a biphasic life cycle. The small cell variant (SCV) is the extracellular, spore-like form of *C. burnetii* (44). SCVs are electron-dense (58), and are resistant to environmental stresses such as high temperatures, UV radiation, and osmotic pressure (3). *C. burnetii* SCVs are between 0.2-0.5 μm in size (59). The large cell variant (LCV) is the replicative, metabolically active, intracellular form of *C. burnetii* (60). LCVs are approximately 1 μm in size (58). Studies comparing protein expression levels and transcriptomic profiles between the two forms of *C. burnetii* have identified processes which are important for the maintenance, as well as morphological differentiation between SCV and LCV *C. burnetii* (59, 61-64).

SCV *C. burnetii* show a higher abundance of proteins which may be involved in chromatin condensation, such as ScvA and Hq1 (59, 61). Other proteins that were in

higher abundance may be involved in stabilising outer membrane structures, as well as regulating cell division (62). Transcriptional analysis of SCV *C. burnetii* has also demonstrated that this form upregulates genes involved in the oxidative stress response, amino acid transport, and the remodelling of the bacterial cell wall (63), with another study demonstrating that these responses are regulated by the master stress response regulator, RpoS (64). These traits may contribute to the environmental hardiness of SCV *C. burnetii*.

Proteomic analysis of LCVs have demonstrated that this form of *C. burnetii* have a higher abundance of proteins relating to cell division, transcription and translation (62). These reflect the association of LCVs as the replicative form of *C. burnetii*.

1.4.2 The *Coxiella*-containing vacuole

During natural infection through the inhalation of contaminated aerosols, *C. burnetii* typically infect alveolar macrophages (65, 66). However, *C. burnetii* have the capacity to replicate within a variety of mammalian cells, including epithelial cells (67) and fibroblasts (68). Once internalised, *C. burnetii* passively undergo endocytic maturation, with the endosome/phagosome acquiring key markers of early and late endosomes, such as Rab5 and Rab7, respectively (69, 70). This delivery of *C. burnetii* to the lysosome is essential, as the bacteria require this environment for replication and virulence (71, 72). This highlights the uniqueness of *C. burnetii*, as unlike most intracellular pathogens, the bacteria are not destroyed by this niche and do not attempt to escape. Studies where endosomal trafficking has been inhibited have shown detrimental effects to *C. burnetii*

replication (70, 71). When the bacterium reaches the acidic lysosomal environment of approximately pH 4.5 (69, 72, 73), the conversion to the LCV form is triggered. The transcriptionally active LCVs actively remodels the vacuole, leading to the formation of a single *Coxiella*-containing vacuole (CCV) via homotypic fusion. This expansion of the CCV relies on the high fusogenicity of this vesicular compartment, with studies showing the incorporation of other microbes and latex beads in the CCV (74, 75).

A critical component of CCV expansion is host cell autophagy. Disruption of autophagy was shown to alter CCV morphology, leading to the presence of multiple, smaller CCVs within the host cell (76-78). A *C. burnetii* mutant deficient in a protein involved in the recruitment of autophagic vesicles shows this same multi-vacuolar phenotype, and virulence is reduced in the insect model using *Galleria mellonella* wax moth larvae (76, 77). As the mature CCV is decorated with lysosomal and autophagic markers, it would be more accurate to consider the mature CCV to resemble an autolysosome. Another host cell pathway which is utilised for CCV expansion is clathrin-mediated endocytosis, as the surface of the CCV is enriched with clathrin heavy chain (79, 80). Clathrin is not required for the intracellular uptake of *C. burnetii* (80). Recently, it has been shown that clathrin aids in the fusion of autophagosomes and CCVs, further highlighting the importance of these two host pathways for CCV expansion (78, 80). Fusion of multiple vesicular compartments leads to rapid expansion of the CCV, resulting in a spacious vacuole which can grow to occupy almost the entire host cell cytoplasm (60, 74). This rapid expansion combined with high fusogenicity facilitates success of *C. burnetii* infection, not only by providing space, but presumably by providing vital nutrient sources required for replication.

The expansion and maintenance of the mature CCV requires tight regulation of host processes, including host immune mechanisms such as apoptosis (81). This process limits bacterial replication, and alerts the broader, host immune system to the infection (81). Apoptosis is efficiently and actively inhibited by *C. burnetii* during infection of macrophages (82). This inhibition of host cell death prevents host cell-induced bacterial clearance, thus allowing *C. burnetii* to persist for longer periods within the host cell. This would be an important adaptation for slow-growing bacteria such as *C. burnetii* (60), which must preserve and maintain the host cell for longer periods of time.

The host lysosome contains a high abundance of reactive oxygen species (ROS), which a recent study has shown is increased during *C. burnetii* infection in THP-1 human monocytic cells (83). This same study identified a *C. burnetii* short-chain dehydrogenase, SdrA, which was shown to reduce oxidative stress in *C. burnetii* during intracellular replication within THP-1 cells (83).

C. burnetii also modulate the pH of the intravacuolar environment, increasing this to approximately pH 5.2 (84). This suggests that while *C. burnetii* during initial infection will passively undergo endocytic maturation and require acidification of the vacuole for metabolic activation, this acidification is detrimental to bacterial replication. This difference in the intravacuolar pH may be useful in distinguishing the early CCV from a mature CCV. Interestingly, the routine, axenic culture media for *C. burnetii*, acidified citrate cysteine medium (ACCM)-2, has a pH of 4.75 (85). Alteration of this pH above

4.75 is detrimental to *C. burnetii* growth in axenic culture, suggesting that an inability to withstand acidification is not the reason *C. burnetii* regulate the pH of the mature CCV (86). Many hydrolytic and proteolytic enzymes are present within the host phagolysosome, and proteolytic enzymes are active within the CCV (57, 73). These enzymes require a specific pH niche to be active, and work most efficiently at approximately pH 5 (87). Raising the pH may be a mechanism to inhibit lysosomal enzymes, and may contribute to the ability of *C. burnetii* to grow in more acidic conditions during axenic culture, where these host enzymes are not present.

Replication within the CCV continues until 6-8 days post-infection, where the LCV *C. burnetii* transition back to SCVs (60). The mechanisms allowing egress of SCV *C. burnetii* from the host cell are currently unknown.

1.5 Metabolomics

Understanding the mechanisms utilised by intracellular bacteria to replicate within host cells is an important aspect of understanding overall pathogenesis. *C. burnetii* uniquely replicates within a modified phagolysosome, and the exact mechanisms by which the bacteria acquire nutrients in order to facilitate infection are currently unknown.

Metabolomics is an approach used to obtain a broad, yet highly informative view of the overall metabolic pathways utilised in any given organism under specific conditions (88). Approaches may include steady state profiling, which involves the harvesting of cells under relevant replication conditions. Samples are rapidly quenched to halt metabolism,

which deactivates enzymes and preserves intracellular metabolic compounds, termed metabolites, at the point of harvest. Following extraction of metabolites from harvested cells, samples are analysed to generate a metabolite profile, using such techniques as gas or liquid chromatography-mass spectrometry (GC/MS or LC/MS) (89-91). The overall abundance of each metabolite may be analysed and compared across different conditions and/or strains (92).

Steady state profiling does not determine whether a metabolite was synthesised *de novo* by the organism, or whether it was scavenged from the extracellular environment, and does not allow analysis of the flux through different metabolic pathways. Hence, many profiling studies are now coupled with stable isotope labelling using tracers such as ^{13}C, enabling mapping of metabolic pathways and even quantification of the metabolic flux, or reaction rate, in previously uncharacterised biological systems (90, 91, 93). As the ^{13}C-labelled substrate is taken up by the cell, the subsequent processing and interconversion of the metabolite will incorporate the ^{13}C-label into all active pathways, allowing the tracking of a metabolite substrate through its relevant metabolic pathways. For example, ^{13}C-stable isotope labelling was applied to show glucose utilisation in *Leishmania mexicana* is altered to a more stringent state during the intracellular life stage of the parasite (90). ^{13}C-stable isotope labelling was also applied to compare metabolic pathways present in two species of *Mycoplasma* (91). Stable isotope labelling in this study enabled researchers to obtain information on differences in substrate utilisation between the two species, and lead to the discovery of novel pathways that were not apparent through genomic analyses alone (91).

1.5.1 The *C. burnetii* metabolome

Understanding the metabolism of *C. burnetii* has been important for the development of axenic culture conditions. However, further characterisation of the *C. burnetii* metabolome may also reveal essential metabolic pathways, which may be targeted using novel therapeutics.

In the environment, *C. burnetii* is an obligate intracellular pathogen, and laboratory-based cultivation of *C. burnetii* outside host cells is a relatively new technique. The first iteration of ACCM was established by defining the metabolic requirements of *C. burnetii* (94). This media satisfied the significant number of amino acid auxotrophies in *C. burnetii* (94). In addition, optimal replication of *C. burnetii* occurred under microaerophilic conditions, at 2.5% O_2 (94). Further refinements of this media has led to a number of ACCM derivatives, including ACCM-2 (85), which replaced the initial foetal calf serum present in ACCM with methyl-β-cyclodextrin, leading to increased bacterial replication (85). In ACCM-2, bacteria begin replicating after an initial lag phase at 1 day post-inoculation, with mid log phase at approximately 3 days post-inoculation (85). Replication continues until 6-7 days post-inoculation, when bacteria reach stationary phase (85). Defined media such as ACCM-D and D-ACM removed the casamino acids and Bacto^{TM} Neopeptone present in ACCM-2, and instead require the addition of individual amino acids (86, 95). ACCM-D in particular allows the use of amino acid auxotrophies as a selective tool for the genetic manipulation of *C. burnetii* (95). In addition, unlike ACCM-2, ACCM-D does not contain glucose, which demonstrates that

C. burnetii does not require this nutrient source during axenic cultivation. Replication of *C. burnetii* in all derivatives of ACCM, except D-ACM, require conditions at 37°C, 2.5% O_2, 5% CO_2 (85, 94, 95).

Genetic disruption of the gluconeogenic enzyme *pckA*, a phosphoenolpyruvate carboxykinase (PEPCK) in *C. burnetii*, causes partial attenuation during replication in animal cells (86). This suggests that *C. burnetii* requires glucose during infection, despite being able to replicate in glucose-deficient axenic culture media such as ACCM-D (95). Transcripts for glycolytic and gluconeogenic enzymes are upregulated during intracellular replication, indicating bacteria may require glucose while replicating within the phagolysosome during infection (96).

C. burnetii are auxotrophic for many amino acids, some of which are essential for replication during axenic culture (95). These auxotrophies suggest *C. burnetii* must scavenge amino acids from the host cell during infection. Interestingly, recent metabolomic analysis of mammalian lysosomes has shown that this niche contains amino acids at concentrations equivalent to or higher than in the cytoplasm (97). These studies indicate that *C. burnetii* may rely on both sugar and non-sugar carbon sources such as amino acids for replication within host cells.

A recent study has examined the use of a number of carbon sources, including [^{13}C]glucose, [^{13}C]glycerol, and [^{13}C]serine, in axenically cultivated *C. burnetii* (98). This study confirmed that *C. burnetii* generate ATP and anabolic precursors via

glycolysis, despite the apparent absence of a genome annotated hexokinase or functional phosphotransferase system (PTS). The study also indicated that *C. burnetii* is auxotrophic for histidine, isoleucine, leucine, lysine, phenylalanine, proline and valine biosynthesis, confirming that these amino acids are scavenged from the environment (98). However, it remains unclear how and to what extent these bacteria catabolise non-essential amino acids.

1.6 *C. burnetii* virulence factors

The capacity of *C. burnetii* to establish the unique intracellular replicative niche and cause disease is complex and multifactorial. Many other intracellular pathogens typically avoid endocytic maturation, either by escaping the endosome into the cytosolic environment (99), or by preventing the fusion of the lysosome with the phagosome (100, 101). *C. burnetii* virulence factors which facilitate infection include the LPS, as outlined in section 1.3.1. However, *C. burnetii* utilise numerous other virulence factors to manipulate the host cell, which are outlined below.

1.6.1 Dot/Icm type 4B secretion system

The first *C. burnetii* genome to be sequenced revealed that this pathogen encodes a complete Dot/Icm type 4B secretion system (T4BSS) (47). The T4BSS is a multiprotein apparatus which spans the bacterial and host cell membranes. This apparatus allows the bacteria to translocate proteins, termed effectors, directly into the host cell, in order to facilitate the bacterial replication cycle (102, 103). Ancestrally related to the bacterial conjugation system, the *C. burnetii* T4BSS is functionally analogous to a system first

observed in the human pathogen *L. pneumophila* (104, 105). The *L. pneumophila* T4BSS was observed simultaneously by two different groups who were studying *L. pneumophila* genes involved in preventing **d**efects in **o**rganelle **t**rafficking and promoting **i**ntra**c**ellular **m**ultiplication (104, 105). The *C. burnetii* T4BSS shares high functional analogy to the T4BSS utilised by *L. pneumophila*, in that some T4BSS genes of *C. burnetii* are able to function as part of the *L. pneumophila* T4BSS (106).

C. burnetii are unable to replicate intracellularly without this apparatus, highlighting the importance of the T4BSS during infection (107). It is interesting to note, however, that the survival of *C. burnetii* inside the harsh phagolysosomal environment is not dependant on a functioning T4BSS (107, 108). Mutants of the T4BSS remained viable within the host cell, and replication could be restored upon complementation with an inducible system 24 hours post-infection (108), or upon transfer of *C. burnetii* mutants into axenic media after 24, 72 and 120 hours post-infection (107). This indicates that *C. burnetii* have a T4BSS independent strategy to counteract the hostile lysosomal environment. Interestingly, unlike the *L. pneumophila* T4BSS, the *C. burnetii* T4BSS only begins translocating effector proteins several hours after infection, when the vacuole reaches a highly acidic state (71, 107). This has recently been attributed to pathogen detection of specific amino acids in the degradative lysosomal compartment (109).

Both the *C. burnetii* and *L. pneumophila* T4BSS are transcriptionally regulated by the PmrAB two-component system (110). In these systems, a membrane-localised sensory kinase becomes autophosphorylated upon activation by an environmental trigger, which

leads to a phosphotransfer on to the cytosolic response regulator. This response regulator can then bind target DNA and lead to transcriptional regulation of associated genes (111). The environmental trigger for the activation of this system have been determined to be specific amino acids, which are present in the host lysosomal compartment (97, 109). It has been shown that this two-component system is responsible for regulating not only the T4BSS but expression of a subset of T4BSS effectors (109, 110). Thus the PmrAB two-component system is essential for intracellular replication of *C. burnetii* (109, 110).

Translocation of T4BSS effectors can also be regulated at the post-translational level. For instance, the IcmS chaperone in *C. burnetii* has recently been shown to regulate the translocation of a subset of effector proteins (112). Interestingly, while a subset of effector proteins were shown to be reliant on IcmS for translocation, the translocation of a different subset of effectors were inhibited by the presence of IcmS (112).

In addition, *L. pneumophila* has demonstrated the use of c-di-GMP signalling as a post-transcriptional mechanism that regulates effector translocation by the T4BSS (113). Mutants lacking diguanylate cyclase showed delayed translocation of a known *L. pneumophila* effector protein, LepA (113). A homologous system has not been identified in *C. burnetii*. However, it is highly likely that *C. burnetii* also possess similar mechanisms to temporally regulate T4BSS effector translocation.

1.6.2 Dot/Icm effector proteins

The essentiality of the T4BSS is mediated by the collective action of the proteins this apparatus translocates. Therefore, it is important to understand the function of these effector proteins. To date, approximately130 *C. burnetii* Dot/Icm effectors have been identified, with the actual number likely to be in excess of 150, based on bioinformatic predictions (114). Effector identification initially relied on using *L. pneumophila* as a surrogate host, since *Legionella* are much easier to manipulate genetically compared to *C. burnetii* (115, 116). The development of axenic media to cultivate *C. burnetii* (85, 94), as well as the application of reporter assays such as the calmodulin-dependent adenylate cyclase reporter assay and β-lactamase (BlaM) translocation assay, have led to the discovery of many new *C. burnetii* effectors (107, 115-117). Many of these effectors contain eukaryotic-like domains or motifs, such as ankyrin repeats and kinase motifs, which has also been observed with effectors of other bacterial species (115, 116). The presence of these eukaryotic motifs are predicted to allow bacterial effectors to target various host cell functions by interacting in a similar manner to eukaryotic proteins. Many effectors are not well conserved amongst different strains of *C. burnetii*, and are instead found to have disruptions, caused by insertion/deletion and frameshift mutations (47, 50). Effectors found to be conserved across multiple strains without mutations may represent effectors of essential function within the *C. burnetii* life cycle, which have been maintained through evolutionary pressure.

A large portion of identified *C. burnetii* effectors have unknown roles during infection. Many effectors have only been studied by expressing them ectopically, and therefore the importance of these effectors during a natural infection remains unknown. For example,

the effector proteins AnkG, CaeA, and CaeB have anti-apoptotic functions when expressed ectopically (118, 119). This inhibition of apoptosis may allow *C. burnetii* to replicate longer inside host cells. Utilisation of multiple anti-apoptotic effector proteins suggest functional redundancy may be present. Whether these three effector proteins contribute individually to *C. burnetii* pathogenesis remains to be investigated.

T4BSS effector proteins can target a variety of host organelles. For instance, MceA has been shown to integrate into the outer mitochondrial membrane of host cells (120). ElpA is shown to co-localise with host endoplasmic reticulum during ectopic expression (121), CBU1314 was shown to localise to the nucleus during ectopic expression (122), and CBU0635 localises to the Golgi apparatus during ectopic expression (107). It is important to note, however, that localisation during ectopic expression may not reflect true protein localisation during natural infection, as MceA was shown to colocalise with lysosome-derived vacuoles during ectopic expression (107).

Significantly, several effector proteins have been shown to play important roles within the *C. burnetii* life cycle via transposon mutagenesis screens and targeted gene deletion studies (76, 80, 117, 123). The findings from these screens suggest that individual *C. burnetii* effectors have important, non-redundant function in the *C. burnetii* life cycle. This is in contrast to *L. pneumophila* T4BSS effector proteins, many of which have been found to be functionally redundant or required in specific environmental hosts (124, 125). For example, a study utilising a transposon mutagenesis screen observed that the *C. burnetii* effector protein Cig2 is critical for the homotypic fusion of the CCV, a process

which in this context is also reliant on host cell autophagy (76). The effector proteins Cig57 and CvpA have been shown to target clathrin-mediated endocytosis, which is required for efficient *C. burnetii* replication within host cells (79, 80). The exact mechanism of action of these effectors are not yet defined.

1.7 CBU2072

The use of transposon mutagenesis screens have also given some insight into non-effector proteins which are also important for the intracellular replication of *C. burnetii* (67, 76). For instance, the *C. burnetii* invasin OmpA, discovered in this manner, has been demonstrated to induce cellular uptake, particularly in non-phagocytic cells (67).

A previous transposon mutagenesis screen demonstrated that the disruption of a novel gene in the *C. burnetii* Nine Mile phase II RSA439 strain led to a complete defect in intracellular replication (76). The protein encoded by this gene, CBU2072, was subsequently shown to not be a substrate of the T4BSS using a BlaM translocation assay (76). The complete dependence *C. burnetii* has on CBU2072 for intracellular replication, and therefore virulence, warrants further investigation of this novel protein.

1.7.1 NAD(P)(+) transhydrogenases

Bioinformatic analysis using PSI-BLAST indicates that CBU2072 has 33% homology to NAD(P)(+) transhydrogenases between the amino acid residues 24 to 96 (126).

Transhydrogenases exist in either a membrane-bound or soluble form, and function to maintain the balance between NAD(H) and NADP(H) within the cell through hydride ion transfer using the reaction $NADP^+ + NADH \leftrightarrow NADPH + NAD^+$ (93). NADPH production initiated by transhydrogenases is important for the detoxification of potentially damaging ROS by pathogens (127). However, the primary role of NAD(P)(+) transhydrogenase has been attributed to those involved in the regulation of metabolism (93). For instance, *Escherichia coli* transhydrogenases are involved in the regulation of NADPH within central carbon metabolism (93).

PntAB is a well-characterised membrane-bound transhydrogenase complex found in *E. coli*. This enzyme, like many other membrane-bound transhydrogenases, contains three functional and structural domains. Domains I and III are hydrophilic, with domain I responsible for NAD(H)-binding, and domain III responsible for NADP(H)-binding. The region in between these two domains is hydrophobic, and contains the membrane bound domain II, which is responsible for the transport of protons across the membrane (128-131). In *E. coli*, the membrane-bound transhydrogenase comprises two subunits, PntA and PntB, or α and β subunits, respectively. Although domain I is derived from the α subunit, and domain III of the β subunit, domain II is composed of both α and β subunits (129). Domain II of *E. coli* is comprised of 13 transmembrane α helices (132).

In addition to the membrane-bound transhydrogenase, *E. coli* and other species of Enterobacteriaceae encode a soluble transhydrogenase. In *E. coli*, this soluble transhydrogenase is encoded by *sthA*, formerly known as *udhA* (133). Structurally

unrelated to the membrane-bound transhydrogenases, soluble transhydrogenases have not been studied as extensively as the membrane-bound counterpart. Found also in *Azotobacter vinelandii* and members of the *Pseudomonas* species, soluble transhydrogenases interact with flavin adenine dinucleotide (FAD) (133). Although not seen with *E. coli* SthA, some soluble transhydrogenases are able to form large polymers (133-136). It is hypothesised that the physiological role of soluble transhydrogenases is to convert excess NADPH into NADH (93). Unlike membrane-bound transhydrogenases, soluble transhydrogenases catalyse this conversion in a manner which is energy independent (137). Soluble transhydrogenases share homology with flavoprotein disulphide oxidoreductases. These oxidoreductases are known to contain a N-terminal flavin-binding domain, a central NAD(P)-binding domain, and a C-terminal dimerization domain (134, 137).

Many soluble transhydrogenases also contain a GXXXG motif, which is also present in CBU2072 ($_{84}$GVNVG$_{88}$). This motif is important for stabilising the structure of binding domains responsible for interacting with FAD and NAD(P) molecules (138). These interactions are facilitated by the formation of a flat binding surface by the GXXXG motif, which allow other helical structures to come into close proximity to interact with the protein (139). This close binding promotes van der Waals interactions between proteins, which can act to further stabilise helix-helix interactions (140). GXXXG motifs are common in many α-helical structures, which may suggest that this area of soluble transhydrogenases also forms a helical structure (138).

1.8 Aims of this research

The broad focus of this research was to understand the ability of *C. burnetii* to infect and replicate within the modified phagolysosome. *C. burnetii* must utilise novel and unique mechanisms to withstand the degradative environment and cause disease. Therefore, investigating these mechanisms could lead to the identification of essential, *C. burnetii*-specific processes, which could become novel therapeutic targets against Q fever.

Specifically, this research focused on comparing and contrasting the nutrient requirements and metabolic substrate usage of *C. burnetii* phase II RSA439, referred to throughout as wild type (WT). One population was cultivated *in vivo* in mammalian cells, while the other was cultivated axenically *in vitro* in routine ACCM-2 media. Techniques developed from this first aim led to the subsequent identification and characterisation of two *C. burnetii* glucose transporters, CBU0265 and CBU0347. Combined, these results have given greater insights into *C. burnetii* metabolism, which revealed greater metabolic flexibility than previously thought.

Additionally, this research also investigated the function of the novel *C. burnetii* protein CBU2072, renamed essential for intracellular replication A (EirA). This protein was found to localise to the bacterial cytoplasm and inner membrane, and requires an N-terminal signal peptide sequence in order to function. Absence of EirA leads to loss of T4BSS effector translocation, suggesting a novel role in control of T4BSS activity. Future

mechanistic characterisation of EirA may reveal a novel, post-translational control mechanism for *C. burnetii* T4BSS activity.

Collectively, this body of research provides important and novel insights that have improved our understanding of this intracellular pathogen.

Chapter 2

Materials and Methods

2.1 Bacterial strains

Bacterial strains used in this research are listed in Table 2.1. All *Escherichia coli* strains were grown in Luria-Bertani (LB) medium (Appendix 1) supplemented with 50 µg/mL kanamycin (Sigma-Aldrich) or with 100 µg/mL ampicillin (A. G. Scientific) when required. *E. coli* were routinely grown in LB liquid cultures or on 1.5% LB agar plates (Appendix 1) at 37°C overnight or until specific OD_{600} was reached as indicated in relevant sections. All liquid cultures were agitated at 180 rpm during growth.

All *C. burnetii* phase II Nine Mile Strain RSA439 wild type (WT) and mutants were routinely grown in ACCM-2, or ACCM-D (Appendix 1) as previously described (85, 95). Media was supplemented with 350 µg/mL kanamycin or 3 µg/mL chloramphenicol (Boehringer Mannheim) when required. Cultures were routinely grown to stationary phase or indicated time points at 37°C, 5% CO_2, 2.5% O_2.

Table 2.1. Bacterial strains used in this study.

Bacterial strain	Features	Reference
E. coli		
XL1-Blue	*recA1*, *endA1*, *gyrA96*, *thi1*, *hsdR17*, *supE44*, *relA1*, *lac [F'proAB*, *lacI^{q}ZΔM15 Tn10*, *(Tet^R)]*	Novagen
DH5α	F$^-$ ø80d*lacZ*ΔM15 Δ(*lacZYA-argF*)U169 *deoR recA1 endA1 hsdR17*(r_k^-,m_k^+) *phoA*	Clontech
Rosetta II (DE3)	F$^-$ *ompT hsdS*$_B$(r_B^- m_B^-) *gal dcm* (DE3) pRARE2 (Cam^R)	Novagen
C. burnetii		
Nine Mile phase II RSA439	Wild type (WT)	Ted Hackstadt, NIH
0265::Tn	Transposon disrupting *cbu0265* – Kan^R	(76)
0347::Tn	Transposon disrupting *cbu0347* – Kan^R	(76)
2072/*eirA*::Tn	Transposon disrupting *cbu2072*/*eirA* – Kan^R	(76)

2.2 Tissue culture cell lines

HeLa human cervical carcinoma cells (229 or CCL2, ATCC) were cultured in Dulbecco's Modified Eagle's Media GlutaMAX™ (DMEM, Gibco) supplemented with 10% heat inactivated foetal calf serum (FCS, Gibco). During infection, cultures were maintained in DMEM + 5% FCS. HeLa cells were routinely passaged by removing media and washing once with 1x phosphate buffered saline (PBS, Appendix 1) to remove detached cell debris. Cells were then incubated for 2 minutes at 37°C, 5% CO_2 with 1 mL trypsin (Gibco) before being resuspended in 9 mL DMEM + 10% FCS. One mL of this resuspension was passaged into 19 mL fresh DMEM + 10% FCS. THP-1 human monocytic (ATCC) cells were cultured in RPMI 1640 with GlutaMAX™ (Gibco) supplemented with 10% FCS. Cells were routinely passaged by taking 1 mL of culture and adding to 19 mL fresh RPMI + 10% FCS. All cell lines were maintained at 37°C, 5% CO_2 and passaged a maximum 40 times.

2.3 Molecular Biology techniques

2.3.1 Purification of plasmid DNA

Plasmids used in this study are listed in Table 2.2, with antibiotic resistance written as Amp^R, Kan^R, and Cm^R, for ampicillin, kanamycin and chloramphenicol resistance, respectively. Plasmid DNA was extracted from overnight LB broth cultures of *E. coli* XL1-Blue or DH5α, supplemented with appropriate antibiotics for selection, using the QIAprep Spin Miniprep Kit (Qiagen) according to manufacturer's protocol. DNA was eluted in 100 µL nuclease free water (Qiagen). Plasmid yield was measured using a Nanodrop™ Lite (ThermoFisher Scientific).

Table 2.2. Plasmid vectors used in this study.

Plasmid	Features	Antibiotic Selection	Reference
pcDNA4/TO:3xFLAG	Eukaryotic expression vector encoding 5' 3xFLAG tag and multiple cloning site (MCS)	Amp^R	Clontech, Roy Laboratory, Yale University
pcDNA4/TO:3xFLAG-EirA	Encodes 5' 3xFLAG tag and full length *eirA* with 5'BamHI and 3' EcoRI RE sites	Amp^R	Newton Laboratory
pcDNA4/TO:3xFLAG-EirA$_{24\text{-}165}$	Encodes 5' 3xFLAG tag and truncated *eirA* from 70 bp-498bp (amino acid residues 24-165) with 5' BamHI and 3' EcoRI RE sites	Amp^R	Newton Laboratory
pcDNA4/TO:3xFLAG-EirA $_{40}$AAAA$_{43}$	Encodes 5' 3xFLAG tag and *eirA* with bp changes between 118 bp-129 bp from CCAGAGATCAGT into GCAGCGGCCGCT (corresponding to amino acid changes P40A E41A I42A S43A) generated using site directed mutagenesis (SDM) of pcDNA4/TO:3xFLAG-EirA	Amp^R	This study
pcDNA4/TO:3xFLAG-EirA $_{84}$AVNVA$_{88}$	Encodes 5' 3xFLAG tag and *eirA* with bp changes between 241 bp-243 bp and 253 bp-255 bp from GGC and GGT to GCC and GCT (amino acid changes G84A G88A) generated using SDM of pcDNA4/TO:3xFLAG-EirA	Amp^R	This study
pGEM-T Easy	High copy cloning vector	Amp^R	Promega
pGEM-T Easy:0265	Full length *cbu0265* with 5' BamHI and 3' NotI restriction endonuclease (RE) sites	Amp^R	This study
pGEM-T Easy:0347	Full length *cbu0347* with 5' BamHI and 3' NotI RE sites	Amp^R	This study
pJB-Kan:BlaM	*C. burnetii* expression vector encoding for β-lactamase (BlaM) from *Bacillus subtilis* under constitutive expression by the *cbu1169* promoter (P1169)	Kan^R	(107)

pJB-Kan:BlaM-MceA	Encodes 5' BlaM tag and *mceA*/*cbu0077* with 5' and 3' SalI sites	Kan^R	Newton Laboratory
pJB-Kan:3xFLAG	*C. burnetii* expression vector encoding 5' 3xFLAG tag under constitutive expression by the *C. burnetii* P1169 promoter	Kan^R	(85)
pJB-Kan:3xFLAG-MCS	*C. burnetii* expression vector encoding 5' 3xFLAG tag and MCS from pcDNA4/TO under constitutive expression by the *C. burnetii* P1169 promoter	Kan^R	This study
pJB-Kan:3xFLAG-MceA	pJB-Kan:3xFLAG encoding 5' 3xFLAG tag and *mceA*/*cbu0077* with 5' and 3' SalI RE sites	Kan^R	Newton Laboratory
pJB-Kan:3xFLAG-0265	pJB-Kan:3xFLAG-MCS encoding 5' 3xFLAG tag and *cbu0265* with 5' BamHI and 3' NotI RE sites	Kan^R	This study
pJB-Kan:3xFLAG-0347	pJB-Kan:3xFLAG-MCS encoding 5' 3xFLAG tag and *cbu0347* with 5' BamHI and 3' NotI RE sites	Kan^R	This study
pJB-Kan:3xFLAG-EirA	pJB-Kan:3xFLAG encoding 5' 3xFLAG tag and *eirA* cloned with 5' and 3' SalI RE sites	Kan^R	Newton Laboratory
pJB-Kan:EirA-3xFLAG	pJB-Kan:3xFLAG encoding 3' 3xFLAG tagged *eirA* cloned with 5' PstI and 3' SalI RE sites	Kan^R	Newton Laboratory
pJB-Kan:3xFLAG-EirA$_{24\text{-}165}$	pJB-Kan:3xFLAG encoding 5' 3xFLAG tag and truncated *eirA* from 70 bp-498bp (amino acid residues 24-165) with 5' and 3' SalI RE sites	Kan^R	This study
pJB-Kan:3xFLAG-EirA $_{40}$AAAA$_{43}$	pJB-Kan:3xFLAG-MCS encoding 5' 3xFLAG tag and *eirA* with bp changes between 118 bp-129 bp from CCAGAGATCAGT into GCAGCGGCCGCT (corresponding to amino acid changes P40A E41A I42A S43A) cloned with 5' BamHI and 3' XhoI RE sites	Kan^R	This study
pJB-Kan:3xFLAG-EirA $_{84}$AVNVA$_{88}$	pJB-Kan:3xFLAG-MCS encoding 5' 3xFLAG tag and *eirA* with bp changes between 241 bp-243 bp and 253 bp-255 bp from GGC and GGT to GCC and GCT	Kan^R	This study

	(amino acid changes G84A G88A) cloned with 5' BamHI and 3' XhoI RE sites		
pMAL-c2X:EirA$_{24\text{-}165}$	pMAL-c2X encoding 5' MBP tag and truncated *eirA* from 70 bp-498bp (amino acid residues 24-165) with 5' BamHI and 3' PstI RE sites	Amp^R	Newton Laboratory (141)

Underline indicates nucleotides mutated for SDM purposes.

2.3.2 Generation of chemically competent *E. coli*

E. coli XL1-Blue or DH5α were streak diluted onto LB agar (Appendix 1) and incubated overnight at 37°C. A single colony was inoculated into 10 mL LB broth and incubated overnight at 37°C with shaking at 180 rpm. One mL of this overnight culture was transferred into 100 mL Super Optimal Broth (SOB) (Appendix 1), which was incubated at 16°C with shaking between 200-250 rpm until the absorbance (OD_{600}) reached 0.4-0.8. Once the appropriate density had been reached, the culture was incubated on ice for 10 minutes, before cells were pelleted by centrifugation at 2,500 x *g* for 15 minutes at 4°C. Cells were resuspended in 40 mL chilled transformation buffer (TB) (Appendix 1), before being incubated on ice for 10 minutes. Cells were pelleted again as above and resuspended in 4 mL chilled TB. Bacteria were incubated on ice for 10 minutes after the addition of 0.3 mL dimethyl sulphoxide (DMSO) (Sigma-Aldrich). Fifty µL aliquots of these chemically competent *E. coli* were snap frozen in a dry ice-ethanol bath and stored at -80°C long term.

2.3.3 Generation of electrocompetent *E. coli*

E. coli Rosetta II were streak diluted onto LB agar and incubated overnight at 37°C. A single colony was inoculated into 10 mL LB broth and incubated overnight at 37°C with shaking at 180 rpm. One mL of this overnight culture was transferred into 100 mL SOB, which was incubated at 16°C with shaking between 200-250 rpm until the absorbance (OD_{600}) reached 0.6-1.0. Once the appropriate density had been reached, the culture was incubated on ice for 15-30 minutes, before cells were pelleted by centrifugation at 2,500 x *g* for 15 minutes at 4°C. Bacteria were washed twice, first in 100 mL then in

50 mL ice-cold sterile water, centrifuging at 2,500 x *g* 15 minutes at 4°C. Pelleted bacteria were then washed once in 2 mL ice-cold 10% glycerol (v/v in dH_2O) (ThermoFisher Scientific), before being resuspended in 2 mL ice-cold 10% glycerol. Forty µL aliquots of these electrocompetent *E. coli* Rosetta II were snap frozen in a dry ice-ethanol bath and stored at -80°C long term.

2.3.4 Transformation of *E. coli* with plasmid DNA

Chemically competent *E. coli* were transformed using the heat-shock method (142). Chemically competent *E. coli* aliquots as described in 2.3.2 were thawed on ice before the addition of 100-200 µg plasmid DNA or ligation mixture. *E. coli* were incubated for 30 minutes on ice with the DNA, before being heat-shocked at 42°C for 90 seconds. These cells were then incubated on ice for 2 minutes, before the addition of 950 µL Super Optimal Broth with catabolite repression (SOC) (Appendix 1). *E. coli* were incubated for 1 hour in SOC broth, shaking at 180 rpm on a platform shaker at 37°C for recovery. Transformants were selected by plating onto LB agar containing the appropriate antibiotics for selection. Plates were incubated overnight at 37°C.

In order to generate MBP-tagged $EirA_{24\text{-}165}$, pMAL-c2X:$EirA_{24\text{-}165}$ was transformed into *E. coli* Rosetta II strains by electroporation. Briefly, 100 ng of plasmid DNA was added to 50 µL electrocompetent Rosetta II strains. Cells were electroporated at 200 Ω 1.8 kV 25 µF in 2 mm electroporation cuvettes, and 950 µL SOC broth was immediately added. *E. coli* were incubated for 1 hour in SOC broth, shaking at 180 rpm on a platform shaker

at 37°C for recovery. Transformants were selected by plating onto LB agar containing the appropriate antibiotics for selection. Plates were incubated overnight at 37°C.

2.3.5 Transformation of *C. burnetii* with plasmid DNA

All *C. burnetii* expression vectors were transformed into *C. burnetii* as previously described (76). Briefly, 10 mL 6-7 day post-inoculation ACCM-2 cultures of *C. burnetii* were centrifuged at 3,220 x *g*, 15 minutes, 4°C, then washed once in ice-cold 10% glycerol. Bacterial pellets were resuspended in 50 µL ice-cold 10% glycerol, and 1 µg of relevant plasmid DNA was added. Cells were electroporated at 500 Ω 1.8 kV 25 µF in a 1 mm electroporation cuvette, and immediately resuspended in 950 µL RPMI + 10% FCS. Four hundred µL of this resuspension was added to 3 mL ACCM-2 in a 6 well tissue culture plate (Corning), and *C. burnetii* were incubated for 24 hours at 37°C, 5% CO_2, 2.5% O_2.

Transformed *C. burnetii* were then plated onto ACCM-2 agar containing relevant antibiotic selection. For each plate, the bottom layer was formed by mixing 10 mL 2x ACCM-2 with 10 mL 0.5% UltraPure™ agarose (w/v in dH_2O, ThermoFisher Scientific) with relevant antibiotic selection. The top layer consisted of 1.25 mL 2x ACCM-2, 0.75 mL dH_2O, 0.5 mL 0.5% UltraPure™ agarose, and either 200 µL, 400 µL or 600 µL bacterial inoculum with relevant antibiotic selection. Plates were left to incubate at 37°C, 5% CO_2, 2.5% O_2 for 6-7 days before colonies were picked using a wide-bore pipette. Isolated colonies were inoculated into 1 mL ACCM-2 with relevant antibiotic selection

and incubated for another 6-7 days at 37°C, 5% CO_2, 2.5% O_2 before protein expression levels were confirmed by immunoblot (IB) analysis of whole cell lysate.

2.3.6 Polymerase chain reaction (PCR) amplification techniques

All PCR amplifications were performed on either a GeneAmp® PCR system 2400 (Applied Biosystems) or T100™ Thermo Cycler (Bio-Rad) unless otherwise stated.

2.3.6.1 Template DNA preparation and oligonucleotides

gDNA of *C. burnetii* WT was isolated using the Zymo gDNA extraction kit (Zymo Research) as per manufacturer's protocol. All oligonucleotides were obtained from Sigma-Aldrich and are listed in Table 2.3. All oligonucleotides were used at a working concentration of 10 µM.

Table 2.3. Oligonucleotides used in this study.

Primer	Sequence (5' to 3')
Sequencing primers for pcDNA4/TO derivatives	
pcDNA4_F	CGCAAATGGGCGGTAGGCGTG
pcDNA4_R	CTAGAAGGCACAGTCGAGG
Sequencing primers for pGEM derivatives	
M13_F	TGTAAAACGACGGCCAGT
M13_R	TCACACAGGAAACAGCTATGAC
Sequencing primers for pJB-Kan derivatives	
pJB-Kan_F	GAGCTGTTGACAATTAATCATC
pJB-Kan_R	GGATTCATCGACTGTGGCCG
Complementation constructs	
MCS_F (SalI)	AAGTCGACGGATCCACTAGTCCAGTGTG
MCS_R (SalI)	AAGTCGACTTTAAACGGGCCCTCTAGACT
*cbu0265*_F (BamHI)	AAAGGATCCATGAAGTTTTCTTTTCC

*cbu0265*_R (NotI)	AAGCGGCCGCCTAAAAGAAATGAGAATGA
*cbu0347*_F (BamHI)	AAGGATCCATGAATTCAACCGACCAA
*cbu0347*_R (NotI)	AAGCGGCCGCTTATTTTCCTAAATAACG
*eirA*_F (BamHI)	AAAGGATCCATGCGTTATCCGAAATTCAGT
*eirA*_R (NotI)	AAGCGGCCGCTTAAAATCCAATTTCTTGTTG
eirA$_{24\text{-}165}$_F (BamHI)	AAAGGATCCGCCCCTGCAACG
Eukaryotic expression vector constructs	
eirA$_{40}$AAAA$_{43}$_R (XhoI)	AAAGAGCTCTTAAAATCCAATTTCTTGTTGACTGG
Site directed mutagenesis	
eirA $_{40}$AAAA$_{43}$_F	GGCTATCTCACCTGT**G**CAG**C**G**G**C**G**CTAAACTGCAAAAA GATCCC
eirA $_{40}$AAAA$_{43}$_R	GGGATCTTTTTGCAGTTTA**G**C**G**G**C**C**G**CTG**C**ACAGGTGAG ATAGCC
eirA $_{84}$AVNVA$_{88}$_F	GCTCAATGGCAGG**C**CGTTAATGTGG**C**TAATATTACTTGC
eirA $_{84}$AVNVA$_{88}$_R	GCAAGTAATATTA**G**CCACATTAACG**G**CCTGCCATTGAGC
Screening transposon mutants	
Tn7*cat*_F	CTTTTTACGGTTCCTGGGCTT
Tn7ColE1_R	TGTGATGGCTTCCATGTCG
qPCR (143)	
*ompA*_F	CAGAGCCGGGAGTCAAGCT
*ompA*_R	CTGAGTAGGAGATTTGAATCGC

RE sites underlined. Bold nucleotides represent bases mutated for SDM purposes.

2.3.6.2 PCR amplification

PCR was used to amplify *cbu0265*, *cbu0347*, *eirA* fragments, as well as the MCS of pcDNA4/TO:3xFLAG. Each reaction used *PfuUltra* II fusion HS DNA polymerase (Agilent Technologies) according to manufacturer's protocol. Briefly, 100 ng template DNA, 10 µM forward and reverse oligonucleotides, dNTP mix (25 mM of each dNTP, Bioline), 10x *PfuUltra* II reaction buffer, 1 µL *PfuUltra* II fusion HS DNA polymerase was made up to 50 µL total volume with nuclease free water.

2.3.6.3 Colony PCR

GoTaq® Green (Promega) or MyTaq™ Red (Bioline) were used to screen colonies with inserts >1 kb or <1 kb, respectively, according to manufacturer's protocol. For both reactions, 10 μM forward and reverse oligonucleotides were combined with 2x GoTaq® Green or 2x MyTaq™ Red DNA polymerase and made up to 20 μL total volume with nuclease free water.

2.3.6.4 Agarose gel electrophoresis

Agarose gel electrophoresis was performed in order to separate and isolate DNA fragments following PCR or digestion. One percent (w/v) agarose was prepared using molecular biology grade agarose (Bioline) dissolved in Tris acetate EDTA (TAE) buffer (Appendix 1) with 0.01% SYBR® Safe DNA gel stain (ThermoFisher Scientific). Where necessary, DNA samples were mixed with 6x purple loading dye (New England Biolabs) prior to loading. Samples were electrophoresed at 100-110 V for 30-40 minutes alongside 1 kb DNA ladder (New England Biolabs). The G:Box HR Gel Documentation System (Syngene) was used to visualise DNA products, and photographs were obtained using GeneSnap (Syngene).

2.3.6.5 DNA purification from PCR reactions

To isolate DNA from agarose gels, DNA fragments were visualised using the Safe Imager™ Transilluminator (ThermoFisher Scientific) and excised from the agarose gel using a sterile scalpel blade. DNA was purified from resulting fragments using the

ISOLATE II PCR and Gel Kit (Bioline) according to manufacturer's protocol. Purified DNA was eluted in 30 µL nuclease free water.

2.3.6.6 Restriction endonuclease digestion and ligation of DNA

Restriction endonucleases were obtained from New England Biolabs and used according to manufacturer's protocol. DNA ligations using T4 DNA ligase (New England Biolabs) were prepared according to manufacturer's protocol, with a vector:insert ratio ranging 1:3-1:5.

2.3.6.7 Sequencing PCR and analysis

Sequencing PCR was used to confirm correct insert sequence following ligation, plasmid screening, and purification, using the BigDye® Terminator v3.1 Cycle sequencing kit (ThermoFisher Scientific) according to the Australian Genome Research Facility (AGRF) protocol. Briefly, ~300 ng template DNA, 10 µM oligonucleotide, 5x BigDye® Terminator buffer and 0.8 µL BigDye® Terminator v3.2 DNA polymerase was made up to 15 µL with nuclease free water. Samples were initially incubated at 96°C for 2 minutes, before cycling at 96°C for 10 seconds, 50°C for 5 seconds, and 60°C for 4 minutes for a total of 30 cycles. DNA was precipitated by adding 50 µL 100% ethanol (v/v, Chem Supply) and 2 µL 3 M NaOAc (pH 5.2, Sigma-Aldrich). This was incubated at room temperature (RT) for 15 minutes, before being centrifuged at 17,000 x *g* for 20 minutes. Supernatant was removed, and the pellet was washed twice in 200 µL 70% ethanol (v/v), centrifuging at 17,000 x *g* for 5 minutes in between. Residual ethanol was evaporated by incubating at RT until dry.

Samples were sequenced using the Sanger method by AGRF. Analysis of the results was conducted using Sequencher (Gene Codes Corporation) and compared to known GenBank sequences using BLAST (126).

2.4 Treatment of DH5α strains with hydrogen peroxide

E. coli DH5α strains relevant pJB-Kan:3xFLAG constructs were grown at 37°C in LB broth with relevant antibiotics, to OD_{600} = 1, which equated to approximately 10^9 colony forming units (CFU)/mL. Cultures were then serially diluted to 10^3, 10^4, and 10^5 CFU/mL in PBS containing hydrogen peroxide (Chem Supply) at either 0 µM, 0.02 µM, 0.2 µM, 2 µM, 20 µM or 200 µM. One hundred µL from each was plated on to LB agar with relevant antibiotics. Plates were left to incubate at 37°C for 24 hours before colonies were counted.

2.5 Quantification of *C. burnetii* genome equivalents

Quantification of *C. burnetii* genome equivalents (GE) was achieved using an *ompA* specific quantitative PCR (qPCR) as previously described (143). Briefly, cultures of relevant *C. burnetii* strains were centrifuged at 3,220 x *g* for 15 minutes or 17,000 x *g* for 15 minutes, before being resuspended in appropriate volume of media or nuclease free water. Dilutions of these samples at 1:10 and 1:100 were prepared in nuclease free water and run using the SensiFAST™ SYBR No-Rox kit (Bioline). The Mx3005P qPCR system (Agilent Technologies) or QuantStudio™ 7 Flex real-time PCR system (ThermoFisher

Scientific) and respective analysis softwares were used for data export. Microsoft Excel was used for further data analysis and generation of standard curves.

Quantification of *C. burnetii* GE from axenic culture using the Quant-iT™ PicoGreen™ dsDNA assay kit (ThermoFisher Scientific) was performed according to manufacturer's protocol. Samples were read using the CLARIOStar® plate reader (BMG LABTECH). Data was processed using the MARS analysis software (BMG LABTECH) and further analysed using Microsoft Excel.

In both protocols, *C. burnetii* GE were extrapolated by comparing unknown samples to DNA standards or known *C. burnetii* GE.

2.6 *C. burnetii* infections of tissue culture cells

Infections in HeLa CCL2 and THP-1 cells were performed as previously described (120). Briefly, HeLa CCL2 cells were seeded at 2.5 x 10^4 cells/well into 24 well flat bottom tissue culture plates (Corning) and incubated for 24 hours. THP-1 cells were seeded at 5 x 10^5 cells/well and were treated and differentiated with 10 nM phorbol 12-myristate 13-acetate (PMA, Adipogen Life Sciences) for 3 days. Samples for immunofluorescence microscopy (IF) were seeded onto 12 mm sterile glass coverslips. Unless otherwise stated, HeLa CCL2 cells were infected at a multiplicity of infection (MOI) of 100 and THP-1 cells were infected at an MOI of 25. Bacteria were quantified as outlined in 2.5. For intracellular replication assays, following addition of *C. burnetii*, cells were incubated for 4 hours at 37°C, 5% CO_2, before being washed once in PBS and supplemented with fresh

media. For intracellular replication assays, samples were lysed with nuclease free water (Qiagen) for *C. burnetii* quantification at defined time points. For 1, 3, and 5 day post-infection samples, the supernatant from each duplicate well was pooled and collected alongside lysed cells. Collected samples were centrifuged at 17,000 x *g* for 15 minutes before the bacterial and cell debris pellet was resuspended in 100 µL nuclease free water and quantified as outlined in 2.5. For IF, samples were processed at relevant time points as outlined in section 2.10.6.

For 7 day co-infection and phenotype rescue experiments, HeLa CCL2 cells were seeded at 5 x 10^4 cells/well into 24 well flat bottom tissue culture plates containing 12 mm glass coverslips, and incubated for 24 hours to allow cells to adhere to the well before infection. For 7 day co-infection experiments, *C. burnetii* WT and *eirA*::Tn were used to infect at an MOI of 5 for each strain. Cells were fixed for IF at 24 hour intervals for the duration of the infection as outlined in section 2.10.6. For phenotype rescue experiments, cells were first infected with *eirA*::Tn at an MOI of 100. After 5 days incubation, cells were super-infected with either WT or *eirA*::Tn at an MOI of 100 for each strain. Following a further 3 days of incubation, cells were fixed and stained as outlined in section 2.10.6. Cells from both experiments were incubated in DMEM + 5% FCS for 24 hours post-infection, before extracellular bacteria were removed by washing once in PBS and replacing with fresh DMEM + 5% FCS.

2.7 Metabolomics techniques

2.7.1 Metabolite quenching and extraction

To harvest bacteria cultivated in HeLa 229 cells, cells were seeded at 2.5 x 10^4 cells/mL into T175 flasks (Corning) in 50 mL DMEM + 10% FCS. After 3 days, cells were infected with *C. burnetii* WT at an MOI of 100. Twenty-four hours post-infection, these cultures were split across two T175 flasks and incubated for a further 24 hours before harvesting for analysis.

To prepare *C. burnetii* strains for metabolite quenching, strains incubated in ACCM-2 for 6 days were continuously and manually agitated and rapidly quenched to 0°C in a dry ice-ethanol bath to halt metabolic activity. Cultures were centrifuged at 3,220 x *g* for 15 minutes at 0°C to pellet bacteria. For intracellularly cultivated *C. burnetii*, HeLa 229 cells were collected and quenched in 10 mL ice-cold PBS and lysed to release intracellular bacteria by using a Dounce homogeniser (Sigma-Aldrich). Bacteria were separated from cell debris by centrifugation at 164 x *g* for 10 minutes at 0°C, and bacteria-containing supernatant was collected. Supernatant was centrifuged at 3,220 x *g* for 15 minutes at 0°C to pellet bacteria.

The bacterial pellet was washed twice, once in 10 mL ice-cold PBS, centrifuging at 3,220 x *g* for 15 minutes at -2°C, then again with 1 mL PBS, centrifuging at 17,100 x *g* for 15 minutes at -2°C. Metabolites were extracted using chloroform:methanol:water ($CHCl_3$:CH_3OH:H_2O, 1:3:1 v/v) containing 1 nmol [$^{13}C_6$]sorbitol (Sigma-Aldrich) and 10 nmol $^{13}C_5$-^{15}N-labelled valine (Sigma-Aldrich) as internal standards. After addition of

300 µL 100% methanol (v/v, Chem Supply) to 99 µL water with 0.5 µL each of internal standards (CH_3OH:H_2O, 3:1 v/v), bacterial cells were sheared by repeat exposure to liquid nitrogen for 30 seconds, then dry-ice ethanol bath for 30 seconds, for a total of 10 times each. One hundred µL chloroform was then added to bring the solution to the aforementioned 1:3:1 ratio. Following vortex mixing, samples were incubated on ice for 10 minutes. Cell debris was removed by centrifuging samples at 17,100 x *g* for 15 minutes at -2°C. The supernatant was adjusted to 1:3:3 $CHCl_3$:CH_3OH:H_2O (v/v) by the addition of 200 µL water, before vortex mixing and centrifuging at 17,100 x *g* for 15 minutes at -2°C to induce phase separation. The upper aqueous phase, containing polar metabolites, was transferred to a fresh precooled 1.5 mL microcentrifuge tube and stored at -80°C until gas chromatography/mass spectrometry (GC/MS) or liquid chromatography/mass spectrometry (LC/MS) analysis.

For metabolite extractions of ACCM-2 alone, the media was used as the water fraction in the chloroform:methanol:water ($CHCl_3$:CH_3OH:H_2O, 1:3:1 v/v) extraction solvent, with remaining volumes identical to extractions from bacterial cells. The shearing step was omitted, as metabolites were already accessible to the solvent.

2.7.2 Metabolite derivatisation and GC/MS analysis

Aqueous-phase samples were transferred into glass vial inserts and dried in a rotational vacuum concentrator (RVC-2-33; John Morris Scientific), with an additional 30 µL of 100% methanol added to ensure samples were completely dry. Free aldehyde groups were derivatized in 20 µL methoxyamine chloride (30 mg/mL in pyridine; Sigma-Aldrich)

with continuous mixing for 2 hours at 37°C. Twenty µL of *N*,*O*-bistrimethylsilyltrifluoroacetamide (Thermo Scientific) containing 1% trimethylchlorosilane (Thermo Scientific) was then added, and samples were incubated for 1 hour at 37°C, with continuous shaking, using a Gerstel MPS2 autosampler robot. For GC/MS analysis, 1 µL of derivatized sample was injected into an Agilent 7890A gas chromatograph (split/splitless inlet, 250°C) containing a VF-5ms column (30 m/250 µm/0.25 µm/10 m Eziguard precolumn) coupled to an Agilent 5975C mass selective detector. Helium was used as the carrier gas at a constant flow rate of 1 mL/minute. The GC temperature was ramped from 35°C, at which it was initially held for 2 minutes, to 325°C, at 25°C/minute, and then held for 5 minutes at 325°C. The 5975C mass selective detector was used in scan mode, and mass spectra data were collected at a rate of 9.19 scans/second over an *m/z* range of 50-600 atomic mass units.

2.7.3 LC/MS analysis

Polar metabolites were also analysed by LC/MS using an Agilent Technologies 1200 series LC system. Samples were stored in an autosampler at 4°C. Ten µL of sample was injected on a SeQuant Zwitterionic ion chromatography-hydrophilic interaction liquid chromatography column (150 mm x 2.1 mm, 5 µm) maintained at 40°C with solvent A (20 mM $(NH_4)_2CO_3$, pH 9.0; Sigma-Aldrich) and solvent B (100% acetonitrile; Sigma-Aldrich) at a flow rate of 250 µL/minute. The gradients used were time (t) = 0 minutes, 90% B; t = 0.5 minutes, 90% B; t = 12 minutes, 40% B; t = 14 minutes, 40% B; t = 15 minutes, 5%, t = 18 minutes, 5% B; t = 19 minutes, 90% B. Analysis was performed on an Agilent Technologies 6520 series quadrupole time of flight (TOF) mass spectrometer The LC flow was directed to an electrospray ionisation (ESI) source where

metabolite ionisation was performed with an N_2 drying gas pressure of 30 lb/in^2 with a gas flow rate of 7 L/minute, 325°C capillary gas temperature, capillary voltage of 3,500 V, and fragmentor skimmer cap voltages of 125 V and 65 V, respectively. Data was collected in centroid mode with a scan range of 50-1,700 *m*/*z* at an acquisition rate of 1.2 spectra/second in negative MS mode.

Prior to analysis, mass calibration was performed for the negative mode to 0.5 ppm accuracy of the *m/z* value. Internal mass calibration was performed using the Agilent ESI-TOF reference mass solution containing purine (*m*/*z*, 119.036320) and hexakis(1H,1H,3H-tetrafluoropropoxy)phosphazene (*m*/*z* 981.99509), which was continuously infused into the ESI source at a flow rate of 200 µL/minute.

2.7.4 Identification of metabolites

For GC/MS, metabolites from *C. burnetii* were identified from chromatograms by using the Agilent MSD Productivity Chemstation for GC and GC/MS. Fragmented ion patterns were used to identify each metabolite using NIST, Fiehn, and Wiley libraries, and retention times were matched to in house libraries to confirm identifications (90). Data matrices were generated using PyMS (144).

For LC/MS, profiles obtained were filtered to remove noise peaks above the specific abundance threshold. Metabolites were then identified using in-house standards from the Metabolomics Australia library by comparing retention times and molecular masses. Metabolites not present in the in-house standards were putatively identified using the

MAVEN database, with molecular masses requiring >70% mass score match to be assigned putative identification.

2.7.5 Statistical analysis and comparison of metabolite profiles

Data matrices generated from the PyMS analyses for profiling studies were missing value imputed, log-transformed, and then median normalised as outlined previously (91, 144). R analysis was used to perform univariate analysis and generate a list of metabolites which were significantly different (P value < 0.05 and Benjamini-Hochberg [BH] adjusted P value < 0.05) between compared conditions and *C. burnetii* strains. Metabolites which were both significantly and non-significantly different between the two conditions were identified as described above.

2.7.6 Mapping identified metabolites onto metabolic pathways

Metabolites identified in these studies were mapped onto predicted metabolic pathways using the *C. burnetii* RSA493 strain from the Kyoto Encyclopedia of Genes and Genomes (KEGG) database as a guide. Metabolic pathways defined on the KEGG database for *C. burnetii* RSA493 are based on genome annotation data. Any enzymes missing from the KEGG database annotations were searched for in *C. burnetii* RSA439 using BLASTp (126), with *L. pneumophila*, *E. coli*, or other bacterial sequences, and human sequences as references.

2.7.7 [$^{13}C_6$]glucose/[$^{13}C_5$]glutamate labelling studies

[$^{13}C_6$]glucose and [$^{13}C_5$]glutamate labelling studies were conducted using detection of incorporated ^{13}C-label into polar metabolites.

To prepare THP-1 cell derived *C. burnetii*, THP-1 cells seeded at 3.5 x 10^5 cells/mL into T175 flasks in 50 mL RPMI + 10% FCS with 10 nM PMA for 3 days. Differentiated THP-1 cells were then infected with *C. burnetii* WT at an MOI of 100 for 24 hours, at which point cells were washed once in PBS and incubated at 37°C, 5% CO_2 in fresh 50 mL RPMI + 10% FCS until 3 and 6 days post-infection.

To prepare bacteria for ^{13}C stable isotope labelling, axenically cultivated (AX) cultures were centrifuged at 3,220 x *g* for 15 minutes at RT to pellet bacteria, while intracellularly cultivated (IC) *C. burnetii* were prepared by scraping infected HeLa or THP-1 cells in warm PBS, then lysing and isolating as described for steady state experiments in section 2.7.1, except samples were kept at RT throughout instead of 0°C. Mock samples using uninfected THP-1 cells were also prepared alongside IC samples to account for contamination by host enzyme activity. THP-1 cells were lysed and cell debris was removed as per IC sample preparation. Supernatants which would normally contain the bacteria were harvested, labelled, quenched and extracted as per AX and IC conditions outlined below.

Isolated AX and IC *C. burnetii* were labelled for 10 minutes at 37°C, 5% CO_2, 2.5% O_2 in either 5 mL fresh ACCM-2 supplemented with 11.11 mM [$^{13}C_6$]glucose or ACCM-D

supplemented with 3 mM [$^{13}C_5$]glutamate. Cultures were quenched, and polar metabolites were extracted and analysed by GC/MS as described for steady state experiments, except 1 nM *scyllo*-inositol (Sigma-Aldrich) was used as the internal standard.

Labelled metabolites were identified as described in section 2.7.4 for steady state experiments. ^{13}C-label incorporation, where a representative unlabelled ion (M0), and mass isotopologues of up to M+1 of the possible number of labelled carbon atoms were integrated using Agilent MassHunter software. Natural background ^{13}C was subtracted from labelled samples as previously described (145). The level of label incorporation for each replicate was normalised against the maximum labelling that occurred for glucose or glutamate for that replicate. Replicates were averaged to obtain labelling percentage values, and any labelling occurring in uninfected THP-1 samples was subtracted for each metabolite in day 3 and day 6 THP-1 harvested IC samples. Label incorporation graphs were generated using Visualization and Analysis of Networks conTaining Experimental Data (VANTED) (146). Unpaired student's *t*-tests were performed using Microsoft Excel.

2.8 Antibiotic sensitivity testing of *C. burnetii*

C. burnetii strains grown for 6 days in ACCM-2 were quantified for GE as defined in section 2.5. Strains were passaged at 10^6 GE/mL and incubated for a further 4 days in 3 mL ACCM-2, at which point cultures were treated with defined concentrations of ampicillin or polymyxin B (Sigma-Aldrich). One hundred µL from each sample was taken and quantified using qPCR or PicoGreen™, as defined in section 2.5, or plated in

serial dilutions on ACCM-2 agar plates. Semi-solid ACCM-2 agar plates were incubated for 12 days at 37°C, 5% CO_2, 2.5% O_2 before viability counts were manually performed. Following addition of antibiotics, cultures were incubated at 37°C, 5% CO_2, 2.5% O_2 for 24 hours, and 100 µL from each condition was taken and analysed as per the previous day. Fold change values for GE and CFU/mL were calculated as 24 hours post-treatment relative to pre-treatment with antibiotics.

2.9 β-lactamase translocation assay

HeLa CCL2 cells were seeded at 5 x 10^3 cells/well in a 96 well flat clear bottom black assay plate (Corning) and incubated at 37°C, 5% CO_2 for 24 hours. Relevant *C. burnetii* strains were quantified using qPCR, as described in section 2.5, and added to cells at indicated MOIs. For co-infection conditions with two different strains, infections were performed with *C. burnetii* WT and *eirA*::Tn at a 1:1 (total MOI 100), 1:3 (total MOI 150) or 1:5 (total MOI 300) ratio. At 46 hours or 70 hours post-infection, CCF2-AM (ThermoFisher Scientific) was added to cells according to manufacturer's protocol. After 2 hours incubation in the dark, fluorescence was measured using a CLARIOStar plate reader (BMG LABTECH). Emissions at 450 nm and 520 nm were read upon excitation at 410 nm. Data was processed using the MARS analysis software (BMG LABTECH) and analysed using Microsoft Excel.

2.10 Protein-based techniques

2.10.1 Sodium dodecyl sulphate-polyacrylamide gel electrophoresis (SDS-PAGE)

Whole cell lysates of *C. burnetii* were centrifuged at 17,000 x *g* for 15 minutes, before pellets were resuspended in 20 µL 2x SDS loading dye (Appendix 1). All protein samples were lysed using 2x SDS loading dye by incubating at 95°C for 10 minutes, unless otherwise stated. Lysed proteins were separated at 165 V for 40 minutes on NuPAGE Bis-Tris gels (Life Technologies) with MES running buffer (Life Technologies). SeeBlue^{TM} Plus2 Pre-stained protein standard (ThermoFisher Scientific) was used as a molecular ladder. When required, protein gels were stained with Coomassie brilliant blue (Appendix 1) for 20 minutes before being destained (Appendix 1).

2.10.2 Protein purification

Ten mL LB broth inoculated with *E. coli* Rosetta II carrying pMAL-c2X:EirA$_{24\text{-}165}$ was incubated overnight at 37°C with agitation at 180 rpm. Two mL of this overnight culture was added to 200 mL LB broth and incubated at 37°C until OD_{600} reached 0.6-0.8. Once the appropriate density had been reached, 0.5 mM isopropyl-β-D-thiogalactoside (IPTG) was added to log phase cultures, and cells were incubated overnight at 18°C with agitation. Cultures were centrifuged at 10,000 x *g* for 15 minutes and the bacterial pellets were resuspended in 25 mL column buffer (Appendix 1). Cells were lysed using the Dounce-homogeniser and EmulsiFlex-C3 high-pressure homogeniser (Avestin) according to manufacturer's protocol. Purification was performed according to manufacturer's protocol (New England Biolabs), except samples were diluted 1:2 in column buffer prior to resin binding. All elutions were pooled for dialysis, and samples

were dialysed within the Cellu·Sep® Regenerated Cellulose Tubular Membrane (Membrane Filtration Products) overnight at 4°C in 2 L Tris-buffered saline (TBS, Appendix 1) with gentle mixing. Protein expression and purification was confirmed using SDS-PAGE as outlined in section 2.10.1. Defined concentrations of bovine serum albumin (BSA; Gibco) were run alongside purified protein samples to estimate protein concentration. Gels were stained with Coomassie brilliant blue and destained as outlined in section 2.10.1. All elutions were then diluted to 2 mg/mL for long-term storage at -80°C. Polyclonal antibodies were raised against MBP-EirA$_{24\text{-}165}$ at the Walter and Eliza Hall Institute (WEHI) Antibody Facility. Briefly, 200 µg of MBP-EirA$_{24\text{-}165}$ was injected into the rabbit on three separate occasions. Serum was collected twice, once after the second immunisation and again after the third immunisation.

All collected serum was preadsorbed against *C. burnetii eirA*::Tn to reduce the amount of antibodies cross-reactive against other, non-EirA *C. burnetii* proteins. Twenty mL 6-7 day post-inoculation cultures of *eirA*::Tn *C. burnetii* were centrifuged at 3,220 x *g* for 15 minutes, before being resuspended in 50 mL of serum. Serum was left to incubate overnight at 4°C on a rotating wheel, before being centrifuged at 3,220 x *g* for 15 minutes at 4°C. Supernatant was filtered through a 0.2 µm filter, before being stored at -80°C in 20 µL aliquots.

2.10.3 Immunoblot analysis

Proteins were separated using SDS-PAGE as outlined in section 2.10.1. Protein gels were transferred to a nitrocellulose membrane using the iBlot2 system (Life Technologies).

Membrane was blocked in either TBS + 0.1% Tween-20 (TBST, Appendix 1) + 5% (w/v) skim milk powder or TBST + 5% (w/v) BSA to match primary antibody solutions, for 1 hour at RT. Relevant primary antibodies (Table 2.4) were added to the membrane and incubated as indicated. Membrane was washed three times at 10 minute intervals in TBST before relevant secondary antibodies (Table 2.4) were added to the membrane for 1 hour at RT. Membrane was washed as before, and developed using Clarity Western ECL Reagents (BioRad) and detected with MF-ChemiBIS, version 3.2 (DNR Bio-Imaging Systems, Ltd.) or Amersham Imager (AI) 600 imager (GE Healthcare). Immunoblots were exposed for 1 minute and assessed with GelCapture, version 7.0.18 software (DNR Bio-Imaging Systems, Ltd.) for the MF-ChemiBIS system to ensure band detection was within the linear range. Immunoblots were exposed on auto settings for the AI600 with subsequent manual adjustment to exposure time as required. Images were processed using Fiji software (147).

Table 2.4. Antibodies used in this study.

Antigen	Manufacturer	Type	Concentration	Host species	Buffer	Incubation condition
Primary antibodies						
BlaM	QED Biosciences	Monoclonal antibody	IB – 1:1500	Mouse	TBST + 5% skim milk	1 hour RT or overnight 4°C
EirA	WEHI Antibody Facility	Polyclonal sera	IB – 1:2000	Rabbit	TBST + 5% skim milk	Overnight 4°C
C. burnetii	Roy Laboratory, Yale University	Polyclonal sera	IF – 1:1000	Rabbit	PBS + 2% BSA + 0.05% saponin	1 hour RT
C. burnetii	WEHI Antibody Facility	Polyclonal sera	IF – 1:1000	Mouse	PBS + 2% BSA + 0.05% saponin	1 hour RT
DotB	Robert A. Heinzen, Edward I. Shaw	Polyclonal sera	IB – 1:2000	Rabbit	TBST + 5% BSA	Overnight 4°C
FLAG	Sigma-Aldrich	Monoclonal antibody	IF – 1:250	Mouse	IF – PBS + 2% BSA + 0.05% saponin	IF – 1 hour RT
			IB – 1:2000		IB – TBST + 5% skim milk	IB – 1 hour RT or overnight 4°C
IcmD	Robert A. Heinzen, Edward I. Shaw	Polyclonal sera	IB – 1:2000	Rabbit	TBST + 5% BSA	Overnight 4°C
IcmK	Robert A. Heinzen, Edward I. Shaw	Polyclonal sera	IB – 1:2000	Rabbit	TBST + 5% BSA	Overnight 4°C
IcmX	Robert A. Heinzen, Edward I. Shaw	Polyclonal sera	IB – 1:2000	Rabbit	TBST + 5% BSA	Overnight 4°C
LAMP-1	Developmental Studies Hybridoma Bank (DSHB)	Monoclonal antibody	IF – 1:500	Mouse	PBS + 2% BSA + 0.05% saponin	1 hour RT
mCherry	Novus Biologicals	Polyclonal antibody	IF – 1:500	Rabbit	PBS + 2% BSA + 0.05% saponin	1 hour RT

RPoA	Biolegend	Monoclonal antibody	IB – 1:5000	Mouse	TBST + 5% BSA	Overnight 4°C
Secondary antibodies						
AlexaFluor-488 mouse	ThermoFisher Scientific	Polyclonal antibody	IF – 1:2000	Goat	PBS + 2% BSA + 0.05% saponin	1 hour RT
AlexaFluor-568 rabbit	ThermoFisher Scientific	Polyclonal antibody	IF – 1:2000	Goat	PBS + 2% BSA + 0.05% saponin	1 hour RT
Mouse-HRP	Perkin Elmer	Polyclonal antibody	IB – 1:3000	Goat	TBST + 5% skim milk	1 hour RT
Rabbit-HRP	Perkin Elmer	Polyclonal antibody	IB – 1:3000	Goat	TBST + 5% skim milk	1 hour RT

IB – Immunoblot

2.10.4 Analysis of EirA present in axenic culture media

One hundred mL day 6 *C. burnetii* ACCM-2 cultures were centrifuged at 3,220 x *g* for 15 minutes at 4°C. Supernatants were passed through a 0.2 µm filter to remove any bacterial cells, before being precipitated in 20% trichloroacetic acid (Sigma-Aldrich) overnight at 4°C on ice. Samples were centrifuged at 20,000 x *g* for 20 minutes at 4°C, before resulting protein pellets were washed once in 80% ice-cold acetone (Chem Supply) and centrifuged at 17,000 x *g* for 20 minutes at 4°C. Protein pellets were dried at 60°C until all residual acetone was removed, before being resuspended in 50 µL 2x SDS loading dye. *C. burnetii* harvested from the initial centrifugation step to separate the ACCM-2 supernatant were washed once in ice-cold PBS, then resuspended in 1 mL ice-cold PBS. This resuspension was diluted 1:10 to a total volume of 50 µL in 2x SDS loading dye. All samples were processed for immunoblot analysis as outlined in section 2.10.1 and 2.10.3.

2.10.5 Fractionation of *C. burnetii*

One hundred mL day 6 *C. burnetii* ACCM-2 cultures were centrifuged at 3,220 x *g* for 15 minutes at 4°C, washed once in ice-cold PBS, and then resuspended in 3 mL ice-cold lysis buffer (Appendix 1). Samples were sonicated on ice using a 600 W S-4000 sonicator (Misonix) at 50 W for 10 seconds, followed by 20 seconds of rest, until total sonication time reached 3 minutes. Samples were then centrifuged at 3,220 x *g* for 15 minutes at 4°C to remove intact bacterial cells. Fifty µL of the supernatant was reserved as the whole cell lysate sample. Supernatants containing lysed bacteria were centrifuged at 100,000 x *g* for 1 hour at 4°C to separate the membranes from the cytoplasmic fraction. Fifty µL of the resulting supernatant was collected as a portion of the cytoplasmic fraction. The pellet

was resuspended in lysis buffer using a 26 G needle (Terumo) and centrifuged as before to remove residual cytoplasmic proteins. Pelleted proteins containing the membrane fractions were resuspended in 500 µL ice-cold membrane solubilisation buffer (Appendix 1) using a 26 G needle, then left to incubate for 2 hours on a rotating wheel at 4°C. Samples were made up to equivalent total volume as the supernatant, representing the cytoplasmic fraction, using solubilisation buffer, before being centrifuged as above to separate the outer and inner membranes. The TX-100 soluble fraction was considered to contain inner membrane contents and the TX-100 insoluble fraction was considered to represent the outer membrane. Fifty µL of the TX-100 soluble fraction was reserved for further analysis. The TX-100 insoluble pellets were resuspended in 2x SDS loading dye in equivalent volumes to other fractions, and 50 µL was reserved for further analysis. All reserved samples were diluted 1:1 in 2x SDS loading dye and incubated at 60°C for 30 minutes before immunoblot analysis as outlined in section 2.10.1 and 2.10.3.

2.10.6 Immunofluorescence microscopy

All antibodies and concentrations used are listed in Table 2.4. For intracellular replication assays, infected HeLa CCL2 and THP-1 cells were fixed for 20 minutes at RT with 4% paraformaldehyde (in PBS, w/v) at 3 days post-infection. Cells were then blocked and permeabilised using PBS + 2% BSA + 0.05% saponin (Sigma-Aldrich), before being incubated with relevant primary antibodies (Table 2.4). After three 5 minute washes in PBS, cells were incubated in the dark with relevant secondary antibodies (Table 2.4). PBS containing 4′,6-diamidino-2-phenylindole (DAPI, Life Technologies) at 1:10,000 was added to cells for 5 minutes, before two 5 minute washes in PBS.

For 7 day coinfections and phenotype rescue experiments, cells were fixed and stained at given time points using relevant antibodies (Table 2.4). Anti-mCherry primary antibody was used to stain *eirA*::Tn, as mCherry fluorescence from the transposon was too low for imaging. For 3xFLAG-MceA staining, cells were fixed and stained at given time points as above, except MitoTracker^{TM} Red CMXRos (ThermoFisher Scientific) staining was performed prior to fixing, according to manufacturer's protocol.

Coverslips were mounted onto glass slides with ProLong Gold reagent (Life Technologies). All samples were imaged using a Zeiss LSM700 instrument with Zen software. All images were analysed using Fiji (147).

For phenotype rescue experiments, the total 568 nm fluorescence from a x20 objective image was quantified using Fiji (147). This numerical value was then made relative to the total number of host cell nuclei in the image.

2.11 Transmission electron microscopy of *C. burnetii*

One hundred mL day 6 ACCM-2 cultures of *C. burnetii* were centrifuged for 15 minutes at 3,220 x *g* at RT, before being washed once in PBS before centrifuging as before. Pellets were resuspended in 2.5% glutaraldehyde (ProSciTech) and fixed for 2 hours at RT. Bacteria were then rinsed twice in PBS without resuspension to remove any residual fixative. Samples were post-fixed in 1% osmium tetroxide (Electron Microscopy

Sciences) before dehydrating in a graded series of acetone (Merck), infiltrated and embedded with EPON™ resin (ProSciTech). Ninety nm thick sections were cut and stained with uranyl acetate (BDH) and lead citrate (BDH) before imaging on a CM120 transmission electron microscope (Phillips) at 120 kV.

2.12 *Galleria mellonella* infection model

G. mellonella larvae were cultured in-house and kept at 30°C in the dark until use. The food mixture used to cultivate *G. mellonella* larvae are listed in Appendix 1. Larvae were maintained in autoclave safe glass jam jars filled with food mixture. Four to six larvae were placed in each jar and left to grow into adult *G. mellonella* to breed. To prepare for infections, larvae were harvested from these propagation jars.

Infections were conducted as described previously (54). Briefly, 10^6 GE of relevant *C. burnetii* strains were injected in the right proleg of *G. mellonella* larvae. Larvae were incubated at 37°C, and survival was monitored every 24 hours across 11 days. PBS controls were included with each experiment. Each condition consisted of 12 larvae.

To harvest haemocytes for IF, three larvae per condition were anaesthetised on ice for 15 minutes, before a small incision was made near the tail end of the larvae with a scalpel. Haemolymph from three larvae were pooled and immediately resuspended in 500 µL PBS. These resuspended cells were seeded onto 12 mm coverslips in a 24 well flat bottom plate, which was centrifuged for 10 minutes at 500 x *g* to allow cell adherence. Cells were then fixed and stained as outlined in section 2.10.6.

Chapter 3

Metabolic pathway analysis of *C. burnetii*

3.1 Introduction

In order to survive and cause disease, intracellular pathogens must generate or obtain essential nutrients for replication. Many of these pathogens have developed mechanisms to scavenge nutrients from the host cell during infection, and may therefore become dependent on the host to provide essential nutrients. For instance, the human bacterial pathogen *Salmonella enterica* serovar Typhimurium (*S.* Typhimurium) was found to be highly dependent on host glucose and glucose phosphate during intracellular infection in mice (148). Deleting enzymes involved in glucose uptake, or in the catabolism of glucose via glycolysis, led to severe attenuations in intracellular replication and virulence of *S.* Typhimurium (148). With host nutrient sources shaping bacterial metabolism and replication to such an extent, identifying the metabolic pathways utilised by these pathogens inside cells is key to understanding their pathogenesis (90, 98). In addition, identifying these potentially unique and essential metabolic pathways may lead to the discovery of novel therapeutic targets.

The intracellular bacterium *C. burnetii* is the causative agent of Q fever, which in humans causes a number of symptoms ranging from acute life-threatening infection to debilitating chronic disease (24). Upon inhalation of contaminated aerosols, *C. burnetii* are typically phagocytosed by alveolar macrophages (66). The *C. burnetii* containing phagosome passively undergoes endocytic maturation, eventually fusing with the host lysosomal compartment. Acidification of this phagosome leads to metabolic activation and initiation of bacterial replication.

Amino acids present within the host lysosome also trigger the activation of the *C. burnetii* Dot/Icm type 4 secretion system, which translocates approximately 130 effector proteins into the host cell (71, 109, 114). These effector proteins allow the establishment of the specialised vacuolar compartment, termed the *Coxiella*-containing vacuole (CCV), which allow the bacteria to replicate to large numbers (57, 107, 108). The highly fusogenic nature of this unique replicative niche leads to the mature CCV resembling an autolysosome (76, 77). Unlike most intracellular pathogens, *C. burnetii* are not destroyed within this hostile niche, but require the acidified environment to replicate.

Axenic cultivation conditions for *C. burnetii* have recently been established (94, 108). Acidified citrate cysteine medium (ACCM) supports axenic replication of *C. burnetii* in low oxygen conditions (94, 108). The constituents of this media were established by studying the metabolic requirements of *C. burnetii* (94, 108). ACCM, and its derivatives, contain an abundance of amino acids, which are required to satisfy the auxotrophic requirements of *C. burnetii*. The large number of amino acid auxotrophies in *C. burnetii* suggests that this pathogen may scavenge these nutrients from the host cell during infection. In support of this, recent metabolomic analysis of the lysosomal compartment of mammalian cells indicates that this organelle contains amino acids at levels which are equivalent to or higher than in the cytoplasm (97). Use of amino acids as a carbon source during *C. burnetii* replication is also supported by the ability of axenic bacteria to proliferate in defined ACCM (ACCM-D) lacking glucose (95). However, genetic disruption of the gene encoding the gluconeogenic enzyme phosphoenolpyruvate carboxykinase (PEPCK) causes partial attenuations in *C. burnetii* virulence in mammalian cells (86). This study showed that intracellular bacterial replication had

significantly decreased in this mutant strain compared to WT when incubated at a lower, 5 mM glucose concentration, as opposed to the standard 11 mM glucose concentration. This suggests that in low glucose environments, gluconeogenesis via catabolism of other carbon sources, such as amino acids, is required for intracellular replication of *C. burnetii*. Transcripts for glycolytic and gluconeogenic enzymes are both up-regulated during intracellular replication (96). Thus, it remains unclear whether intracellular *C. burnetii* also utilise or co-utilise sugars scavenged from the phagolysosomal compartment.

During the course of this Ph. D, a study examined the use of a number of carbon sources, including [^{13}C]glucose, [^{13}C]serine, and [^{13}C]glycerol, in axenically grown (AX) *C. burnetii* (98). This study confirmed that *C. burnetii* generate ATP and anabolic precursors via glycolysis. In addition, this study demonstrated that *C. burnetii* is auxotrophic for histidine, isoleucine, leucine, lysine, phenylalanine, proline and valine, confirming that these amino acids are scavenged from the environment (98). However, it remains unclear how and to what extent these bacteria catabolise non-essential amino acids.

This chapter used metabolomic analyses to define the metabolic pathways of AX and intracellularly cultivated (IC) *C. burnetii*, both through the use of steady state metabolite profiling, as well as [^{13}C]glutamate and [^{13}C]glucose labelling approaches. The results demonstrated that both populations of *C. burnetii* are able to utilise glutamate and glucose, which are primarily catabolised by the TCA cycle and via glycolysis, respectively. Strikingly, the results also indicated that the TCA cycle operates differently between these

two populations, with the use of a continuous, oxidative cycle in AX and discontinuous, partial TCA cycle and increased gluconeogenesis in IC *C. burnetii*. These findings demonstrate that intracellular *C. burnetii* has the capacity to switch between different hexose and non-essential amino acid carbon sources *in vitro* and *in vivo* and exhibits surprising flexibility in its central carbon metabolism.

3.2 Results

3.2.1 Metabolite profiling of axenic and intracellular *C. burnetii*

C. burnetii WT were cultured either axenically for 6 days in ACCM-2 media (AX) or intracellularly (IC) for 2 days in HeLa cells. At the respective time points, *C. burnetii* were rapidly quenched to halt metabolism and harvested as described in section 2.7.1. Polar metabolites were then extracted and analysed using GC/MS (Figure 3.1). Two independent experiments were performed and analysed, each with 6 technical replicates. A total of 58 metabolites were identified across the two independent experiments, covering a range of pathways within central carbon metabolism (Figure 3.2, Table 3.1 and Appendix 2 and 3). Eleven of the identified metabolites were not predicted from existing metabolic pathway maps in the KEGG database and may either be salvaged from the medium or reflect the presence of non-annotated enzyme/pathway activities (Figure 3.2 and Appendix 3). Seven of these unmapped metabolites were not detected in the GC/MS metabolite profile of the ACCM-2 medium (Table 3.2), indicating that they may be synthesized *de novo* by as yet unannotated enzymes or pathways. Bioinformatic analysis using BLASTp similarity searching was unable to identify putative enzymes to link these metabolites to existing annotated *C. burnetii* pathways.

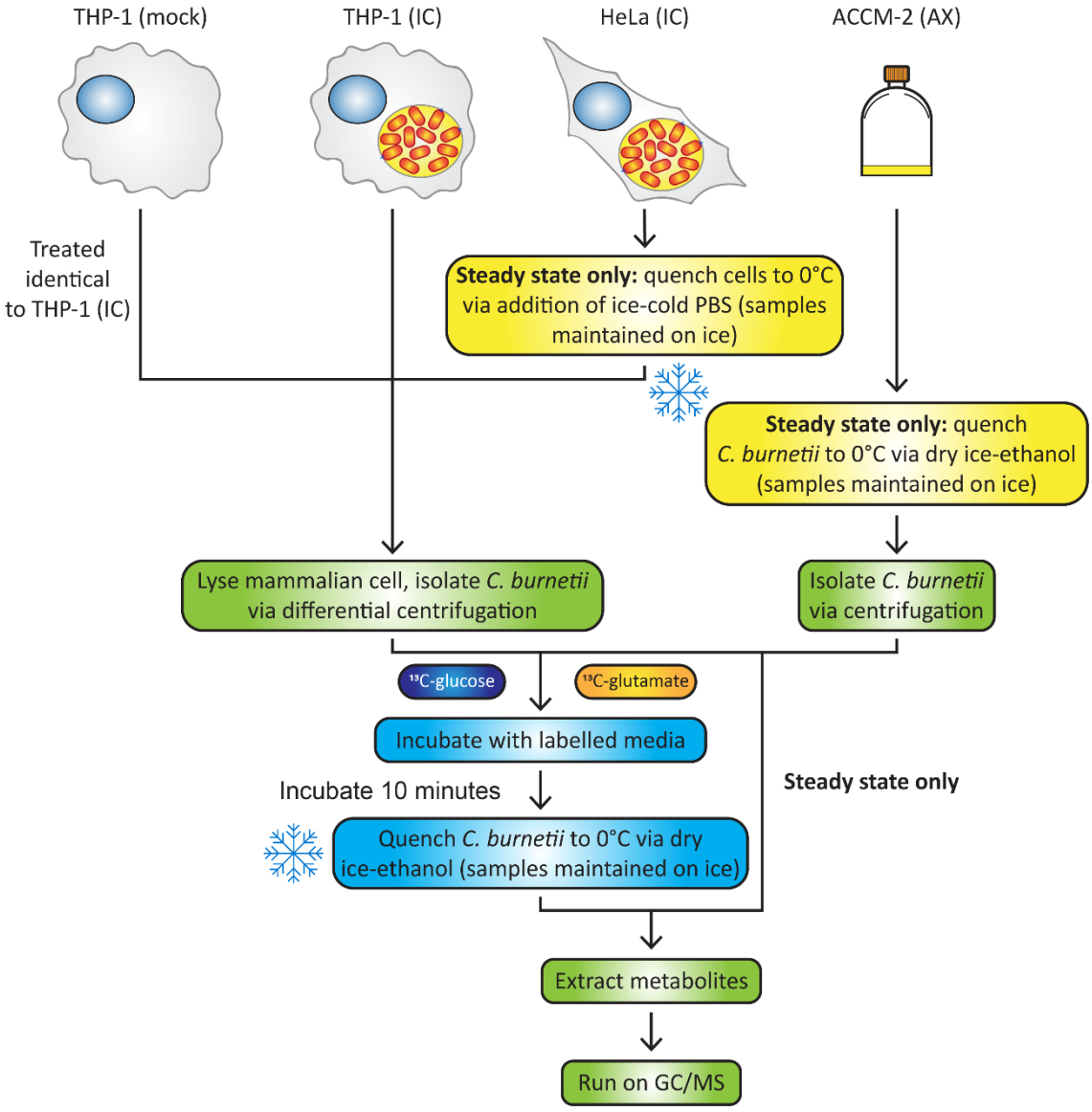

Figure 3.1. Schematic of overall workflow for various metabolomic analyses. Yellow indicates steps which were only used for steady state profiling analysis. Light blue indicates steps which were only used for ^{13}C-labelling experiments. Green indicates steps which were common across both experimental procedures.

Table 3.1. Identified metabolites from steady state data across the two conditions.

Metabolite	Compound ID (KEGG)	Retention time (minutes)		Fragmented ion		[A]Level of ID
		Experiment 1	Experiment 2	Experiment 1	Experiment 2	
G6P	C00668	12.246		387		1
F6P	C05345		12.358	315		1
3P-D-glycerate	C00197	10.304	10.462	357	357	1
2P-D-glycerate	C00631	10.181		211, 299, 315, 369, 459		2
Pyruvate	C00022	6.551		59, 174		2
Malate	C00149		8.980		233	1
Fumarate	C00122	8.127	8.295	245	245	1
Succinate	C00042	7.950		247		1
Citrate	C00158		10.520		273	1
Isocitrate	C00311	10.358		245, 273		1
D-Gluconic acid	C00257	11.111	11.264	333	205, 217, 292, 319, 333	1
D-Glycerate	C00258		8.157		189	1
R5P	C00117		11.648		315	1
D-Ribose	C00121	9.697		307		1
Guanosine	C00387		13.862		230, 245, 280, 296, 324, 368	2
Xanthine	C00385	11.243	11.404	279, 294, 353, 368	158, 265, 279, 294, 353, 368	2
Hypoxanthine	C00262	10.429		265		1
Inosine	C00294	13.142	13.295	103, 193, 217, 230, 245, 281	103, 217, 230, 245, 259, 281	2

Urea	C00086	7.656		189		1
Adenine	C00147	10.705		264		1
AMP	C00020		14.895		169	1
Adenosine	C00212	13.350	13.498	192, 217, 230, 236, 259, 280	192, 217, 230, 236, 259, 280	2
Uridine	C00299	12.824	12.902	103, 169, 217	169	1
UMP	C00105	13.974		169, 211, 230, 243, 299, 315		2
Uracil	C00106		8.262		241, 256	2
CMP	C00055	11.206	11.362	169, 211, 243, 258, 299, 315	169, 227, 243, 258, 299, 315	2
L-Ala	C00041	6.669	6.963	116	116	1
L-Asp	C00049	8.994		232		1
L-Asn	C00152	9.737	9.897	231	100, 132, 188, 218, 202, 231	1
L-Glutamate	C00025		9.640		246, 128, 100, 218, 230, 348	1
L-Thr	C00188	8.294	8.455	218	218	1
L-Ser	C00065	8.319	8.158	204	204	1
L-Cys	C00097		9.358		100, 132, 204, 218, 220, 294	2
Glycine	C00037	7.926	8.088	86, 174, 248, 370	248	1
Cys-Gly	C01419	11.368		100, 220, 275		2
L-Met	C00073	9.040		176		1
L-Val	C00183	7.410	7.573	144	144	1
L-Ile	C00407	7.837	7.995	158	158	1
L-Lys	C00047	10.579	10.744	174	174	1
L-Pro	C00148	7.900	8.061	142	142	1
L-Ornithine	C00077	10.378	10.541	142	142	1

L-Phe	C00079		9.591		192	1
L-Tyr	C00082	10.911	11.074	218, 280	280	1
L-Trp	C00078		12.174		202, 218	1
Hydroxyproline	C01157	9.030		230		1
5'-Methylthioadenosine	C00170		14.040		236, 188, 175, 129, 165	2
LL-2,6-Diaminopimelate	C00666	11.048	11.207	100, 128, 181, 200, 272	128, 200, 272	2
D-Fructose	C00095		10.551		307	1
Myo-inositol	C00137	11.475	11.638	305	305	1
Inositol-1P	C01177	12.661	12.765	318	318	1
Glycerol	C00166	7.679	7.835	103, 117, 175, 191, 205, 218	205, 218, 293	2
Galactose-6P	C01113		12.332		387	1
GlcNAc	C00140	11.428	11.585	100, 205, 202, 319	100, 205, 202, 319	2
Taurine	C00245	9.789		326		1
Pidolic acid	C01879	9.084	9.249	156, 230, 258	156	1

[A]Level of identification (ID) according to standards proposed by (149), where 1 denotes absolute identification and 2 denotes putative identification.

Table 3.2. Metabolites detected in ACCM-2 on the GC/MS.

Metabolite	Compound ID (KEGG)	Retention time (minutes)	Fragmented ion	[A]Level of ID
Glucose	C00031	10.885	205	1
Citrate	C00158	10.554	183	1
Glycine	C00037	8.134	174	1
L-Ala	C00041	7.018	116	1
L-Asp	C00049	9.203	232	1
L-Asn	C00152	9.939	116	1
L-Glutamate	C00025	9.689	246	2
L-Thr	C00188	8.500	218	1
L-Ser	C00065	8.363	204	1
L-Cys	C00097	9.404	220	2
L-Cystine	C00491	12.429	411	1
L-Met	C00073	9.248	176	1
L-Val	C00183	7.617	144	1
L-Ile	C00407	8.040	158	1
L-Leu	C00123	7.904	158	1
L-Lys	C00047	11.034	174	1
L-Pro	C00148	8.112	142	1
L-Phe	C00079	9.796	192, 218	1
L-Tyr	C00082	11.128	218	1
L-Trp	C00078	12.174	202, 218	1
L-Ornithine	C00077	9.664	142	1
L-His	C00135	11.075	154	1
L-Citrulline	C00327	10.662	142, 157, 256	2
Myo-inositol	C00137	11.674	305	1
Pidolic acid	C01879	9.299	156	1

[A]Level of identification (ID) according to standards proposed by (149), where 1 denotes absolute identification and 2 denotes putative identification.

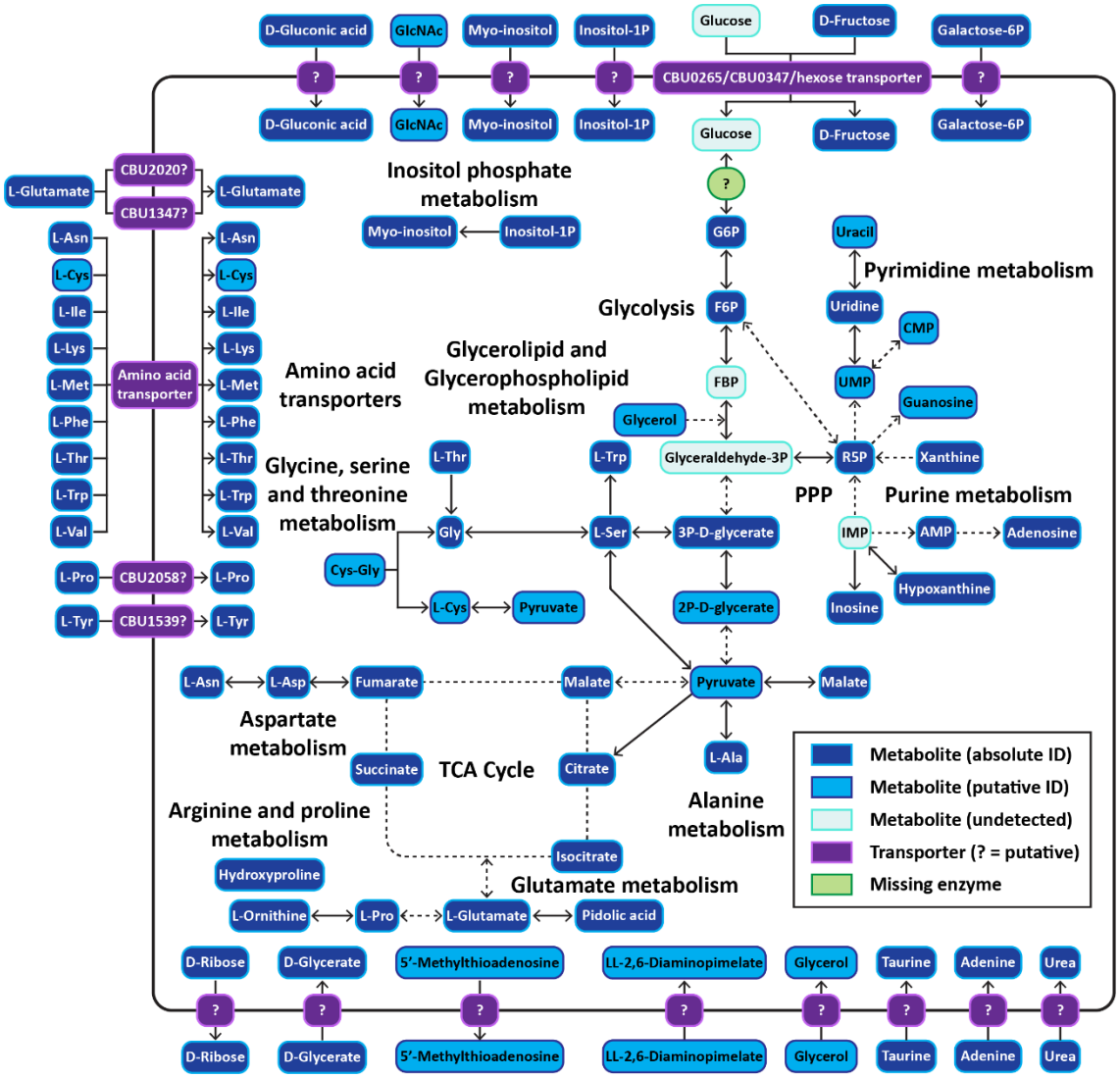

Figure 3.2. Metabolic pathway map of *C. burnetii* constructed from steady state GC/MS data. Dark blue boxes indicate metabolites detected using GC/MS with absolute identifications. Azure boxes indicate putatively identified metabolites and pale blue boxes indicate metabolites not detected on the GC/MS. Purple denotes transporters, where '?' indicates putative transporters. Pale green circle indicates missing enzyme based on genome annotation data in KEGG. Unlinked metabolites do not have annotated enzymes involved in their conversions based on KEGG. Dotted arrows indicate pathways which have been abbreviated. Metabolite abbreviations are listed in Appendix 2.

3.2.2 *C. burnetii* can utilise both [^{13}C]glutamate and [^{13}C]glucose during intracellular replication

To analyse metabolic substrate utilisation and metabolic flux during *C. burnetii* replication, *C. burnetii* WT were isolated at 2 days post-infection of HeLa cells and labelled with either ACCM-D containing 3 mM [^{13}C]glutamate or ACCM-2 containing 11.11 mM [^{13}C]glucose for 10 minutes. Bacteria were rapidly chilled to quench metabolism, then polar metabolites were extracted and analysed using GC/MS (Figure 3.1). Levels of ^{13}C-label incorporation into various downstream metabolites are shown, using the existing pathway maps derived from the KEGG database (Figure 3.3).

Detected labelling for each metabolite was normalised against the maximum labelling that occurred for glutamate within each replicate, as described in section 2.7.7. As glutamate was provided only as [^{13}C]glutamate in the media, detection of only [^{13}C]glutamate in extracted metabolites from bacterial cells, prior to normalisation (raw percentage labelling), indicates that the exogenous [^{13}C]glutamate equilibrated fully with intracellular pools within 10 minutes of labelling. No ^{12}C forms of glutamate was detected in bacterial cells. Internalised [^{13}C]glutamate incorporated into the TCA cycle, via succinate, fumarate and malate, which demonstrates that *C. burnetii* uses the oxidative cycle (Figure 3.3). Interestingly this population of *C. burnetii* appears to undergo a cataplerotic TCA cycle rather than further rounds of oxidation, with ^{13}C-label being shunted away from citrate/isocitrate into gluconeogenesis via the C4 dicarboxylic acids (Figure 3). *C. burnetii* was also able to utilise the carbon backbones derived from glutamate to synthesise L-alanine, L-aspartate and glycine (Figure 3.3).

Unexpectedly, following [^{13}C]glutamate labelling, there was detection of almost 20% ^{13}C-label incorporation into lactate (Figure 3.3). The *C. burnetii* genome lacks an annotated L/D-lactate dehydrogenase, which suggests the presence of an alternative mechanism for synthesising lactate that does not involve direct conversion from pyruvate. Lactic acid bacteria such as *Oenococcus oeni* express alternative malolactic enzymes which convert malate into lactate (150). BLASTp analysis revealed the presence of a putative malolactic enzyme in *C. burnetii*, CBU0823. This protein, which is currently annotated as an NAD-dependent malic enzyme, possesses 43% identity with the *O. oeni* malolactic enzyme across 63% of the predicted amino acid sequence. This raises the possibility that CBU0823, much like the *O. oeni* enzyme, may function to convert malate to both pyruvate and lactate (Figure 3.3).

Labelling IC *C. burnetii* with [^{13}C]glucose demonstrated utilisation of this sugar substrate (Figure 3.3). Raw percentage labelling data showed intracellular pools of glucose had equilibrated with exogenous [^{13}C]glucose, also within 10 minutes of labelling, which indicates rapid intake of substrate. Catabolism of [^{13}C]glucose has previously been reported in AX *C. burnetii*, but not in IC *C. burnetii* (98). The exact mechanism used by *C. burnetii* to phosphorylate glucose to form glucose 6-phosphate is currently unknown. Given *C. burnetii* appears to lack an annotated hexokinase or phosphotransferase system (PTS), it is likely that *C. burnetii* possesses an alternative mechanism to phosphorylate sugars. Levels of ^{13}C within TCA cycle substrates were generally much lower in [^{13}C]glucose-fed *C. burnetii* compared to [^{13}C]glutamate-fed bacteria, which indicates efficient compartmentalisation of these two carbon sources (Figure 3.3). Following

glucose labelling, ^{13}C-enrichment also occurred in some amino acids, such as L-aspartate, L-glutamate, and L-serine, in addition to lactate (Figure 3.3).

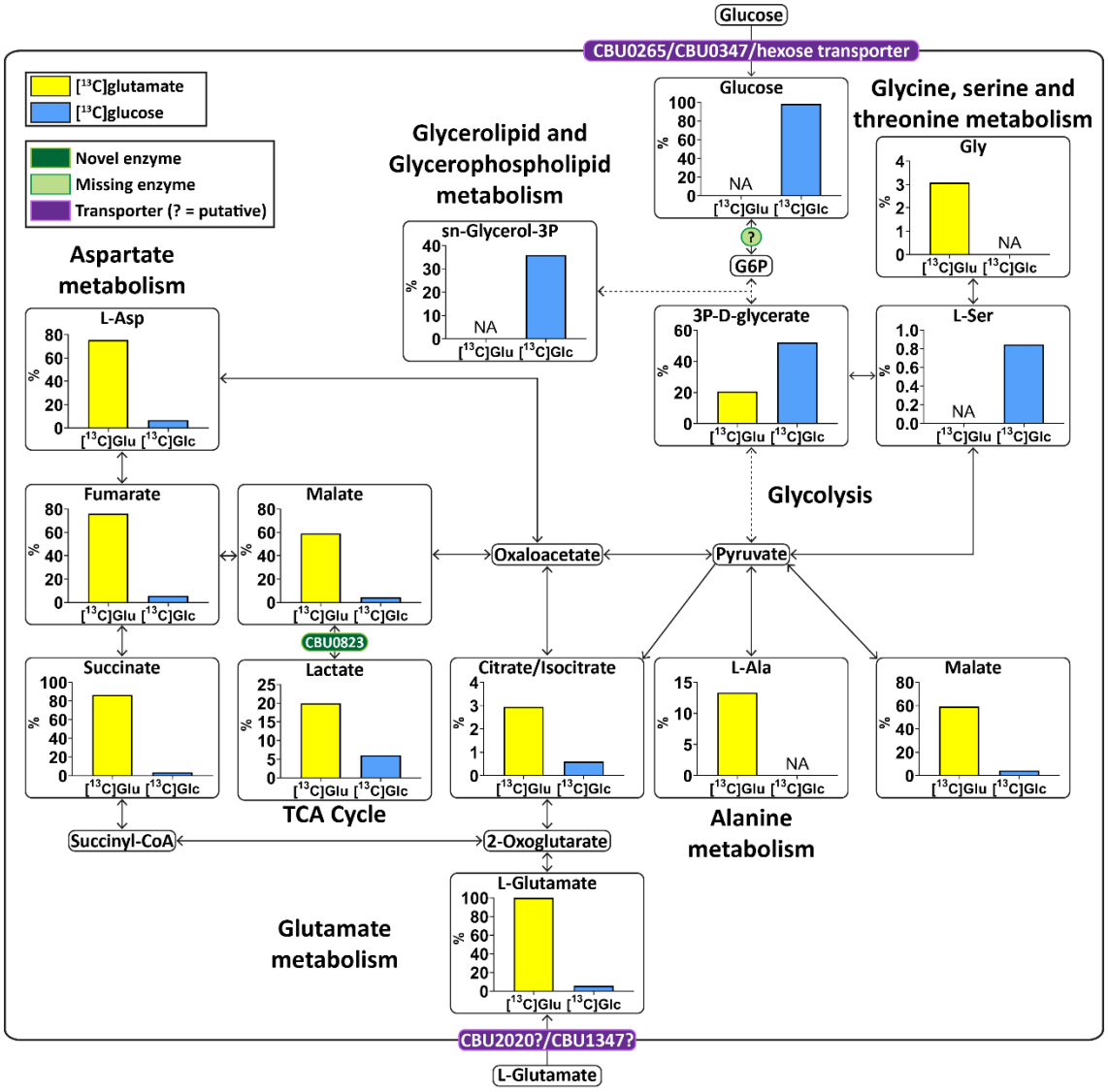

Figure 3.3. HeLa cell-derived IC *C. burnetii* utilise both glutamate and glucose. Metabolic pathway map of HeLa cell-derived IC *C. burnetii* labelled with either [^{13}C]glutamate or [^{13}C]glucose. Metabolites detected on the GC/MS as having incorporated ^{13}C-label are shown in larger boxes, with percentage labelling in bar graphs. Yellow bars indicate samples labelled with [^{13}C]glutamate. Light blue bars indicate samples labelled with [^{13}C]glucose. Pale green circles indicate missing enzymes based on genome annotation data in KEGG. Dark green circles indicate putative enzymes with novel functions. Purple denotes metabolite transporters, where '?' indicates those with putative functions. Dotted arrows indicate pathways which have been abbreviated. NA indicates metabolites which were unable to be detected in a given condition. Metabolite abbreviations are listed in Appendix 2.

3.2.3 Comparison of ^{13}C-substrate usage between axenically and intracellularly cultivated *C. burnetii*

IC samples derived from HeLa cells could only be harvested at 2 days post-infection. This was due to the technical constraints of maintaining a high bacterial load for detection of *C. burnetii* metabolites, while balancing normal host cell division. The discrepancy in replication stage between AX (harvested at day 6 post-inoculation) and IC *C. burnetii* limited any direct comparison between the metabolism of these two distinct environments. In addition, these initial experiments did not account for host metabolic enzymes, which may be carried across during isolation of IC *C. burnetii*, resulting in false labelling of metabolites not produced by bacterial enzymes.

To address these limitations, *C. burnetii* WT were cultivated in non-replicating, differentiated macrophage-like THP-1 cells. Given the tropism of *C. burnetii* toward infections within alveolar macrophages, this cell type was more biologically relevant to natural infection. In order to measure host cell contamination, mock infected THP-1 cells were also prepared alongside the IC *C. burnetii*, and any ^{13}C-label incorporation occurring in these mock samples was subtracted from the bacterial samples (Figure 3.1, Table 3.3). THP-1-derived IC *C. burnetii* were harvested at both 3 and 6 days post-infection to represent late logarithmic and stationary phase *C. burnetii*, respectively. AX *C. burnetii* were also grown to 3 and 6 days post-inoculation before being harvested. Both AX and IC *C. burnetii* were then labelled with either [^{13}C]glutamate and [^{13}C]glucose as before, and polar metabolites were extracted and analysed on the GC/MS (Figure 3.1).

Table 3.3. Metabolites with detectable ^{13}C-label incorporation values in mock THP-1 cell samples.

Metabolite	Percentage ^{13}C-label incorporation
[^{13}C]glutamate	
Succinate	18.53%
Lactate	0.92%
[^{13}C]glucose	
Succinate	12.43%
Lactate	0.53%

Much like with the previous HeLa-derived IC *C. burnetii*, both AX and THP-1-derived IC *C. burnetii* were able to utilise [^{13}C]glutamate (Figure 3.4). Interestingly, while IC *C. burnetii* demonstrated the use of a discontinuous TCA cycle (with ^{13}C being converted into gluconeogenic intermediates), AX *C. burnetii* underwent further rounds of the TCA cycle via citrate/isocitrate (Figure 3.4). Stationary phase AX *C. burnetii*, 6 days post-inoculation, also showed significantly lower incorporation of ^{13}C-label into gluconeogenic intermediates compared to 3 days post-inoculation, which is consistent with this population requiring less nucleotide precursors (Figure 3.5 and Table 3.4). IC *C. burnetii* on the other hand maintained high levels of ^{13}C-label incorporation at both time points, suggesting these bacteria require ongoing production of nucleotide precursors within the vacuolar compartment. Overall these data suggest that while both AX and IC *C. burnetii* are able to utilise [^{13}C]glutamate, IC *C. burnetii* use this substrate primarily to synthesise anabolic precursors, and AX *C. burnetii* undergo a cyclic TCA cycle.

^{13}C-label incorporation into lactate was detected at much lower levels when host cell contamination was accounted for, with percentage labelling of approximately 6% for AX *C. burnetii* and below 3% in IC *C. burnetii* (Figure 3.4).

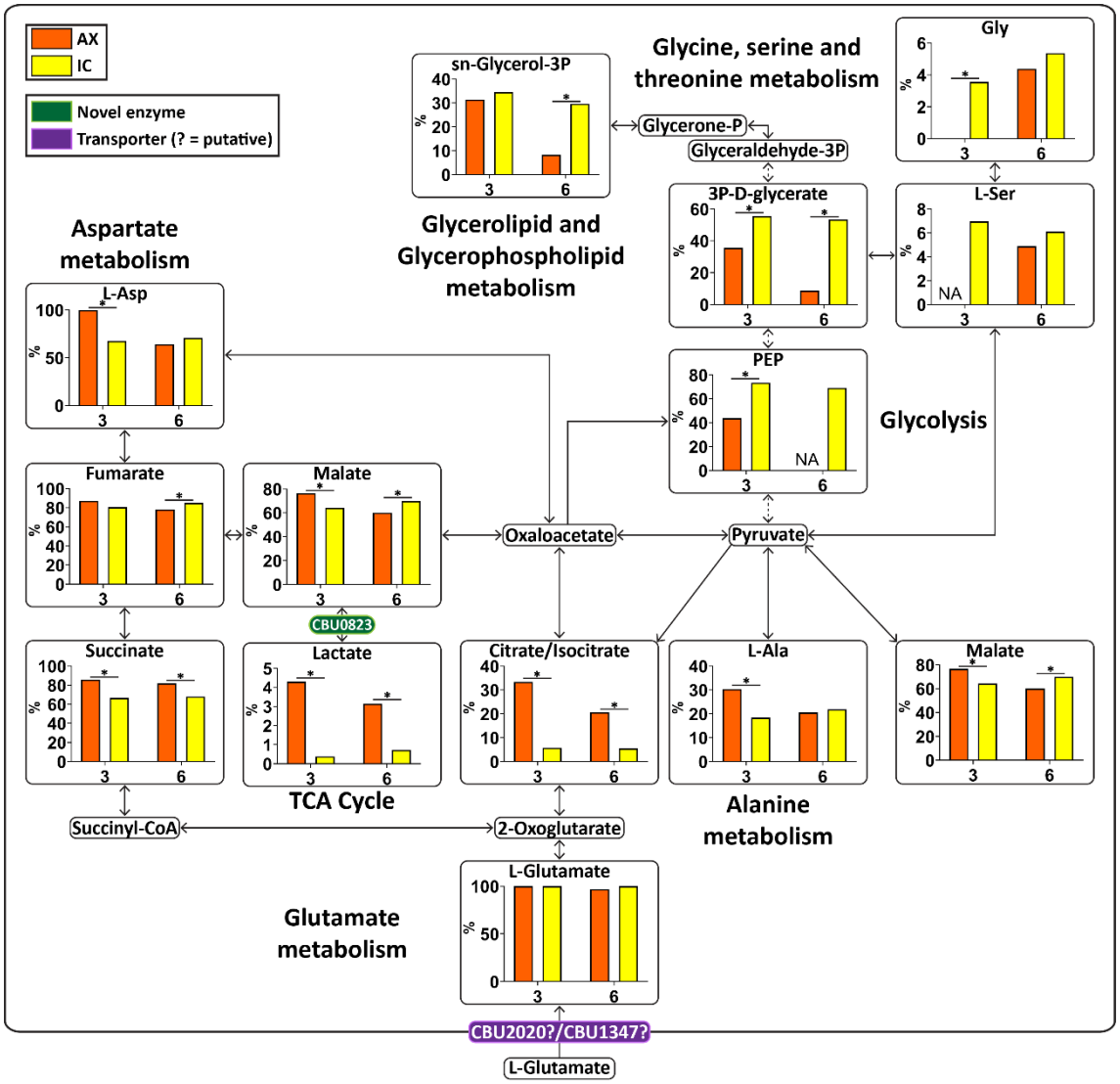

Figure 3.4. Both AX and IC *C. burnetii* are able to catabolise [^{13}C]glutamate. Metabolic pathway map of *C. burnetii* comparing ^{13}C-label incorporation between AX and IC *C. burnetii* after 10 minute incubation with [^{13}C]glutamate. Metabolites detected on the GC/MS as having incorporated ^{13}C-label are shown in larger boxes, with percentage labelling in bar graphs. Orange bars indicate AX samples and yellow bars indicate IC samples. Dark green circles indicate putative enzymes with novel functions. Purple denotes metabolite transporters, where '?' indicates those with putative functions. Dotted arrows indicate pathways which have been abbreviated. * = p<0.05 using unpaired student's t-test. NA indicates metabolites which were unable to be detected in a given condition. Metabolite abbreviations are listed in Appendix 2.

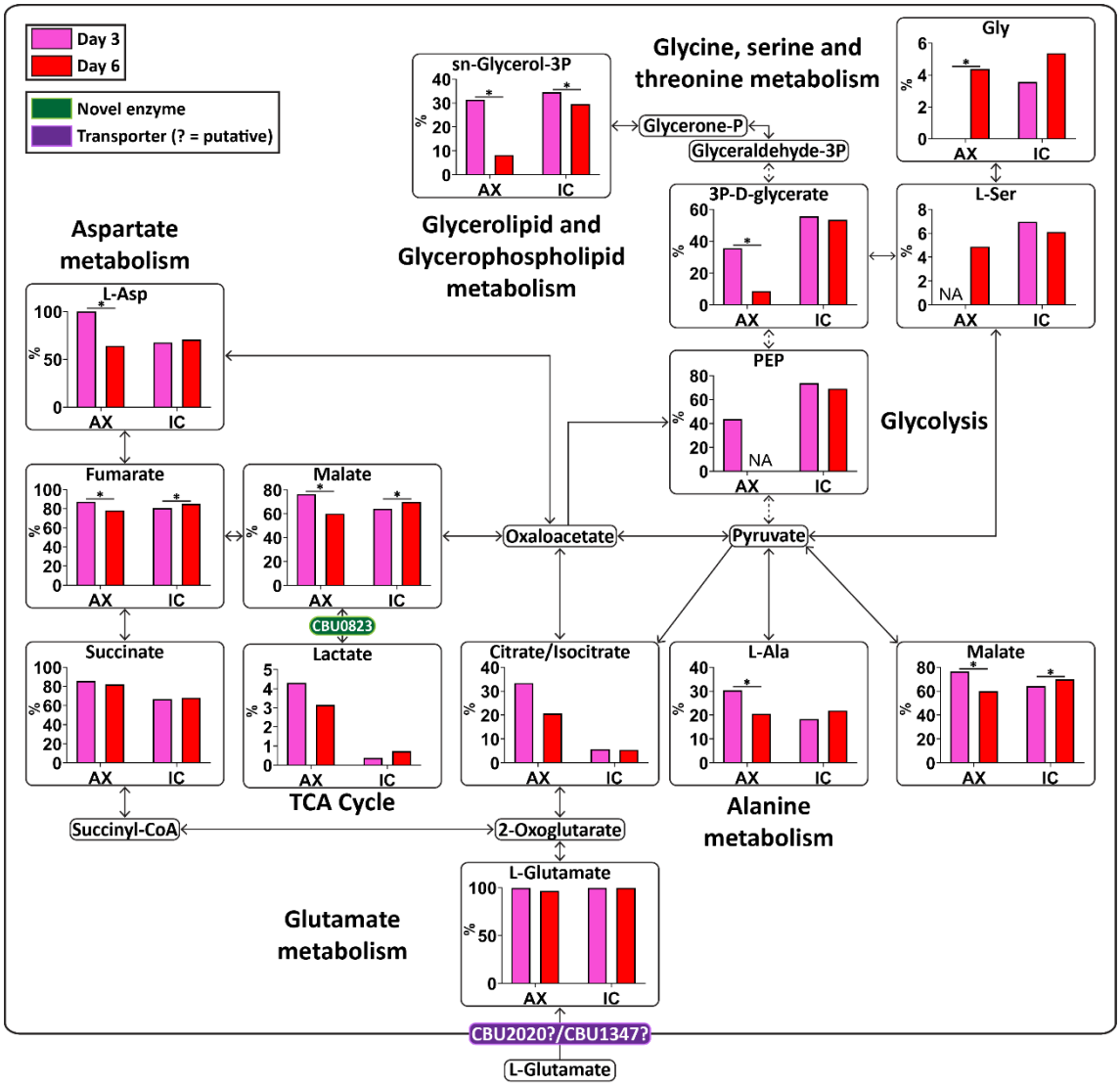

Figure 3.5. Day 3 vs day 6 comparisons of [^{13}C]glutamate labelled *C. burnetii*. Metabolic pathway map of *C. burnetii* comparing ^{13}C-label incorporation at day 3 and day 6 within the same culture condition after 10 minute incubation with [^{13}C]glutamate. Metabolites detected on the GC/MS as having incorporated ^{13}C-label are shown in larger boxes, with percentage labelling in bar graphs. Pink bars indicate day 3 samples and red bars indicate day 6 samples. Dark green circles indicate putative enzymes with novel functions. Purple denotes metabolite transporters, where '?' indicates those with putative functions. Dotted arrows indicate pathways which have been abbreviated. * = p<0.05 using unpaired student's *t*-test. NA indicates metabolites which were unable to be detected in a given condition. Metabolite abbreviations are listed in Appendix 2.

Table 3.4. Metabolites with significant day 3 vs day 6 differences within AX and IC conditions during [^{13}C]glutamate labelling using an unpaired student's *t*-test.

Elevated at day 3		Elevated at day 6	
Metabolite	***p* value**	**Metabolite**	***p* value**
AX			
3P-D-glycerate	2.4×10^{-3}		
Malate	3.4×10^{-7}		
Fumarate	6.4×10^{-3}		
L-Ala	1.0×10^{-2}		
L-Asp	2.9×10^{-5}		
sn-Glycerol-3P	3.2×10^{-7}		
		Gly	3.4×10^{-2}
IC			
		Malate	4.5×10^{-3}
		Fumarate	2.9×10^{-2}
sn-Glycerol-3P	1.4×10^{-2}		

[^{13}C]glucose utilisation by AX and IC *C. burnetii* indicates AX *C. burnetii* are able to utilise this substrate more readily than IC *C. burnetii*, with significantly higher ^{13}C-label incorporation into TCA cycle intermediates and some amino acids in the AX population (Figure 3.6). Interestingly the IC *C. burnetii* showed significantly reduced labelling in citrate/isocitrate compared to AX *C. burnetii*, similar to what was observed in the [^{13}C]glutamate-fed population (Figure 3.6). This suggests one or more enzymes involved in channelling glycolytically derived acetyl-coA into the TCA cycle is differentially regulated between AX and IC *C. burnetii*. In addition, levels of ^{13}C-enrichment in C4 dicarboxylic acid intermediates were generally higher than in citrate for IC *C. burnetii*, which suggests pyruvate may be converted to malate to undergo anaplerosis. ^{13}C-label incorporation was once again observed in lactate, for both AX and IC *C. burnetii*, supporting the notion that malate can also be converted into lactate (Figure 3.6).

AX *C. burnetii* at 3 days post-inoculation showed significantly higher incorporation of [^{13}C]glucose compared to day 6, consistent with these populations being at a more rapid growth phase than at 6 days post-inoculation (Figure 3.7 and Table 3.5). In contrast, IC *C. burnetii* showed the opposite phenotype, with more ^{13}C-label incorporation occurring at 6 days post-infection.

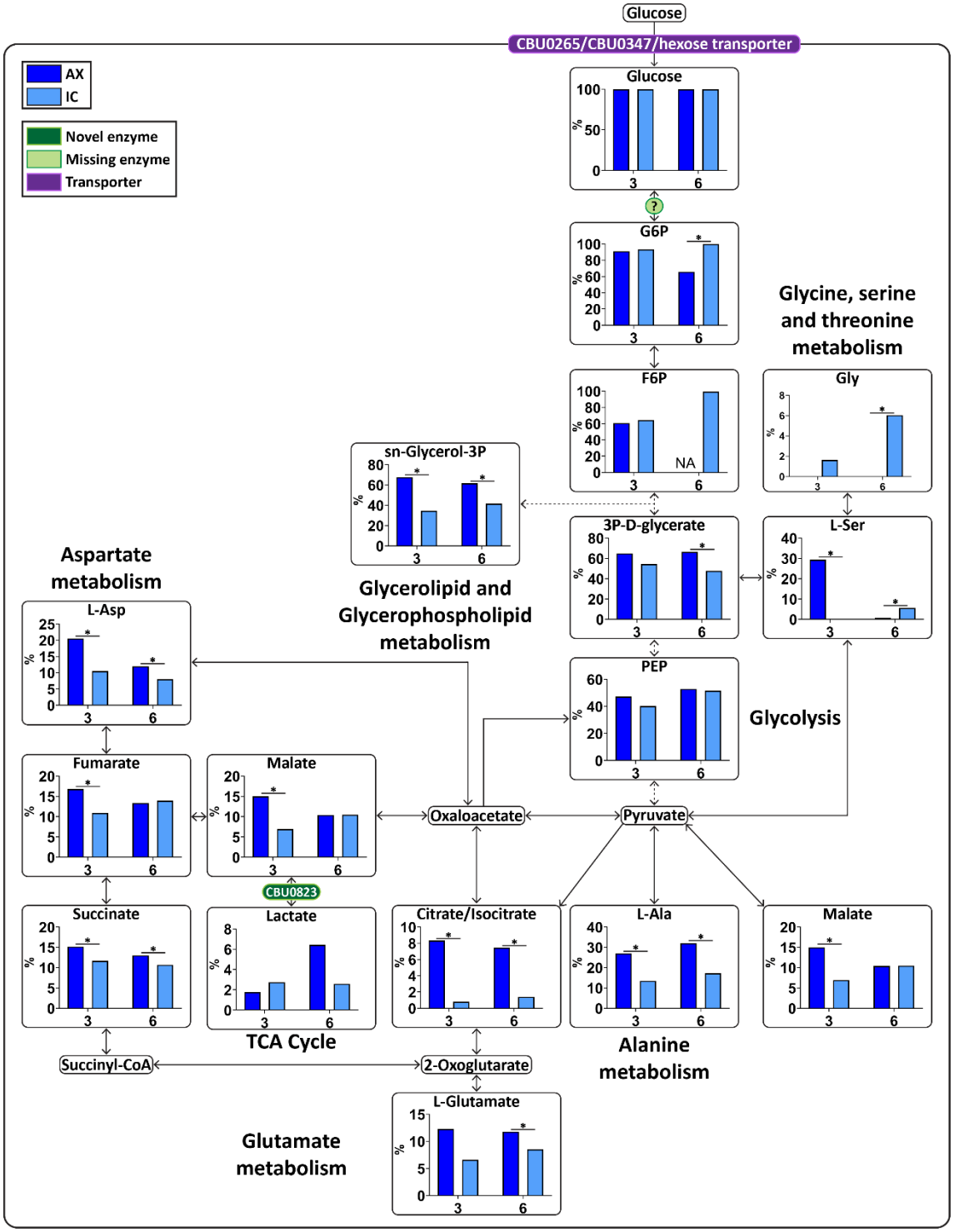

Figure 3.6. AX *C. burnetii* are able to utilise [^{13}C]glucose more readily than IC. Metabolic pathway map of *C. burnetii* comparing ^{13}C-label incorporation between AX and IC *C. burnetii* after 10 minute incubation with [^{13}C]glucose. Metabolites detected on the GC/MS as having incorporated ^{13}C-label are shown in larger boxes, with percentage labelling in bar graphs. Dark blue bars indicate AX samples and light blue bars indicate

IC samples. Pale green circles indicate missing enzymes based on genome annotation data in KEGG. Dark green circles indicate putative enzymes with novel functions. Purple denotes metabolite transporters. Dotted arrows indicate pathways which have been abbreviated. * = $p<0.05$ using unpaired student's *t*-test. NA indicates metabolites which were unable to be detected in a given condition. Metabolite abbreviations are listed in Appendix 2.

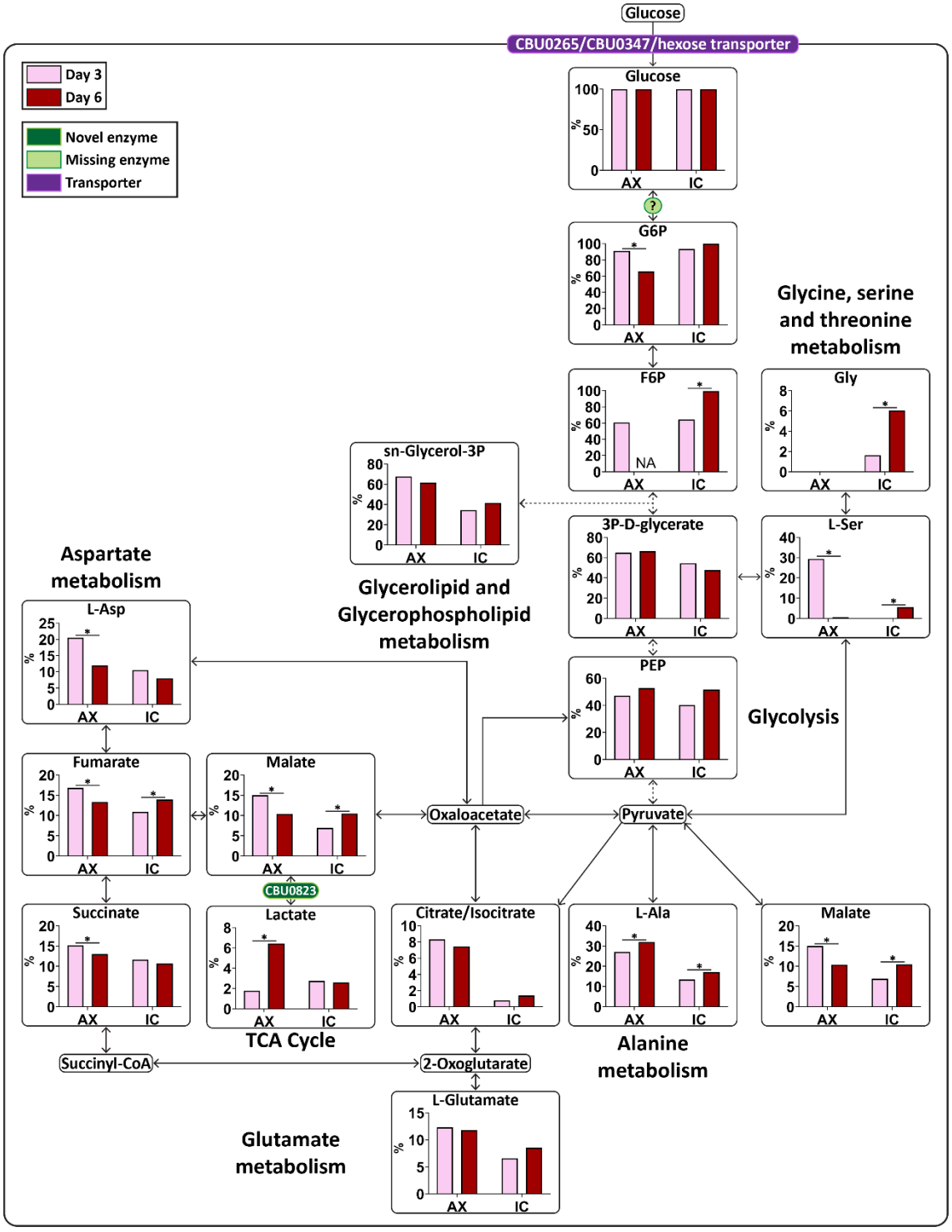

Figure 3.7. Day 3 vs day 6 comparisons of [^{13}C]glucose labelled *C. burnetii.* Metabolic pathway map of *C. burnetii* comparing ^{13}C-label incorporation at day 3 and day 6 within the same culture condition after 10 minute incubation with [^{13}C]glucose. Metabolites detected on the GC/MS as having incorporated ^{13}C-label are shown in larger boxes, with percentage labelling in bar graphs. Light pink bars indicate day 3 samples and maroon

bars indicate day 6 samples. Pale green circles indicate missing enzymes based on genome annotation data in KEGG. Dark green circles indicate putative enzymes with novel functions. Purple denotes metabolite transporters. Dotted arrows indicate pathways which have been abbreviated. * = $p<0.05$ using unpaired student's *t*-test. NA indicates metabolites which were unable to be detected in a given condition. Metabolite abbreviations are listed in Appendix 2.

Table 3.5. Metabolites with significant day 3 vs day 6 differences within AX and IC conditions during [^{13}C]glucose labelling using an unpaired student's *t*-test.

Elevated at day 3		Elevated at day 6	
Metabolite	***p* value**	**Metabolite**	***p* value**
AX			
Malate	2.2×10^{-8}		
Fumarate	1.0×10^{-5}		
Succinate	4.2×10^{-2}		
L-Asp	5.4×10^{-5}		
L-Ser	4.0×10^{-5}		
		Lactate	1.6×10^{-2}
IC			
		F6P	2.9×10^{-2}
		Malate	8.4×10^{-3}
		Fumarate	9.0×10^{-3}
		L-Ala	4.2×10^{-4}
		L-Ser	3.9×10^{-6}
		Gly	1.8×10^{-2}

3.3 Discussion

Understanding the nutrient requirements and metabolic pathways required for *C. burnetii* to survive and replicate within the host cell will assist in elucidating how this pathogen proliferates inside a normally hostile intracellular compartment. A number of recent studies have investigated the metabolism of axenic *C. burnetii*, yet little is known about the metabolic potential of intracellular *C. burnetii*. Within this study, the use of steady state metabolite profiling has facilitated the construction of a *C. burnetii* metabolic map, providing an overview of the types of nutrients *C. burnetii* utilise within both axenic and intracellular compartments. [^{13}C]glutamate and [^{13}C]glucose labelling data has shown that both of these populations are capable of utilising these substrates for use in central carbon metabolism. This indicates that enzymes involved in glycolysis and TCA cycle are constitutively active in both axenically and intracellularly cultivated *C. burnetii*. However, there were significant differences between axenic and intracellular *C. burnetii* in terms of the extent to which both carbon sources are catabolised within the TCA cycle. This demonstrates a capacity of *C. burnetii* to remodel carbon metabolism depending on nutrient availability and environment.

Current technological limitations mean *in situ* labelling of intracellular bacteria with ^{13}C-substrates is not possible. Such techniques would need to overcome the difficulties involved in discerning whether the incorporation of ^{13}C-label into detected metabolites occurred through host or bacterial enzyme activity. The methodology used in this study is the closest indicator of *C. burnetii* metabolism *in vivo*. While it is difficult to account for any rapid metabolic changes due to the altered environment during harvesting of IC

C. burnetii, our data still demonstrates significant differences between AX and IC *C. burnetii*.

Recent studies profiling lysosomal content suggest that the lysosome of mammalian cells contain elevated levels of many amino acids, including glutamate. These amino acids are generated by proteolysis of luminal proteins and/or reverse transport from the cytosol (97). The CCV shares many properties in common with mature lysosomes, including high fusogenicity with endosomal and autophagosome compartments, and is likely to have similar luminal nutrient levels.

In this context, utilisation of [^{13}C]glutamate by IC *C. burnetii* may represent an important adaptation to this intracellular niche. The labelling studies indicate IC *C. burnetii* primarily catabolise glutamate in a discontinuous TCA cycle by converting α-ketoglutarate to malate/oxaloacetate, with production of reducing equivalents such as NADH as well as carbon backbones for gluconeogenesis.

Gluconeogenesis appears important *in vivo*, as disruption of the *C. burnetii* gluconeogenic enzyme PEPCK leads to a decrease in intracellular replication in Vero cells (86). Operation of a discontinuous TCA cycle may also prevent production of excess reducing equivalents and leakage of reactive oxygen species (ROS) from the respiratory chain, and thereby minimise oxidative stress in the CCV compartment. The mechanisms in IC *C. burnetii* which regulate TCA cycle flux, for instance in increasing the conversion of malate/oxaloacetate to PEP and gluconeogenesis, remain to be elucidated. The

^{13}C-label incorporation into gluconeogenic intermediates in IC *C. burnetii* supports the notion that these bacteria are accustomed to generating sugars and sugar phosphates by catabolising amino acids rather than via glycolysis.

Furthermore, AX *C. burnetii* cultured in ACCM-2 medium, which contains a higher abundance of glucose than that present in a lysosome, more readily utilised [^{13}C]glucose than IC *C. burnetii*. This was evident through higher ^{13}C-label incorporation within the TCA cycle, particularly at 3 days post-infection when *C. burnetii* have been actively dividing in the late logarithmic growth phase.

Interestingly, in contrast to AX *C. burnetii*, at 6 days post-infection, IC *C. burnetii* incorporated more ^{13}C-label than at day 3, particularly for [^{13}C]glucose-labelled samples. IC *C. burnetii* at 6 days post-infection are likely to contain a mixture of stationary phase bacteria alongside those which have newly infected cells. While it would be difficult to remove host turnover as a factor regarding these samples, further investigations are warranted to determine the cause of this apparent late-stage increase in metabolic activity in this population of bacteria.

These labelling studies have also provided new insights into *de novo* amino acid biosynthesis in *C. burnetii*. For instance, the high ^{13}C-label incorporation into intracellular pools of aspartate, for both [^{13}C]glutamate and [^{13}C]glucose labelled samples, suggest the interconversion of oxaloacetate and aspartate through transamination reactions may have an important role in regulating carbon-nitrogen metabolism.

Aspartate is also the precursor to essential metabolites such as NAD. The aspartate oxidase NadB (CBU0101) in *C. burnetii* has previously been shown to have an important role in *de novo* NAD synthesis, which is important for intracellular replication (151).

Unexpectedly, this study showed both [^{13}C]glutamate and [^{13}C]glucose were catabolised into lactate in AX and IC *C. burnetii*. The production of lactate from [^{13}C]glucose has previously been reported in *C. burnetii* (98). Initial studies using HeLa cells at 2 days post-infection showed almost 20% ^{13}C-label incorporation into lactate for [^{13}C]glutamate labelled samples, and approximately 5% for [^{13}C]glutamate labelled samples. However, a limitation of this HeLa cell-derived dataset was that host cell-induced turnover had not been addressed, giving rise to the possibility that these percentages may not be a true representation of *C. burnetii* metabolism.

Another limitation to this dataset was the inability to observe the metabolism of *C. burnetii* at later times during infection (rather than 2 days post-infection). Combined, this resulted in the development of a new methodology to study IC *C. burnetii* metabolism using THP-1 cells. Using this model, the percentage labelling occurring in mock THP-1 cells were subtracted from the detected percentage labelling occurring in IC *C. burnetii*. Only succinate and lactate showed ^{13}C-label incorporation in mock samples, with percentage labelling in lactate at 0.92±0.42% and 0.53±0.24% for [^{13}C]glutamate and [^{13}C]glucose, respectively. Removing these values from the IC *C. burnetii* datasets resulted in ^{13}C-label incorporation of lactate below 3%. This suggests that while there are host-derived enzymes that are able to convert [^{13}C]glucose into lactate, present alongside

isolated IC *C. burnetii*, there must also be a *C. burnetii* enzyme that is able to synthesise lactate.

Genome annotation suggests *C. burnetii* lacks an NAD^+-dependent lactate dehydrogenase (LDH), which can generate lactate from pyruvate (152). However, the *C. burnetii* genome does encode an NAD^+-dependent malate dehydrogenase (MDH), which is predicted to convert malate into pyruvate or oxaloacetate (153). MDH has been postulated in *Mycoplasma* species to also catalyse the reversible interconversion of pyruvate to lactate (154). There is, however, no evidence to suggest dual functioning MDHs exist in these bacteria (155).

An alternative possibility is that *C. burnetii* possesses a malolactic enzyme, capable of converting malate to lactate, which are found in lactic acid bacteria (150). BLASTp analysis indicates *C. burnetii* possesses a malolactic enzyme homologue, CBU0823. CBU0823 is currently annotated as an NAD-dependent malic enzyme, but no biochemical analyses have been performed to determine substrate preferences or enzymatic activities of this protein. Further investigations are needed to confirm whether CBU0823 has malolactic enzyme activity.

Biosynthesis of lactate may be a carbon storage mechanism utilised by *C. burnetii*, where this substrate could be catabolised at later times during infection, or under conditions where other carbon sources are limited. Utilisation of lactate as a sole carbon source was recently demonstrated in the intracellular pathogen *Mycobacterium tuberculosis*, which

also infects alveolar macrophages (156). Rates of lactate uptake and/or utilisation at various times throughout infection may help elucidate how this substrate is processed by *C. burnetii*. If lactate is indeed used as a carbon storage mechanism, supplementation of media with lactate during nutrient deprivation may also determine how vital lactate is for *C. burnetii*, and thus assist in establishing the importance of lactate biosynthesis in *C. burnetii* pathogenesis.

This research has demonstrated that both AX and IC *C. burnetii* are able to utilise glucose. Utilisation of exogenous glucose has previously been reported in AX *C. burnetii* (98). The mechanism by which *C. burnetii* either transports or phosphorylates exogenous glucose remains to be elucidated, as the bacteria lack an identifiable hexokinase or PTS. Glucose uptake in *C. burnetii* will be further investigated in Chapter 4 of this thesis.

A number of metabolic traits in IC *C. burnetii* are shared with *Leishmania* species, a group of protozoan parasites that also invade macrophages and proliferate within a similar phagolysosomal environment (157). Both pathogens are auxotrophic for many amino acids, purines, and vitamins. This suggests both pathogens are completely reliant on salvage of these metabolites from the host lysosome (158). Both pathogens also utilise hexoses *in vivo* and exhibit an incomplete TCA cycle, minimising the production of respiratory ROS (90). Interestingly, and in contrast to IC *C. burnetii*, intracellular *Leishmania mexicana* down-regulate metabolism of glutamate as a carbon source, when compared to extracellular cultivated stages (90). *L. mexicana* mutants with reduced capacity to utilise glucose adapt by increasing their capacity to uptake glutamate (90).

This adaptation, however, does not restore virulence in macrophages or animal models, due to the associated increase in endogenous ROS production (159). It is possible that *C. burnetii* are able to tolerate higher levels of respiratory activity or have a more efficient respiratory chain compared to *Leishmania*. This ability to tolerate higher levels of ROS is supported by the labelling data, where the pattern of ^{13}C-label incorporation suggests reduced activity of enzymes such as isocitrate dehydrogenase and glutamate dehydrogenase in IC *C. burnetii*. Both enzymes, when NADP(H)-dependent, are involved in reducing ROS build up and avoiding oxidative stress in other pathogenic bacteria (160). In addition, recent studies have shown that the ROS levels in THP-1 cells during *C. burnetii* infection are elevated when compared to uninfected cells (83). ROS levels were elevated even further during infection with a mutant strain of *C. burnetii* lacking the enzyme SdrA (CBU1276). This enzyme was shown to increase levels of NADP(H), an essential cofactor involved in reducing the accumulation of intracellular ROS, thus highlighting the importance of SdrA in resisting oxidative stress during intracellular replication (83). Further characterisation of factors involved in ROS tolerance in IC *C. burnetii* may provide important insights into host-pathogen interactions mediated by *C. burnetii*.

This research characterised the nutrient preferences and metabolic pathways of *C. burnetii*, facilitating the construction of a comprehensive metabolic pathway map. Obtaining metabolic information during cultivation of *C. burnetii*, in both axenic and intracellular conditions, has allowed important temporal and environmental comparison of metabolic potential. Stable isotope labelling identified gaps in the existing metabolic pathway data of *C. burnetii*, highlighting the likely existence of novel metabolic enzymes

involved in the phosphorylation of glucose and generation of lactate. Further investigations into these enzymes and pathways may help identify mechanisms unique and essential to *C. burnetii* metabolism and pathogenesis, which have potential to become novel therapeutic targets.

Chapter 4

Glucose transport and utilisation in *C. burnetii*

4.1 Introduction

Exogenous hexose is an essential nutrient source for many organisms. However, in order to utilise this substrate, cells must first import sugars within the cell. Transport of exogenous hexose by bacteria has been studied extensively in *E. coli*. In these bacteria, uptake of sugars typically occur via H^+ symporters and phosphotransferase systems (PTSs) (161, 162) (Figure 4.1).

H^+ symporters require a proton gradient across the bacterial cell membrane to allow simultaneous uptake of sugars and protons (161) (Figure 4.1). These membrane-bound proteins share homology to mammalian hexose transporters such as GLUT1-4, which are major facilitator superfamily (MFS) transporters (163). In addition to bacteria and animals, MFS transporters are found ubiquitously in archaea, fungi, protozoa, and plants (161). Members of this family of transporters appear to show some promiscuity in substrates, with some transporters able to uptake more than one type of hexose (163, 164). *E. coli* encodes at least six MFS sugar transporters, allowing uptake of a range of sugars including arabinose, rhamnose, fucose, lactose, galactose, and xylose (161, 164, 165).

In contrast to H^+ symporters, which do not alter their substrates during transport, PTSs add phosphate groups to their sugar substrates as they enter the cytoplasm (162). In addition to the membrane-bound transporter, PTSs also include three enzymes, termed Enzyme I (EI), Enzyme II (EII), and Histidine Protein (HPr) (162). The soluble protein kinase EI catalyses the phosphorylation of HPr using phosphoenolpyruvate (PEP). HPr

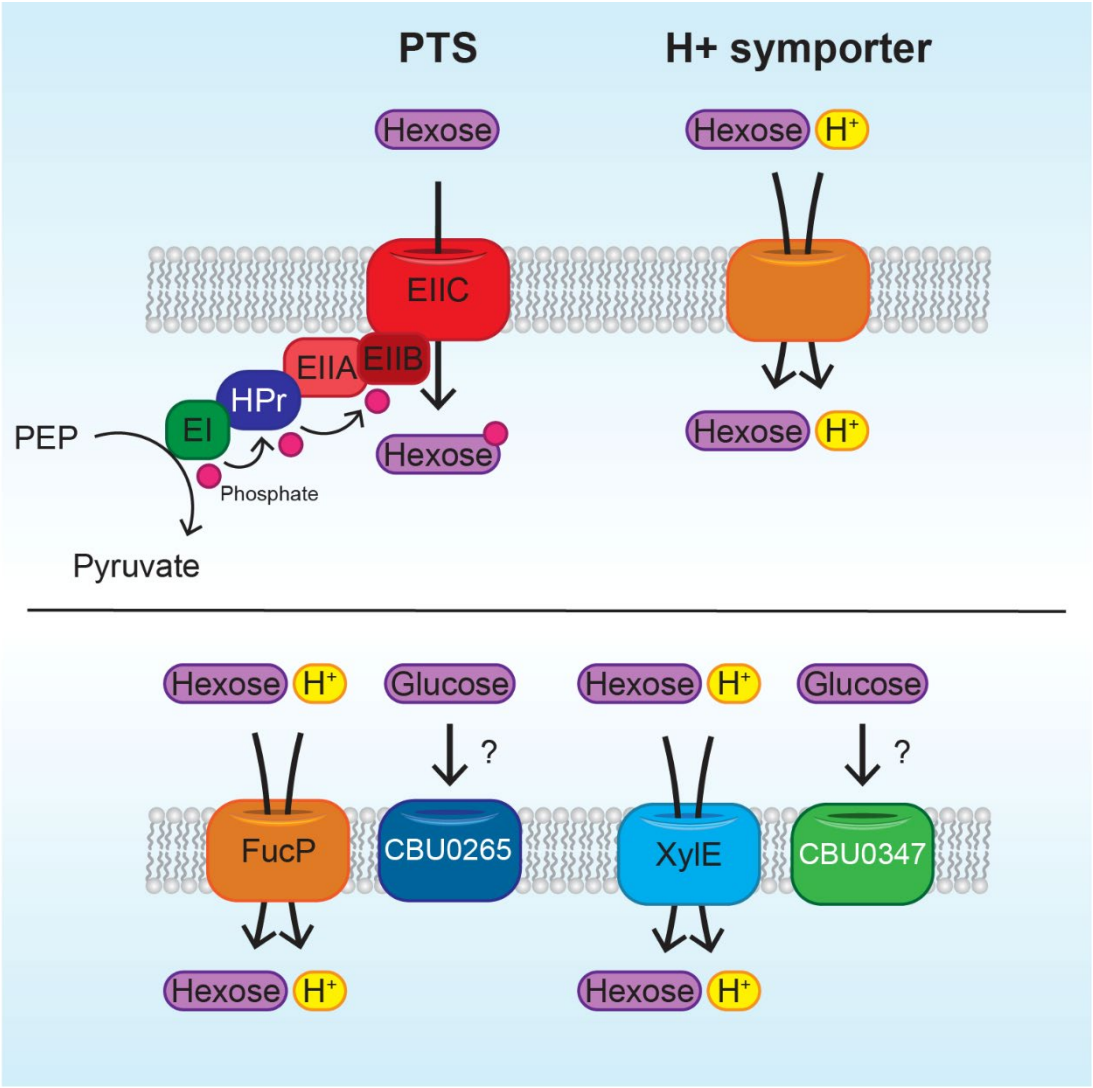

Figure 4.1. Schematic representation of sugar transport in Gram-negative bacteria. Top panel indicates prototypical sugar transport in Gram-negative bacteria, with components of the phosphotransferase system (PTS) including Enzyme I (EI), Enzyme II components A-C (EIIA-C), and Histidine Protein (HPr). Bottom panel denotes systems present in *C. burnetii*, based on genome annotation, which include CBU0265 (homologous to the *E. coli* H^+ symporter FucP) and CBU0347 (homologous to the *E. coli* H^+ symporter XylE).

in turn phosphorylates EII, comprised of three domains termed EIIA, EIIB, and EIIC, which then transfers this phosphoryl group on to incoming sugars (162). This system, therefore, allows the generation of additional sugar phosphate groups such as glucose 6-phosphate during glucose uptake, independent of hexokinases. This system appears specific to prokaryotes (including Archaea), with no homologous systems present in eukaryotic cells (166, 167).

Utilisation of exogenous glucose has previously been shown for AX *C. burnetii* (98), which was also independently verified in Chapter 3 of this thesis. Additional data from Chapter 3 showed IC *C. burnetii*, cultivated in both HeLa and THP-1 cells, were able to utilise exogenous glucose via classical glycolysis. Given the metabolism of exogenous glucose and demonstration that exogenous glucose appears important for *C. burnetii* during infection in Vero cells (86), glucose may be an important nutrient source for *C. burnetii*. However, *C. burnetii* lack an identifiable hexokinase or PTS, which raises questions as to how the bacteria phosphorylate glucose.

This chapter identified and characterised proteins involved in glucose transport in *C. burnetii*, using [^{13}C]glucose labelling techniques developed from Chapter 3. In addition, this study has further investigated the importance of glucose transport to intracellular replication and virulence in *C. burnetii*, using both mammalian and insect models of infection.

4.2 Results

4.2.1 Bioinformatic identification of putative *C. burnetii* hexose transporters

C. burnetii lacks a functional PTS capable of internalising hexose with concomitant phosphorylation, suggesting that sugars are internalised via an active or facilitative transporter. Analysis of the RSA439 *C. burnetii* genome indicates that *C. burnetii* encodes two putative hexose transporters (47). CBU0265, annotated as a putative glucose/galactose transporter, has 31.6% identity with FucP in *E. coli* between amino acids 8-376 (126, 168, 169). FucP, an MFS transporter, has been shown to transport L-fucose, D-arabinose, and L-galactose in *E. coli* (165). Similar to FucP, CBU0265 contains 12 predicted transmembrane domains (170) (Figure 4.2A). The predicted molecular weight of CBU0265 is 44.8 kDa (Figure 4.2A). Amino acid sequence alignment between CBU0265 and FucP is shown in Figure 4.3.

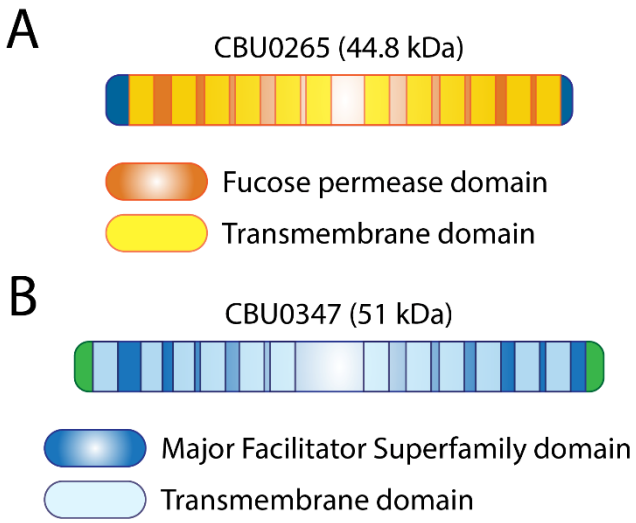

Figure 4.2. Schematic representation of CBU0265 and CBU0347. (A) CBU0265 shown in dark blue, with area of homology to FucP shown in orange. Yellow indicates transmembrane domains. (B) CBU0347 shown in green, with area of homology to XylE shown in blue. Light blue indicates transmembrane domains.

The second putative *C. burnetii* hexose transporter, CBU0347, is currently annotated as a D-xylose-proton symporter, as this protein contains 34.7% identity with the *E. coli* xylose transporter, XylE, between amino acids 13-449 (126, 164, 171). XylE, which is also an MFS transporter, has been shown to bind D-xylose and D-glucose (163). CBU0347 is predicted to have a molecular weight of 51 kDa, and similar to CBU0265, XylE, and FucP, also contains 12 predicted transmembrane domains (170) (Figure 4.2). Sequence similarity between CBU0347 and XylE is shown in Figure 4.4.

Both CBU0265 and CBU0347 are conserved across numerous *C. burnetii* strains outside of RSA439, including virulent phase I strains isolated from clinical samples. This conservation suggests both proteins are important for *C. burnetii*.

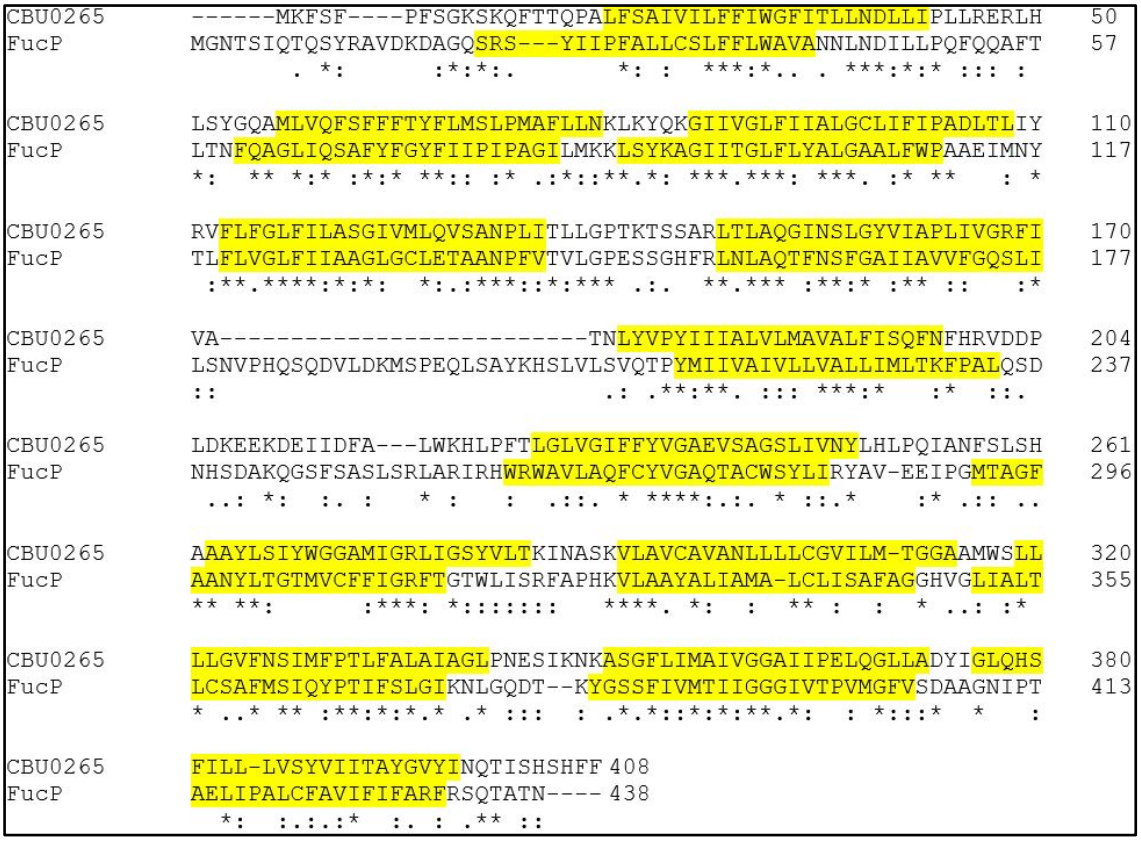

Figure 4.3. Amino acid sequence homology between CBU0265 and FucP. Sequence alignment between CBU0265 and the *E. coli* homologue FucP generated using Clustal Omega (172). '*' indicates conserved residues. ':' indicates conservation between amino acids of strongly similar properties. '.' indicates conservation between amino acids of weakly similar properties. Yellow highlighting indicates amino acid sequences predicted to be transmembrane domains (170).

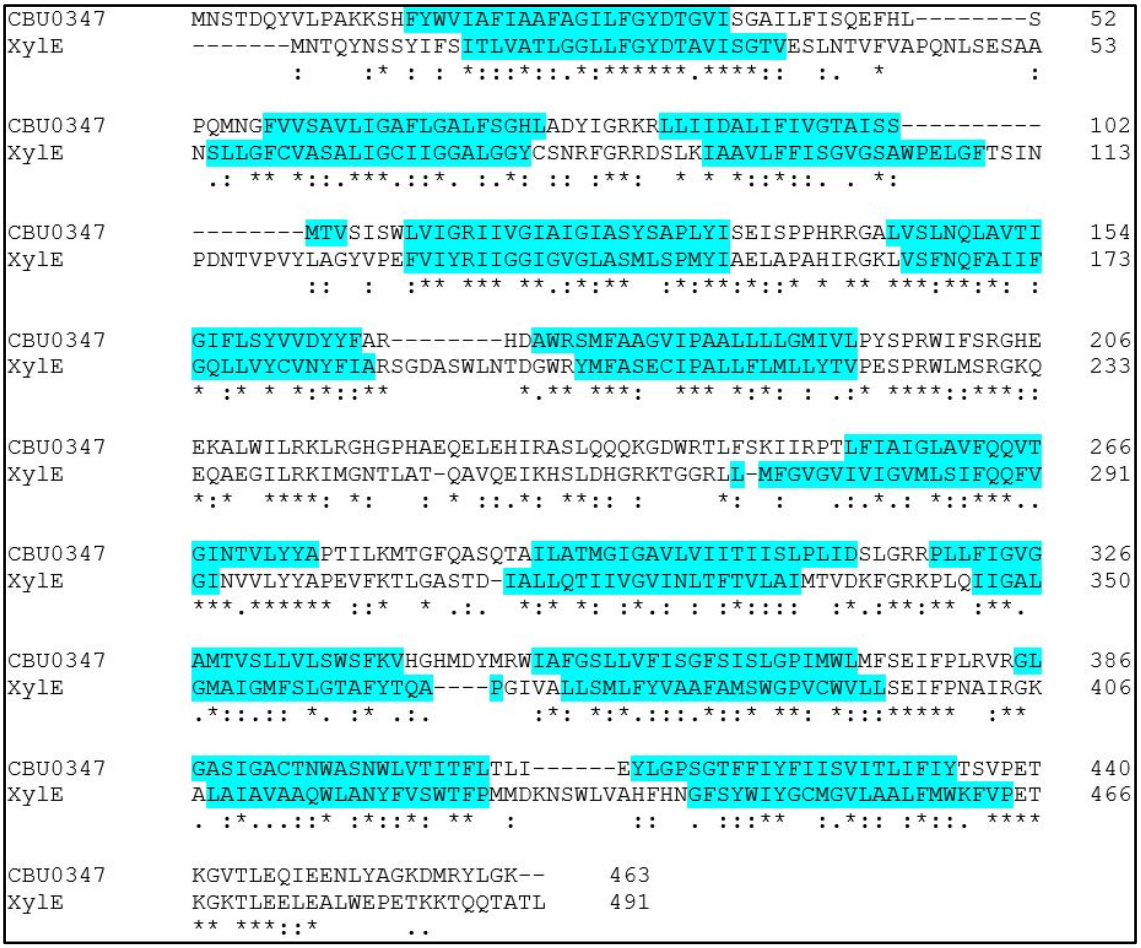

Figure 4.4. Amino acid sequence homology between CBU0347 and XylE. Sequence alignment between CBU0347 and the *E. coli* homologue XylE generated using Clustal Omega (172). '*' indicates conserved residues. ':' indicates conservation between amino acids of strongly similar properties. '.' indicates conservation between amino acids of weakly similar properties. Pale blue highlighting indicates amino acid sequences predicted to be transmembrane domains (170).

4.2.2 CBU0265 is a functional glucose transporter in *C. burnetii*

C. burnetii CBU0265 has previously been identified as a putative proton-driven glucose/galactose transporter, and may be responsible for glucose uptake (47, 86, 95, 96, 98).

A previous study generated and identified a *C. burnetii* transposon mutant in which *cbu0265* was disrupted (*0265*::Tn) (Figure 4.5A) (76, 173). The transposon insertion occurred 297 bp from the start codon (Figure 4.5A). This disruption is predicted to create a CBU0265 deficient strain as the insertion site would only allow the production of a 11.4 kDa truncated protein, including only 2 of the 12 predicted transmembrane domains. In order to examine the role of CBU0265, a complemented *0265*::Tn mutant was constructed, in which a 3xFLAG tagged CBU0265 was constitutively expressed from the pJB-Kan expression plasmid (*0265*::Tn pFLAG-0265). Expression of 3xFLAG-0265 in the complemented strain was confirmed via western blot (Figure 4.5B). The predicted molecular weight of CBU0265 is 44.8 kDa (Figure 4.2A). However, 3xFLAG-0265 expressed by *C. burnetii 0265*::Tn migrates at approximately 35 kDa (Figure 4.5B). This is consistent with previously characterised H^+-rich sugar transporters, which have been observed to migrate on SDS-PAGE at 65-75% of their true molecular mass. This shift in mass has been speculated to be due to the high hydrophobicity of these membrane proteins, which leads to an unusually high binding with SDS (174). This has been previously reported for FucP, the *E. coli* CBU0265 homologue (168, 169).

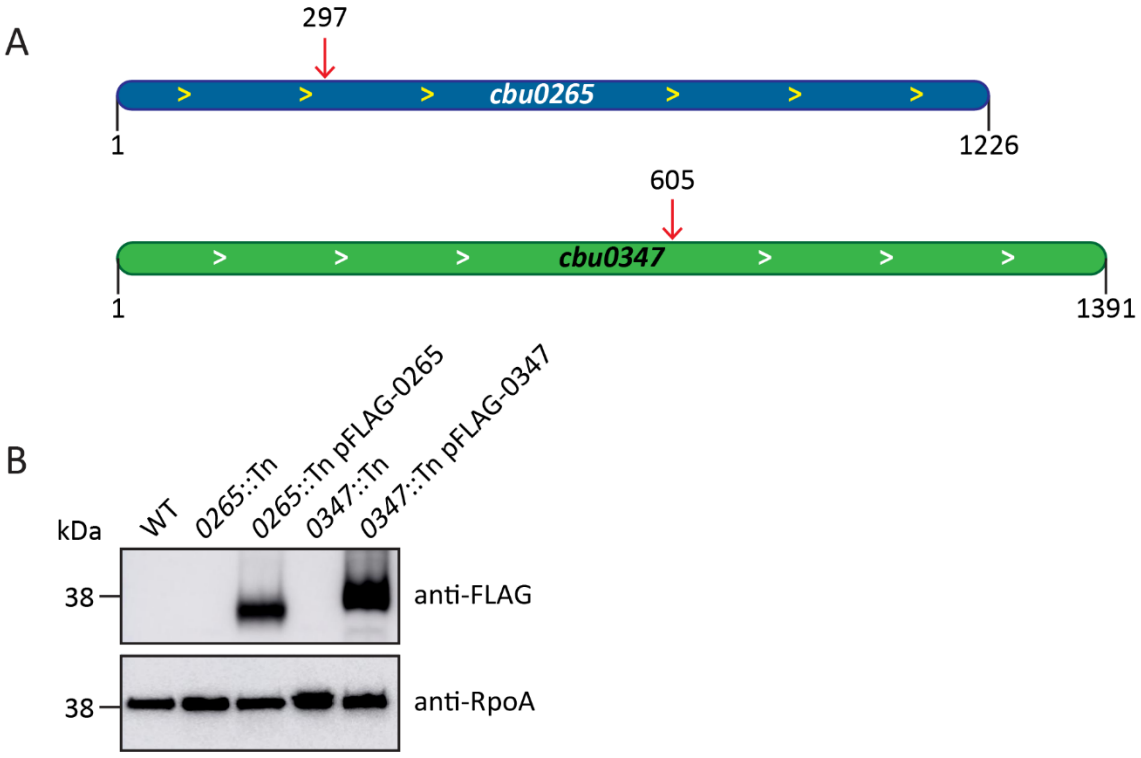

Figure 4.5. Transposon insertion sites and confirmation of transposon mutant complementation. Schematic of transposon insertions sites in *0265*::Tn and *0347*::Tn mutants (A). Red arrows indicate insertion sites for *cbu0265* (blue) and *cbu0347* (green). Direction of internal arrows indicate direction of open reading frame. Numbers indicate base pairs within *C. burnetii* RSA439 genome. Western blot of *C. burnetii* lysate showing expression of 3xFLAG-0265 or 3xFLAG-0347 in *C. burnetii* strains (B). RpoA used as loading control.

To determine whether CBU0265 is responsible for glucose uptake, [^{13}C]glucose labelling was performed on *C. burnetii* WT, *0265*::Tn and *0265*::Tn pFLAG-0265 at 6 days post-inoculation. Axenic cultures were labelled for 10 minutes with ACCM-2 containing 11.11 mM [^{13}C]glucose, after which bacteria were rapidly quenched to halt metabolism and harvested. Polar metabolites were extracted and analysed on the GC/MS, as outlined in section 2.7.

C. burnetii WT strains exhibited detectable levels of substrate utilisation, with incorporation of ^{13}C-label in glycolytic intermediates and the TCA cycle, similar to what was seen in Chapter 3 (Figure 4.6). However, ^{13}C-enrichment in these intermediates was significantly reduced in the *0265*::Tn mutant compared with WT (Figure 4.6). For instance, ^{13}C-enrichment in 3P-D-glycerate for *C. burnetii* WT was at 41±6.3% (Figure 4.6). However, in the *0265*::Tn mutant, this was significantly lower, at 29±5.8% (p = 3.01 x 10^{-2} compared to WT) (Figure 4.6). Complementation of the *0265*::Tn mutant resulted in ^{13}C-enrichment at 54±1.8% (p = 7.6 x 10^{-3} compared to WT) (Figure 4.6). This increase relative to WT likely reflects the increased expression of the plasmid encoded CBU0265 compared to chromosomally encoded CBU0265. Similar trends were present in TCA cycle intermediates such as fumarate, where ^{13}C-enrichment was at 11±0.9% in WT, 6±1.5% in *0265*::Tn (p = 9.0 x 10^{-4} compared to WT) and 17±1.6% in *0265*::Tn pFLAG-0265 (p = 1.4 x 10^{-3} compared to WT). These data also strongly suggest that *C. burnetii* express additional hexose transporters to account for the residual level of [^{13}C]glucose utilisation in the *0265*::Tn strain.

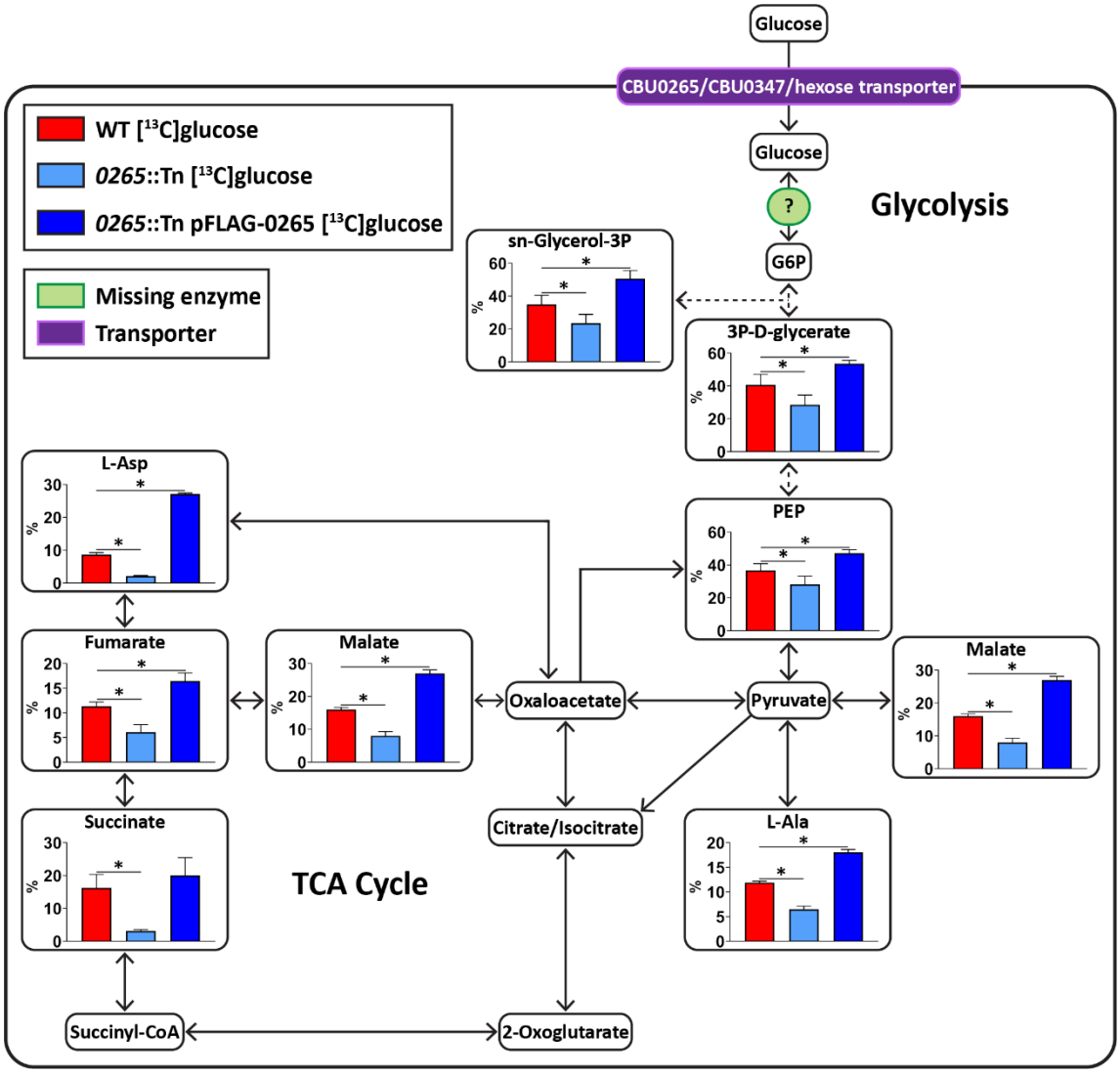

Figure 4.6. CBU0265 is required for efficient glucose utilisation in *C. burnetii*. Metabolites detected on the GC/MS as having incorporated ^{13}C-label from [^{13}C]glucose shown in larger boxes, with percentage labelling depicted in accompanying graphs. *C. burnetii* WT in red, *0265*::Tn in light blue, and *0265*::Tn pFLAG-0265 in dark blue. Pale green circles indicate missing enzymes based on genome annotation data in KEGG. Purple denotes metabolite transporters. Dotted arrows indicate pathways which have been abbreviated. Error bars indicate standard deviations. * = p<0.05 using an unpaired student's *t*-test comparing strains against WT. Metabolite abbreviations are listed in Appendix 2.

4.2.3 CBU0265 is not required for intracellular replication in human cell lines or virulence in *Galleria mellonella*

C. burnetii do not require extracellular glucose during axenic cultivation (95). However, previous research suggests reduced glucose availability during intracellular replication can negatively impact *C. burnetii* replication. This was shown in a *C. burnetii* strain defective in gluconeogenesis, which replicated less efficiently inside Vero cells grown in glucose-restricted medium, when compared with *C. burnetii* WT (86).

To observe whether the loss of glucose uptake via CBU0265 affects intracellular replication, intracellular replication assays were performed in HeLa and THP-1 cells using *C. burnetii* WT, *0265*::Tn and *0265*::Tn pFLAG-0265 (Figure 4.7A-D). At 5 days post-infection of HeLa cells the *C. burnetii* GE fold change, compared to day 0, was 167.7 ± 33 for WT, 158.7 ± 33 for *0265*::Tn, and 153.4 ± 16 for *0265*::Tn pFLAG-0265 (Figure 4.7A). In THP-1 cells, GE fold change at 5 days post-infection was 298.1 ± 129 for WT, 285.3 ± 190 for *0265*::Tn, and 316 ± 186 for *0265*::Tn pFLAG-0265 (Figure 4.7B). At no stage was a significant difference noted between these different strains. In addition, IF images from both HeLa and THP-1 cell lines show no impact to CCV biogenesis in the absence of CBU0265 (Figure 4.7C and D). Together, these results demonstrate that CBU0265 is not required for replication within mammalian cells.

G. mellonella in vivo infection models are a relatively recent tool for studying *C. burnetii* virulence (54, 77, 123). In this model, infection of *G. mellonella* larvae with *C. burnetii* phase II is lethal. To determine whether CBU0265 is required for *C. burnetii* virulence

during infection, *G. mellonella* larvae were injected with 10^6 GE of *C. burnetii* WT, *0265*::Tn or *0265*::Tn pFLAG-0265, and survival was monitored every 24 hours for 11 days. All infected larvae died within 11 days, with similar kinetics observed across all three strains (Figure 4.7E), demonstrating that CBU0265 is not required for virulence in *G. mellonella*.

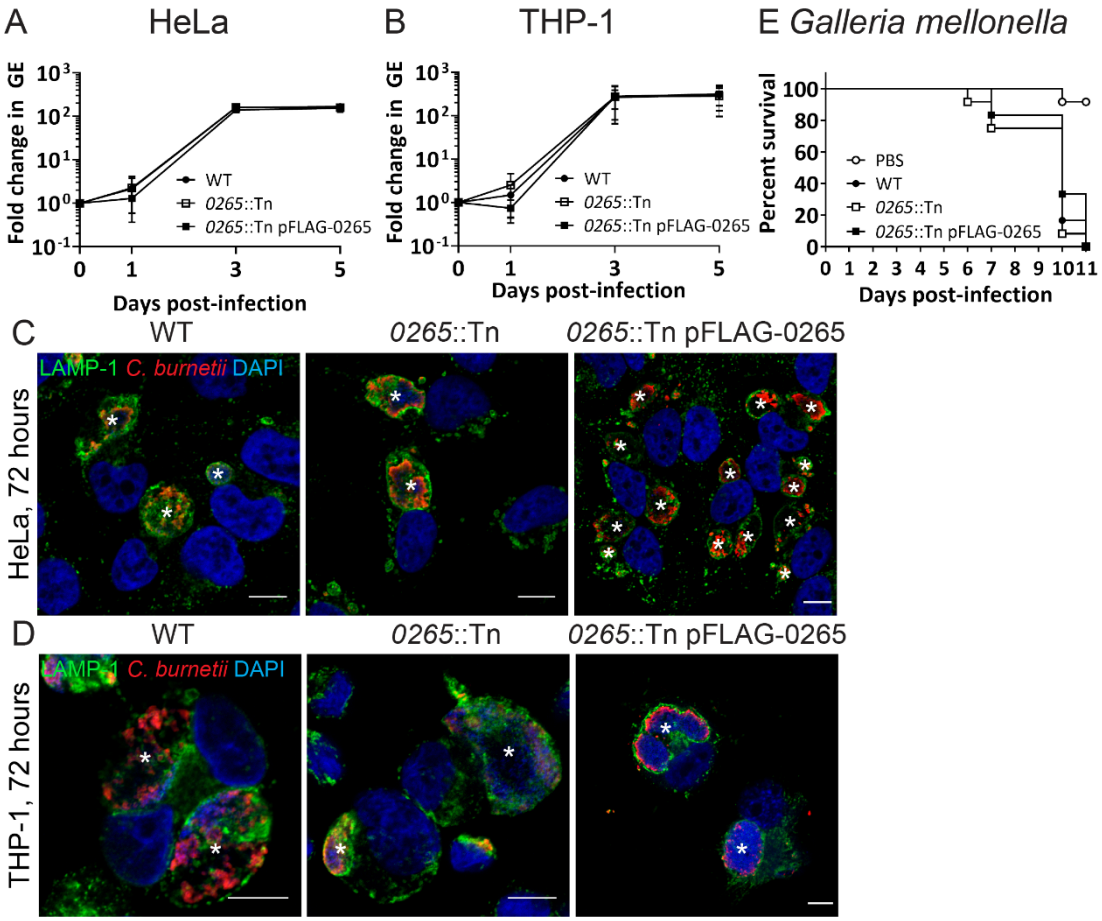

Figure 4.7. CBU0265 is not required for intracellular replication or virulence of *C. burnetii*. Intracellular replication of WT (black circle), *0265*::Tn (white square) and *0265*::Tn pFLAG-0265 (black square) *C. burnetii* in HeLa CCL2 cells (A) and THP-1 cells (B), n=3. Error bars represent standard deviation. Representative confocal immunofluorescence images at 3 days post-infection for infected HeLa CCL2 (C) and THP-1 (D) cells demonstrate normal CCV biogenesis. Samples were stained with LAMP-1 (green), *C. burnetii* (red) and DAPI (blue). Scale bar = 10 μm. * indicates CCV. (E) Survival of *G. mellonella* following infection with *C. burnetii* WT (black circle), *0265*::Tn (white square), *0265*::Tn pFLAG-0265 (black square) at 10^6 GE. A PBS control (white circle) was also included. Results are shown as a representative of two replicates, each with 12 larvae per condition.

4.2.4 The putative xylose transporter CBU0347 can also import glucose into *C. burnetii*

C. burnetii encodes a second putative sugar transporter, which is currently annotated as a D-xylose-proton symporter. CBU0347 contains a domain that is similar to the MFS domain present in the xylose transporter XylE of *E. coli* (Figure 4.2B and 4.4) (164, 171). To determine whether CBU0347, in addition to CBU0265, is capable of importing glucose into *C. burnetii*, [^{13}C]glucose labelling was performed using a previously generated CBU0347 transposon mutant (Figure 4.5A) (76). The transposon insertion occurred 605 bp from the start codon (Figure 4.5A). This disruption is predicted to create a CBU0347 deficient strain as the insertion site would only allow the production of a 29 kDa truncated protein, including only 7 of the 12 predicted transmembrane domains. A complemented *0347*::Tn mutant with constitutively plasmid-expressed 3xFLAG-0347 (*0347*::Tn pFLAG-0347) was generated. Expression of 3xFLAG-0347 was confirmed via western blot (Figure 4.5B). Similar to 3xFLAG-0265 and XylE, 3xFLAG-0347 also migrated on SDS-PAGE at a smaller molecular mass (~38 kDa) compared to its true molecular weight (Figure 4.5B) (164, 171).

[^{13}C]glucose labelling of *C. burnetii* WT, *0347*::Tn and *0347*::Tn pFLAG-0347 at 6 days post-inoculation in ACCM-2 showed significant decreases in ^{13}C-label incorporation for downstream pathways in the *0347*::Tn mutant, compared to WT (Figure 4.8). For instance, ^{13}C-enrichment in 3P-D-glycerate for *C. burnetii* WT was at 53±7.5 % (Figure 4.8). However, in the *0347*::Tn mutant, this was reduced to 41±4.5% ($p = 2.70 \times 10^{-2}$ compared to WT) (Figure 4.8). Complementation of the *0347*::Tn mutant showed significantly higher ^{13}C-enrichment compared with WT, similar to what was observed in the *0265*::Tn

complement (Figure 4.6 and 4.8). For instance, ^{13}C-enrichment of 3P-D-glycerate was at 76±2.5% (p = 1.02 x 10^{-3} compared to WT) (Figure 4.8). Similar trends were present in TCA cycle intermediates such as fumarate, where ^{13}C-enrichment was at 13±1.9% in WT, 4±0.5% in *0347*::Tn (p = 7.69 x 10^{-5} compared to WT) and 24±1.6% in *0347*::Tn pFLAG-0347 (p = 4.97 x 10^{-5} compared to WT).

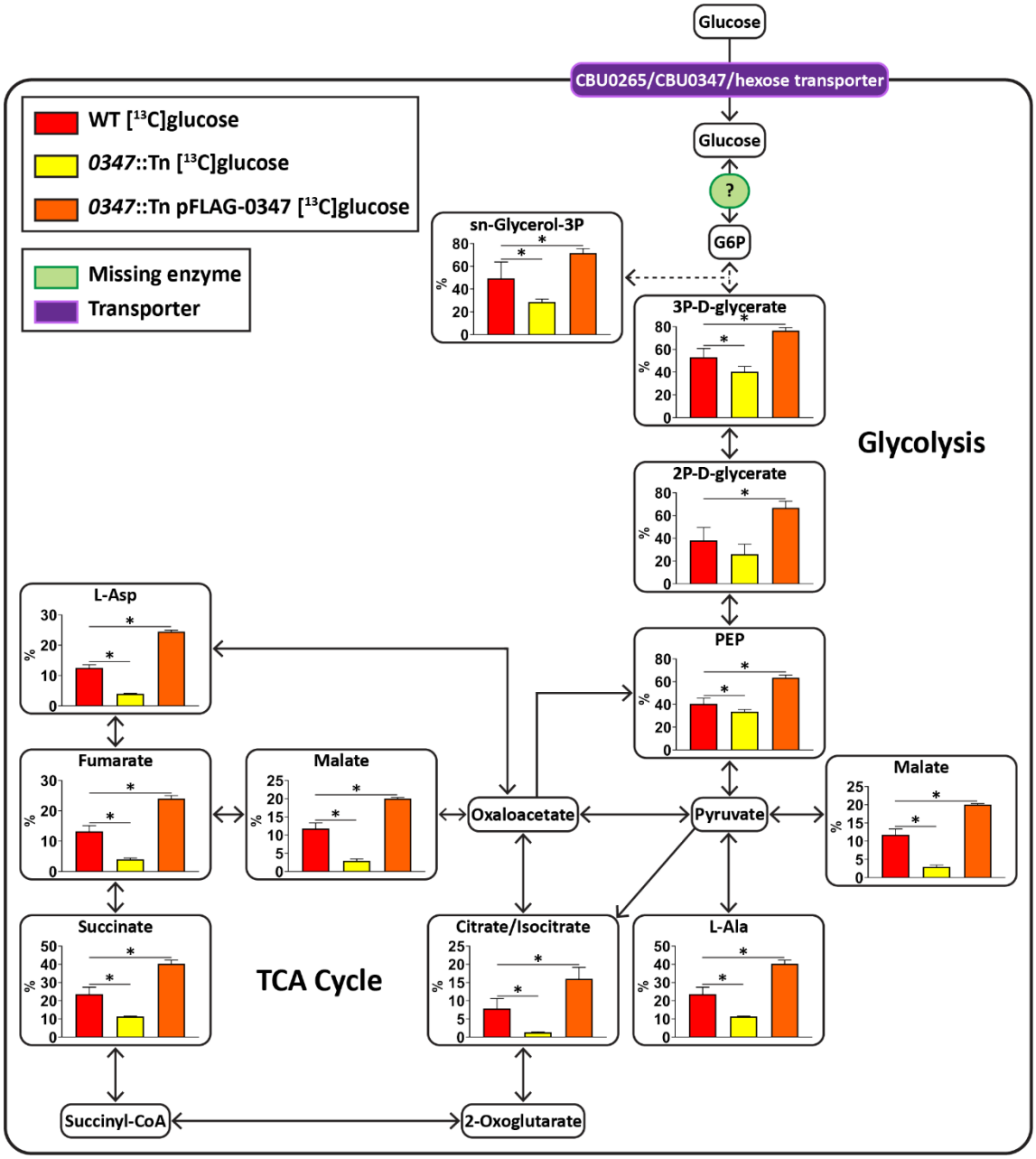

Figure 4.8. CBU0347 is required for efficient glucose utilisation by *C. burnetii*. Metabolites detected on the GC/MS as having incorporated ^{13}C-label from [^{13}C]glucose shown in larger boxes, with percentage labelling depicted in accompanying graphs. *C. burnetii* WT in red, *0347*::Tn in yellow, and *0347*::Tn pFLAG-0347 in orange. Pale green circles indicate missing enzymes based on genome annotation data in KEGG. Purple denotes metabolite transporters. Dotted arrows indicate pathways which have been abbreviated. Error bars indicate standard deviations. * = p<0.05 using an unpaired

student's *t*-test comparing strains against WT. Metabolite abbreviations are listed in Appendix 2.

Mirroring results seen in the absence of CBU0265, no significant differences in replication was observed between WT, *0347*::Tn and *0347*::Tn pFLAG-0347 strains in both HeLa and THP-1 cell models (Figure 4.9A-D). At 5 days post-infection of HeLa cells the *C. burnetii* GE fold change, compared to day 0, was 167.7 ± 33 for WT, 158.7 ± 33 for *0265*::Tn, and 153.4 ± 16 for *0265*::Tn pFLAG-0265 (Figure 4.9A). In THP-1 cells, GE fold change at 5 days post-infection was 298.1 ± 129 for WT, 285.3 ± 190 for *0265*::Tn, and 316 ± 186 for *0265*::Tn pFLAG-0265 (Figure 4.9B).

In addition, there were no attenuations in virulence in the *G. mellonella* model (Figure 4.9E). This demonstrates that, mirroring the results for CBU0265, CBU0347 is not required for replication or virulence in *C. burnetii*. Together, these findings confirm that both CBU0265 and CBU0347 function as hexose transporters in *C. burnetii*.

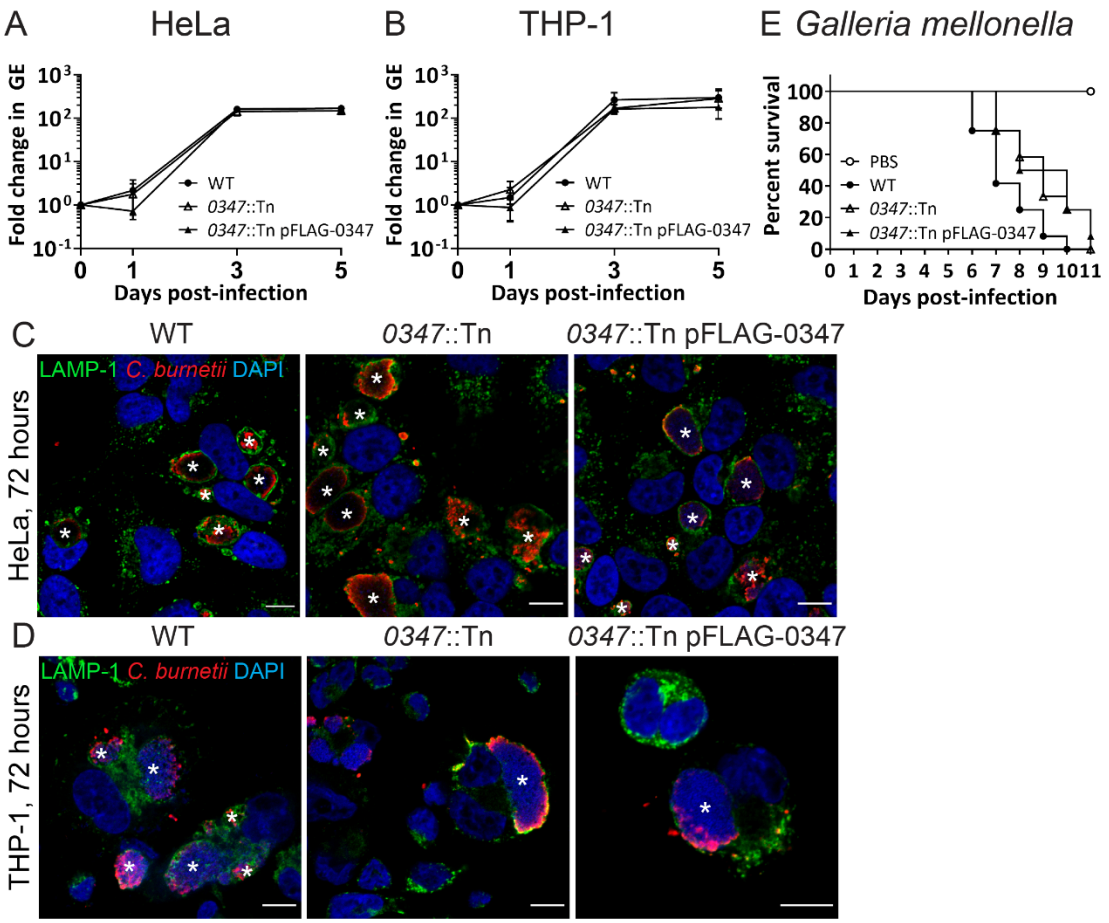

Figure 4.9. CBU0347 is not required for *C. burnetii* intracellular replication or virulence. Intracellular replication assays of WT (black circle), *0347*::Tn (white triangle) and *0347*::Tn pFLAG-0347 (black triangle) C. *burnetii* in HeLa CCL2 cells (A) and THP-1 cells (B), n=3. Error bars represent standard deviation. Representative confocal immunofluorescence images at 3 days post-infection for HeLa CCL2 (C) and THP-1 (D) cells. Samples were stained with LAMP-1 (green), *C. burnetii* (red) and DAPI (blue). Scale bar = 10 µm. * indicates CCV. (E) Survival of *G. mellonella* following infection with *C. burnetii* WT (black circle), *0347*::Tn (white triangle) and *0347*::Tn pFLAG-0347 (black triangle) at 10^6 GE. A PBS control (white circle) was also included. Results are shown as a representative of two replicates, each with 12 larvae per condition.

4.3 Discussion

In conjunction with the results of the previous chapter, this current chapter aims to understand the nutrient acquisition mechanisms utilised by *C. burnetii* to survive and replicate within the normally hostile host phagolysosomal environment. Results presented in Chapter 3 demonstrated that *C. burnetii* are able to catabolise exogenous glucose, which confirms previously reported findings (98). This chapter further investigated glucose usage in *C. burnetii* and confirmed the presence of at least two transporters involved in the uptake of exogenous glucose, CBU0265 and CBU0347.

Disruption of *cbu0265* significantly decreased catabolism of [^{13}C]glucose, while overexpression of this protein on a multi-copy plasmid in the *0265*::Tn strain led to increased glucose catabolism. However, the *0265*::Tn mutant was still able to incorporate ^{13}C from glucose, indicating the presence of at least one additional transporter. CBU0347 is annotated as a putative D-xylose transporter. However, results from this chapter have demonstrated that this protein is also involved in mediating the uptake of glucose, confirming the presence of at least two glucose transporters in *C. burnetii*.

Analysis of the mutant phenotypes in both epithelial and macrophage human cell lines demonstrated no role for these transporters in intracellular replication or CCV biogenesis. This was further supported by demonstrating that both mutants show comparable virulence to WT in the *G. mellonella* insect model of infection.

The lack of a virulence related phenotype for each transposon mutant is not surprising given that both mutants are still capable of internalising some glucose. In order to clearly address whether exogenous glucose supports intracellular success of *C. burnetii*, it would be necessary to characterise a double mutant lacking both *cbu0265* and *cbu0347*. The data presented here would predict that a double mutant would demonstrate an even further decrease in glucose utilisation. However, using a transporter deletion approach to completely abolish glucose uptake is unlikely to succeed, as other transporters capable of glucose transport may compensate for the loss of these specific glucose transporters. The *C. burnetii* genome contains a number of ABC transporters, which could also facilitate hexose uptake (47).

Future studies to fully elucidate proteins contributing to glucose metabolism during *C. burnetii* infection could use transcriptomics or proteomics to compare bacteria cultivated with or without glucose, for instance by using ACCM-D, which normally does not contain glucose (95). Changes observed in the presence of glucose may help elucidate whether any of the *C. burnetii* ABC transporters, or perhaps other proteins, are involved in glucose uptake in *C. burnetii*. Examining the bacterial response to glucose may also provide a strategy to identify the mechanism by which *C. burnetii* phosphorylates glucose into glucose 6-phosphate, likely facilitated by a currently unidentified hexokinase or PTS. Given BLASTp analyses have not been able to identify any putative proteins involved in this conversion, this suggests that the enzyme or system utilised by *C. burnetii* is unique and novel.

Glucose uptake is not essential for *C. burnetii* replication in rich medium (95). However, the co-expression of at least two glucose transporters suggests this substrate may be more important as a nutrient source for *C. burnetii* than previously thought. Indeed, data from Chapter 3 has shown *C. burnetii* are capable of co-utilising hexose and amino acid carbon sources *in vivo*. Similarly, disruption of the gluconeogenic enzyme PEPCK only partially attenuated intracellular *C. burnetii* replication in host cells cultured in glucose restricted medium, indicating that the CCV contains appreciable levels of glucose and/or other sugars (86). Further investigations are warranted to determine the extent to which *C. burnetii* relies on exogenous hexoses during infection. Coupled with a potentially novel mechanism by which glucose is phosphorylated, this may provide a unique, *C. burnetii* specific therapeutic target.

The results of this chapter have focused primarily on glucose transport. However, it may be possible for CBU0265 and CBU0347 to transport other hexose sugars. For instance, *in vitro* assays with FucP has demonstrated that this *E. coli* protein can transport L-fucose, D-arabinose, and L-galactose (168). Future studies may investigate whether CBU0265 and CBU0347 are able to transport other sugars, which may determine whether there are specific hexose sugars that are more important for *C. burnetii* metabolism.

This chapter has investigated the importance of glucose uptake on the replication of *C. burnetii* inside cells. Use of stable isotope labelling has identified at least two glucose transporters in *C. burnetii*, with the possibility that more may exist. Future investigations to characterise these nutrient transporters and metabolic enzymes used in the catabolism

of these substrates may help identify novel systems involved in *C. burnetii* success within eukaryotic host cells.

Chapter 5

EirA is a membrane associated protein essential for the intracellular replication of *Coxiella burnetii*

5.1 Introduction

Upon phagocytosis by alveolar macrophages, *C. burnetii* passively undergo endocytic maturation, where fusion of the lysosome with the *C. burnetii*-containing phagosome is essential for intracellular replication (72). Fusion of bacteria-harbouring phagosomes/endosomes with the lysosome, and the subsequent acidification of the vacuole, triggers the conversion of the pathogen from the non-replicative and environmentally stable small cell variant (SCV) form to the replicative large cell variant (LCV) (60, 72).

Acquisition of nutrients is essential for intracellular replication. This thesis has already demonstrated that *C. burnetii* possesses surprising metabolic flexibility in their ability to utilise various different nutrient sources, as outlined in Chapters 3 and 4. However, in addition to these metabolic activities, *C. burnetii* must also construct a unique replicative niche, which is directed largely by the Dot/Icm type 4B secretion system (T4BSS).

The T4BSS is activated upon fusion of the *C. burnetii*-containing phagosome with the host lysosome (71, 114). This multi-protein apparatus is essential for the pathogen to replicate within the host cell, as disruption of genes encoding the T4BSS apparatus leads to non-replicative but viable bacteria retained within LAMP-1 positive vacuoles (107, 108). The T4BSS translocates approximately 130 effector proteins into the host cell, which modulate host cell responses and directly regulate the establishment of a unique replicative niche called the *Coxiella*-containing vacuole (CCV) (175).

The extent to which *C. burnetii* remodels the lysosomal function and composition remains poorly defined. For many years, it was thought the intravacuolar pH of this compartment was similar to mature lysosomes, at approximately pH 4.5 (176). However, recent studies have suggested that the intraluminal pH of the CCV is approximately pH 5.2, and that maintenance of this higher pH is T4BSS-dependent (84, 177, 178). In addition, T4BSS effector proteins contribute to the increased fusogenic properties of the CCV, which can fuse with other CCVs, autophagosomes, and vesicles from the endocytic pathway (74-78). This process leads to the maturation of the CCV, which is most akin to an autolysosome (76, 77). Replication proceeds up to 6-7 days within the host cell, at which point the bacteria are able to exit the host cell via a currently uncharacterised mechanism (60).

The exact mechanisms allowing *C. burnetii* to withstand lysosomal degradation and replicate within this unique niche are still being investigated. A recent transposon mutagenesis screen revealed that disruption of the gene encoding the *C. burnetii* protein CBU2072 leads to a complete intracellular replication defect (76). This mutant strain, similar to Dot/Icm mutants, remains in LAMP-1 positive vacuoles, but is unable to establish a CCV or replicate (76). Interestingly this mutant presents no replication defect in axenic culture, suggesting that this defect is specific to the intracellular niche (76).

CBU2072 is not a T4BSS effector protein, based on initial screens using a BlaM-CBU2072 fusion protein in a BlaM reporter translocation assay (76). CBU2072 contains 33% homology with soluble transhydrogenases found in *E. coli* (126), which are

enzymes involved in hydride transfer between the cofactors NAD and NADP (93, 133, 137). Given the intracellular replication defect and this low level of homology to soluble transhydrogenases, it was hypothesised that CBU2072 may have a role in *C. burnetii* metabolism. Understanding the exact function of CBU2072 may reveal an essential *C. burnetii* metabolic pathway, which could be targeted by novel therapeutics.

This chapter investigates the role of this protein, referred hereafter as essential for intracellular replication A (EirA, CBU2072), in *C. burnetii* virulence. A putative N-terminal signal sequence was demonstrated to be essential for function, as loss of this region resulted in attenuations to intracellular replication and virulence. Fractionation experiments demonstrate localisation of EirA to the bacterial inner membrane. Significantly, without EirA the *C. burnetii* T4BSS does not translocate effector proteins, suggesting a novel role for EirA in T4BSS activity. These findings demonstrate that EirA is required for *C. burnetii* replication within the host cell and as such may be an important target of novel therapeutic approaches.

5.2 Results

5.2.1 EirA is essential for intracellular replication of *C. burnetii* and contains a key functional region

TMHMM2.0 and TMPred are both bioinformatic analysis tools used to predict transmembrane domains (170, 179). These programs predict that CBU2072 (18.3 kDa) contains an N-terminal signal peptide sequence or transmembrane domain from amino acid 1-29 or 1-25, respectively (Figure 5.1A).

PSI-BLAST analysis of the 165 amino acid protein encoded by *cbu2072* revealed 33% homology, between amino acids 24-96 of CBU2072 to soluble transhydrogenases encoded by *E. coli* (Figure 5.1A and B) (126). Transhydrogenases are metabolic enzymes involved in hydride transfer between NAD^+ and NADP molecules (93, 133, 137). Predictions of such enzymatic activity in CBU2072 cannot be made, as catalytic domains are yet to be characterised in these enzymes.

HHPred provides analysis of amino sequences to determine structural homologies to other proteins (180). This software has shown that CBU2072 has between 20-40% predicted structural homology to hydrolases and lipoproteins found in Gram-positive and Gram-negative bacteria, as well as outer membrane proteins found in Gram-negative bacteria, between amino acids 1-58 (Figure 5.1A).

Despite the presence of these small regions of low homology, most of the protein sequence for CBU2072 showed no close homology to any other proteins. These include

proteins found in the *Legionella* species, which are the closest related organism to *C. burnetii*. However, this gene is conserved across numerous strains of *C. burnetii*, including those which have been isolated from clinical samples (126).

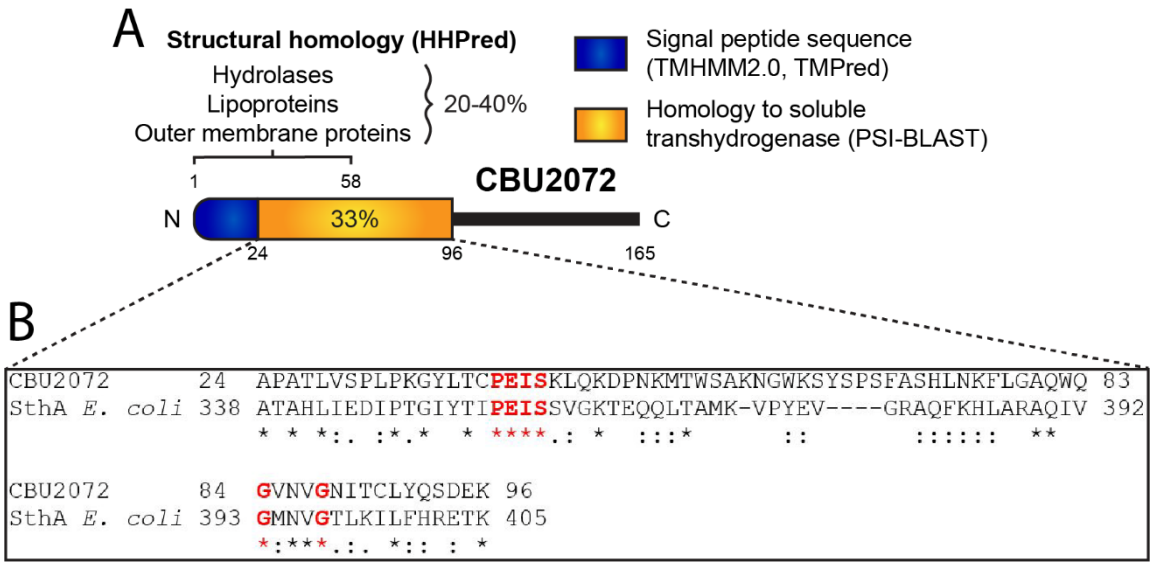

Figure 5.1. Schematic representation of CBU2072 features and homology. (A) Blue indicates predicted signal peptide sequence (170, 179). Orange indicates area of homology to the *E. coli* soluble transhydrogenase, SthA (126). Region of low predicted structural homology based on HHPred analysis is highlighted from amino acids 1-58 (180). Percentages indicative of similarity to homologous proteins. (B) Sequence alignment generated using Clustal Omega (172). '*' indicates conserved amino acid residues. ':' indicates conservation between amino acids of strongly similar properties. '.' indicates conservation between amino acids of weakly similar properties. Amino acids highlighted in red indicate residues which were mutated for complementation experiments in this study. Length depicted as number of amino acids.

A transposon mutant disrupting *cbu2072* 122 bp from the start codon is unable to replicate within HeLa cells (76). To determine whether this intracellular replication defect could be attributed to transposon disruption of *cbu2072*, this strain was complemented with a constitutively plasmid-expressed version of CBU2072 containing either an N-terminal or C-terminal 3xFLAG-tag (*2072*::Tn pFLAG-2072 and *2072*::Tn p2072-FLAG, respectively). Constitutive expression of both 3xFLAG-CBU2072 and CBU2072-3xFLAG restored intracellular replication of *2072*::Tn in both HeLa epithelial cells and THP-1 macrophage like cells to levels comparable with *C. burnetii* Nine Mile phase II, referred to throughout as wild type (WT) (Figure 5.2 and 5.3). For HeLa cells at 3 days post-infection, the fold change in *C. burnetii* GE, compared to day 0, was 168 ± 103 for WT, 2 ± 4 for *2072*::Tn ($p = 3.30 \times 10^{-2}$ compared to WT), 134 ± 119 for *2072*::Tn pFLAG-2072, and 48 ± 27 for *2072*::Tn p2072-FLAG ($p = 1.03 \times 10^{-1}$ compared to WT) (Figure 5.2A). Visual confirmation of this phenotype demonstrated that, in both HeLa and THP-1 cells, *2072*::Tn was only ever observed as individual bacteria tightly enveloped in LAMP-1 positive membranes (Figure 5.2B and 5.3B). Confirmation of this striking phenotype led to CBU2072 being assigned the name EirA, essential for intracellular replication A.

EirA contains a predicted N-terminal signal peptide sequence or transmembrane domain from amino acid 1-29 (170) or 1-25 (179). To determine the role of this N-terminal signal peptide for EirA, a strain expressing truncated protein was generated (*eirA*::Tn pFLAG-EirA$_{24\text{-}165}$). This strain was unable to restore the intracellular replication defect to WT levels (Figure 5.2 and 5.3), suggesting that the N-terminal region is important for the biological function or correct localisation of EirA. For HeLa cells at 3 days

post-infection, the fold change in *C. burnetii* GE compared to day 0 was 2 ± 0.2, $p = 3.17 \times 10^{-2}$ compared to the 168 ± 103 fold change observed for WT (Figure 5.2A), with similar differences observed in THP-1 cells (Figure 5.3A).

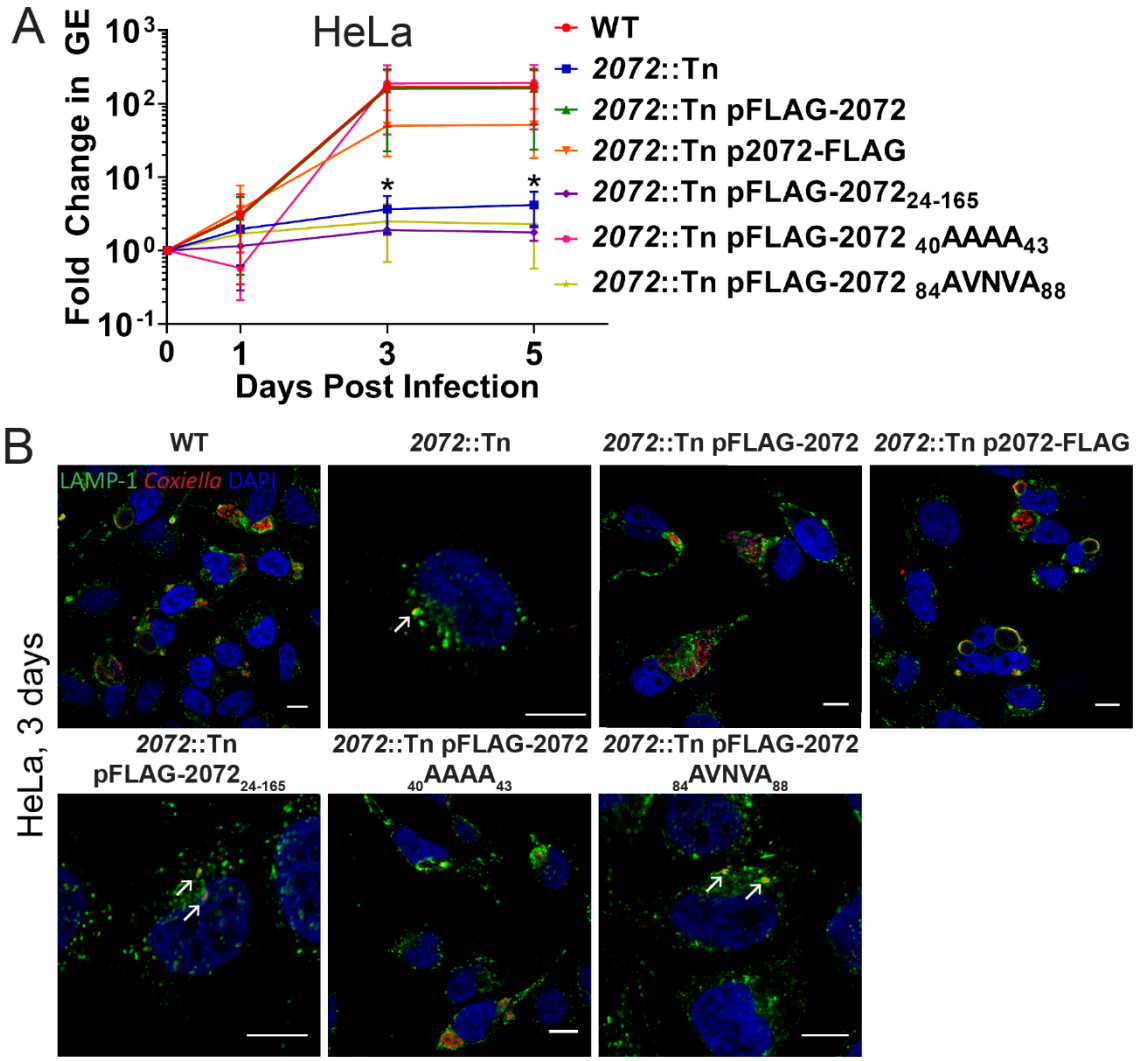

Figure 5.2. CBU2072 is essential for intracellular replication of *C. burnetii*. Intracellular replication of *C. burnetii* WT (red), *2072*::Tn (blue), *2072*::Tn pFLAG-2072 (green), *2072*::Tn p2072-FLAG (orange), *2072*::Tn pFLAG-2072$_{24\text{-}165}$ (purple), *2072*::Tn pFLAG-2072$_{40}$AAAA$_{43}$ (pink) and *2072*::Tn pFLAG-2072$_{84}$AVNVA$_{88}$ (yellow) in HeLa CCL2 cells (A), n = 4 and error bars represent standard deviation. * denotes $p < 0.05$. *p*-values determined using an unpaired student's *t*-test. (B) Representative confocal immunofluorescence images at 3 days post-infection for HeLa CCL2. Cells stained with anti-LAMP-1 (green), anti-*C. burnetii* (red) and DAPI (blue). Scale bar = 10 μm. Arrows indicate individual intracellular *C. burnetii*.

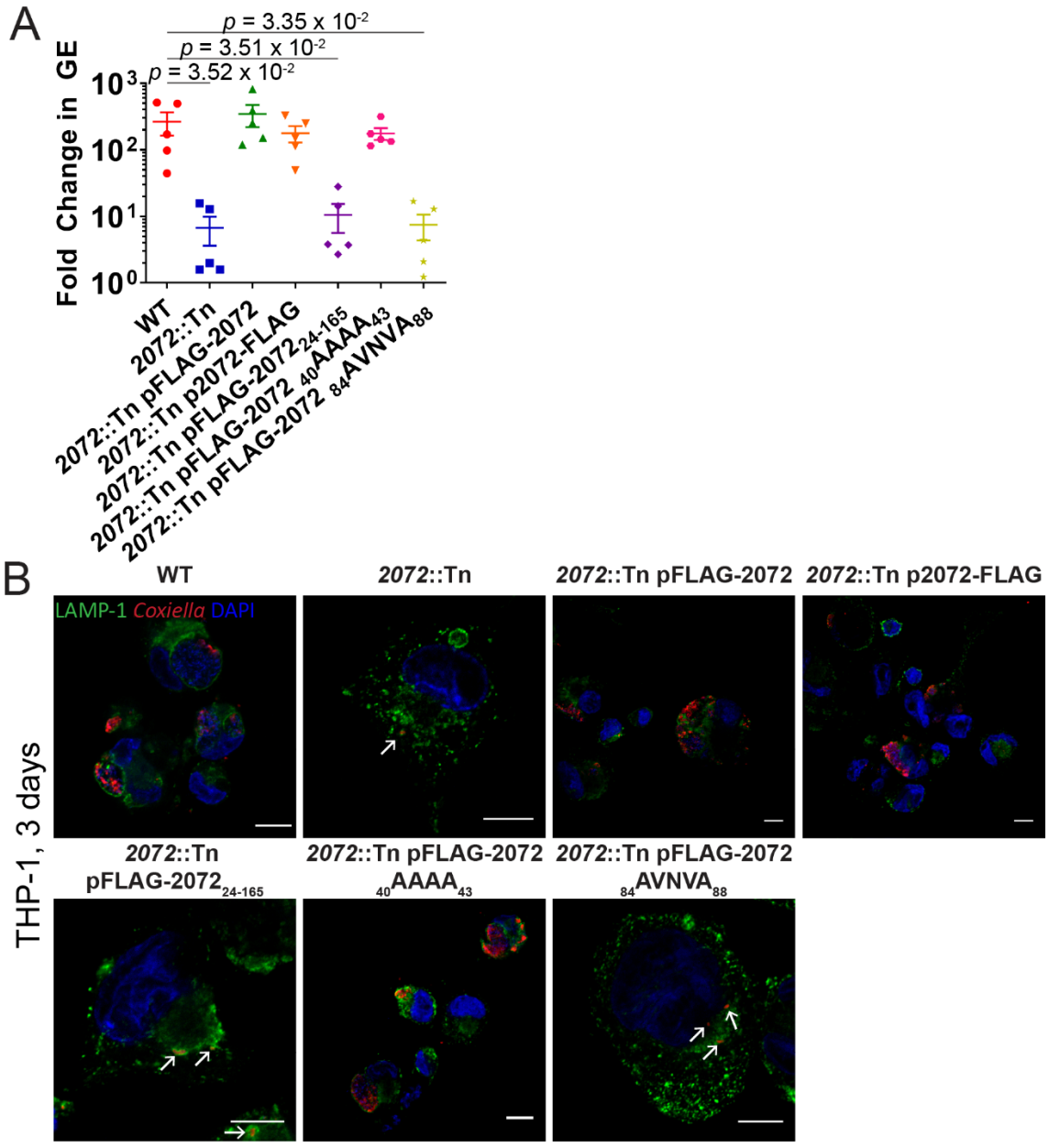

Figure 5.3. Intracellular replication phenotypes are consistent in THP-1 cells. Intracellular replication of *C. burnetii* WT (red), *2072*::Tn (blue), *2072*::Tn pFLAG-2072 (green), *2072*::Tn p2072-FLAG (orange), *2072*::Tn pFLAG-2072$_{24\text{-}165}$ (purple), *2072*::Tn pFLAG-2072$_{40}$AAAA$_{43}$ (pink) and *2072*::Tn pFLAG-2072$_{84}$AVNVA$_{88}$ (yellow) in THP-1 cells (A), n = 5. Data depicts fold change at 3 days post-infection. Error bars represent standard deviation. *p*-values determined using an unpaired student's *t*-test. (B) Representative confocal immunofluorescence images at 3 days post-infection of THP-1 cells. Cells stained with anti-LAMP-1 (green), anti-*C. burnetii* (red) and DAPI (blue). Scale bar = 10 µm. Arrows indicate individual intracellular *C. burnetii*.

In order to identify other regions important for protein function, site directed mutant (SDM) forms of EirA were generated within the region of homology to soluble transhydrogenases. The first SDM altered a cluster of four, conserved residues ($_{40}$PEIS$_{43}$) (Figure 5.1B) into alanines. This mutant version of EirA, EirA$_{40}$AAAA$_{43}$, was cloned into the *C. burnetii* expression plasmid, and used to complement *eirA*::Tn (*eirA*::Tn pFLAG-EirA$_{40}$AAAA$_{43}$). Many soluble transhydrogenases contain a GXXXG motif, which is also found on EirA ($_{84}$GVNVG$_{88}$) (Figure 5.1B). This motif is important for stabilising the structure of binding domains responsible for interacting with FAD and NAD(P) molecules (138). Therefore, another SDM was generated with alanines substituted in place of these glycines, and expressed in *eirA*::Tn (*eirA*::Tn pFLAG-EirA$_{84}$AVNVA$_{88}$). In both HeLa and THP-1 cell models, the *eirA*::Tn pFLAG-EirA$_{40}$AAAA$_{43}$ strain showed replication restored to WT levels (Figure 5.2 and 5.3). However, the *eirA*::Tn pFLAG-EirA$_{84}$AVNVA$_{88}$ was unable to restore intracellular growth, suggesting that this GXXXG motif is important for biological function of EirA (Figure 5.2 and 5.3). For HeLa cells at 3 days post-infection, the fold change in *C. burnetii* GE compared to day 0 for *eirA*::Tn pFLAG-EirA$_{40}$AAAA$_{43}$ was 187 ± 130, $p = 8.47 \times 10^{-1}$ compared to WT. For *eirA*::Tn pFLAG-EirA$_{84}$AVNVA$_{88}$ the fold change was 3 ± 2, $p = 3.17 \times 10^{-2}$ compared to WT (Figure 5.2A). Similar differences were observed in THP-1 cells for both SDM EirA variants (Figure 5.3A).

Recent studies have utilised *Galleria mellonella* larvae to study *C. burnetii* virulence *in vivo*. In this insect model, infection with *C. burnetii* phase II is lethal over an 11 day period (77, 123, 181). To assess whether EirA is required for virulence in this model, *G. mellonella* larvae were infected with 10^6 GE of *C. burnetii* WT, *eirA*::Tn, *eirA*::Tn

pFLAG-EirA and *eirA*::Tn pFLAG-EirA$_{24\text{-}165}$. Survival of the infected larvae was monitored every 24 hours for 11 days. All WT and *eirA*::Tn pFLAG-EirA infected larvae died within 11 days, while all *eirA*::Tn and *eirA*::Tn pFLAG-EirA$_{24\text{-}165}$ infected larvae survived, alongside the PBS control (Figure 5.4A). Isolated infected *G. mellonella* haemocytes, stained with anti-*C. burnetii* and DAPI, showed CCV formation in the WT and *eirA*::Tn pFLAG-EirA infected cells, but *eirA*::Tn and *eirA*::Tn pFLAG-EirA$_{24\text{-}165}$ infected cells presented only individual intracellular *C. burnetii* (Figure 5.4B), consistent with previous observations in HeLa and THP-1 cell models (Figure 5.2B and 5.3B). Overall, these observations support an essential role for *C. burnetii* EirA in intracellular replication and virulence in the *G. mellonella* model and highlight the essentiality of the N-terminal signal peptide for function.

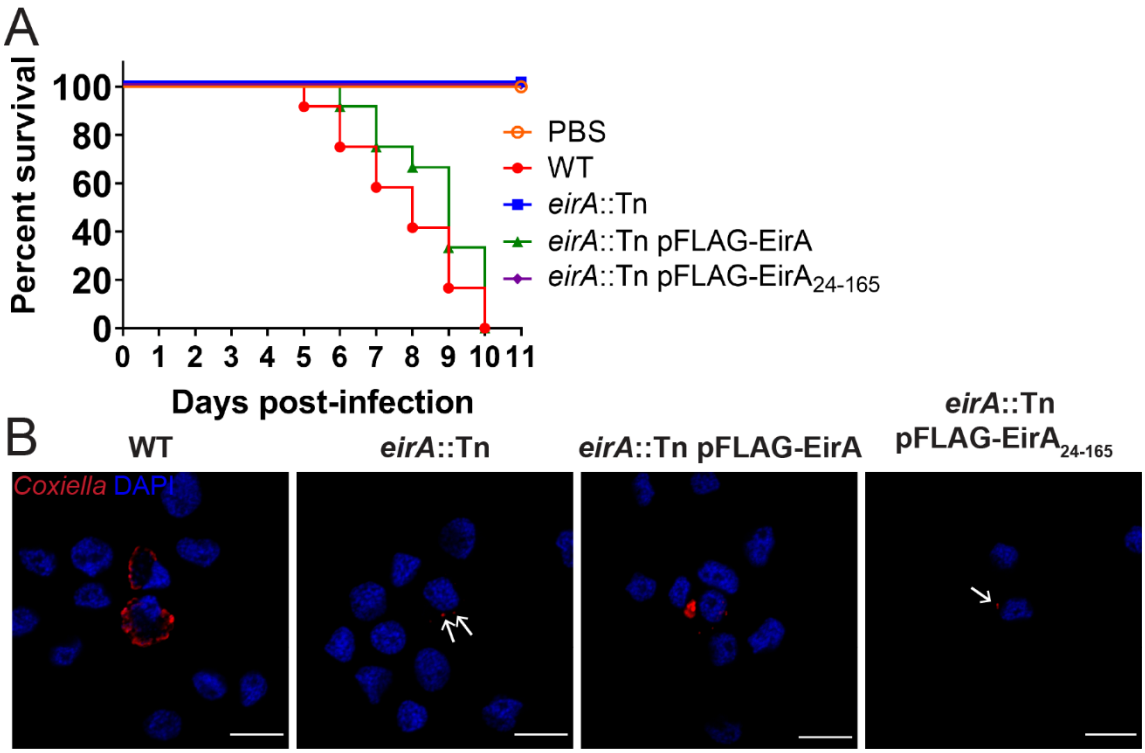

Figure 5.4. EirA is required for virulence in *G. mellonella*. Survival of *G. mellonella* following infection with *C. burnetii* WT (red), *eirA*::Tn (blue), *eirA*::Tn pFLAG-EirA (green) and *eirA*::Tn pFLAG-EirA$_{24\text{-}165}$ (purple) at 10^6 GE (A). A PBS control (orange outline) was also included. Results are shown as a representative of two independent biological replicates, each with 12 larvae per condition. (B) Representative confocal immunofluorescence images at 3 days post-infection of *G. mellonella* hemocytes. Cells stained with anti-*C. burnetii* (red) and DAPI (blue). Scale bar = 10 µm. Arrows indicate individual intracellular *C. burnetii*.

5.2.2 Intracellular replication of the EirA mutant is restored within replication permissive vacuoles

The inability of EirA-deficient *C. burnetii* to replicate intracellularly may indicate that EirA is required to facilitate the replicative environment or may participate in a cell intrinsic aspect of replication that is specific to the intracellular environment. In order to further examine these possibilities, HeLa cells were coinfected with *C. burnetii* WT and *eirA*::Tn at an MOI of 5 for each strain, and replication of the bacteria was visually monitored every 24 hours for 7 days. The transposon disrupting *eirA* also encodes the fluorescent protein mCherry, allowing mutant and WT bacteria to be differentiated during co-infection. By monitoring mCherry fluorescence, *C. burnetii eirA*::Tn displayed intracellular replication in the presence of WT, with large CCVs containing many mCherry-positive *C. burnetii* (*eirA*::Tn) observed by 3 days post-infection (Figure 5.5). This demonstrates that WT *C. burnetii* expressing EirA is able to create an intracellular environment conducive to replication by EirA-deficient *C. burnetii*, thereby supporting a role for EirA in the establishment of the intracellular replicative niche, rather than being required by individual *C. burnetii* for replication.

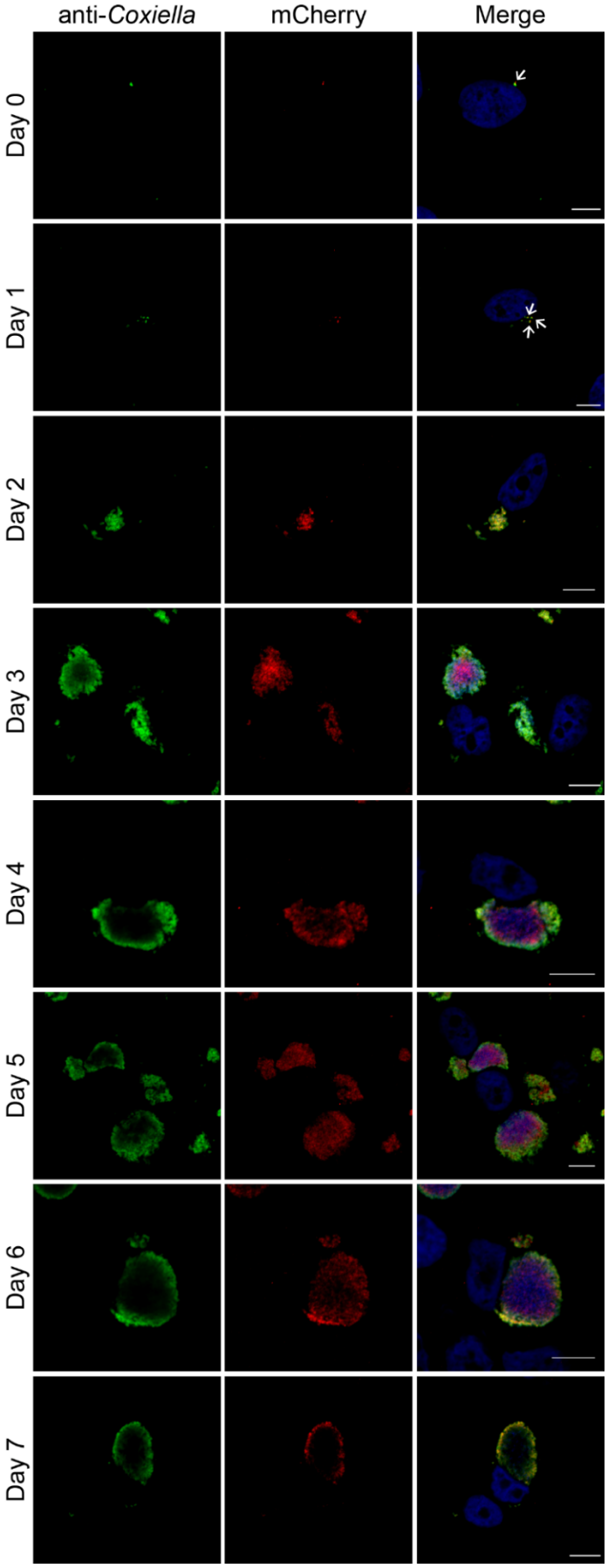
anti-*Coxiella*
mCherry
Merge
Day 0
Day 1
Day 2
Day 3
Day 4
Day 5
Day 6
Day 7

Figure 5.5. *C. burnetii* WT are able to trans-complement *eirA*::Tn during intracellular replication. HeLa CCL2 cells co-infected with *C. burnetii* WT and *eirA*::Tn were fixed and stained every 24 hours across a 7 day infection period. Cells stained with anti-*C. burnetii* (green) and DAPI (blue) while *eirA*::Tn are identified through transposon expression of mCherry (red). Images are representative of three independent biological replicates. Scale bar = 10 μm. Arrows indicate individual intracellular *C. burnetii*.

5.2.3 EirA is not required for intracellular viability of *C. burnetii*

C. burnetii eirA::Tn is observed within individual, tight-fitting LAMP-1 positive vacuoles in both HeLa and THP-1 cells (Figure 5.2 and 5.3). To determine the viability of these bacteria, HeLa cells were infected with *C. burnetii eirA*::Tn at an MOI of 100 and the infection was left to progress for 5 days, allowing for host cell clearance of dead bacteria. At 5 days post-infection, cells were super-infected with either WT or *C. burnetii eirA*::Tn at an MOI of 100, and infection was left to progress for a further 3 days, allowing any viable *C. burnetii eirA*::Tn to replicate in CCVs formed by WT. At this stage, cells were fixed and stained for mCherry and *C. burnetii* to determine whether the *eirA*::Tn mutant was able to replicate (Figure 5.6A). Quantification of fluorescence showed significantly higher levels of mCherry, thereby reflecting the expansion of *eirA*::Tn within the host cell following super-infection with WT (Figure 5.6B). This was further supported by the presence of mCherry-positive CCVs, which were clearly visible in the presence of WT (Figure 5.6C). *C. burnetii eirA*::Tn super-infected with the mutant showed no CCV formation, with only isolated bacteria present intracellularly (Figure 5.6C, arrows). This demonstrates that persistent *C. burnetii eirA*::Tn in individual vacuoles are still viable 5 days post-infection of epithelial host cells.

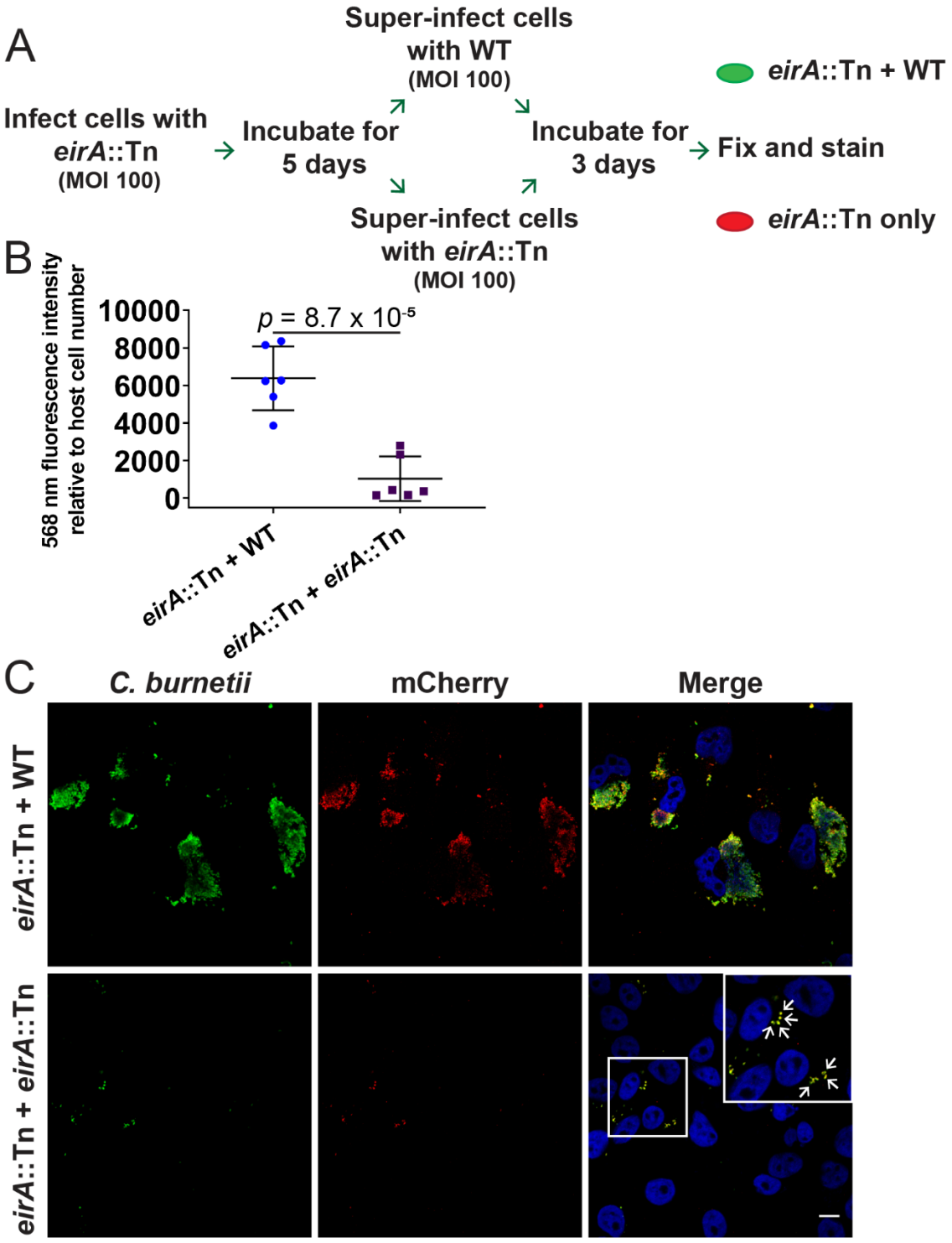

Figure 5.6. EirA is not required for intracellular viability of *C. burnetii*. Schematic representation of experimental procedure (A), in which HeLa cells were infected with *C. burnetii eirA*::Tn and incubated for 5 days, before being super-infected with either *C. burnetii* WT or *eirA*::Tn. After a further 3 days, cells were fixed and stained, and total 568 nm fluorescence levels relative to host cell number was measured using Fiji (147) in

order to quantify mCherry expressing *eirA*::Tn replication (B) n = 6. Error bars represent standard deviation and *p*-value was determined using an unpaired student's *t*-test. (C) Confocal immunofluorescence microscopy images of representative cells stained for all *C. burnetii* (green), mCherry expressing *eirA*::Tn (red) and DAPI (blue). Scale bar = 10 μm. Arrows indicate individual intracellular *C. burnetii*.

5.2.4 EirA is an inner membrane protein of *C. burnetii*

Previous work using mass spectrometry has demonstrated that EirA is present in ACCM-2 culture media during axenic cultivation of *C. burnetii* (182). This was further validated using an inducible, plasmid-expressed C-terminal 3xFLAG-tagged EirA. When expression was induced for 24 hours in transformed WT strains at 2 days post-inoculation, tagged EirA could be detected in the ACCM-2 culture media (182).

Therefore, in order to confirm this finding, *C. burnetii eirA*::Tn, *eirA*::Tn pEirA-FLAG, *eirA*::Tn pFLAG-EirA, and *eirA*::Tn pFLAG-EirA$_{24\text{-}165}$ were harvested at 6 days post-inoculation in ACCM-2, and the presence of EirA in both the bacterial whole cell and the axenic culture media were analysed using immunoblotting techniques as outlined in section 2.10.4 (Figure 5.7).

Despite expression being driven by the same constitutive plasmid, significant differences in protein abundance was observed between each strain (Figure 5.7). For instance, EirA-3xFLAG is more abundant than 3xFLAG-EirA (Figure 5.7C). This may be due to loss of the 3xFLAG tag, which may be cleaved from the N-terminus of this protein, prior to EirA being secreted outside of the bacterial cell. This cleavage may occur due to the N-terminal signal peptide sequence, which is not present in 3xFLAG-EirA$_{24\text{-}165}$. In contrast, EirA-3xFLAG was detected in both the WCL and the culture media (Figure 5.7B). However, there was no observed shift in molecular mass resulting from any cleavage events in EirA-3xFLAG present in the supernatant. A band corresponding to protein of a lower molecular weight was, however, present in the WCL (Figure 5.7B).

This was in contrast to what was observed previously (182), which saw this doublet in the ACCM-2 culture media. In addition, EirA-3xFLAG was present at relatively low levels in ACCM-2, in comparison to the non-functional 3xFLAG-EirA$_{24\text{-}165}$, which was found at a higher proportion in the culture media (Figure 5.7B and D). This suggests that functional, full length EirA may be associated more with the bacterial cell, rather than with the extracellular environment.

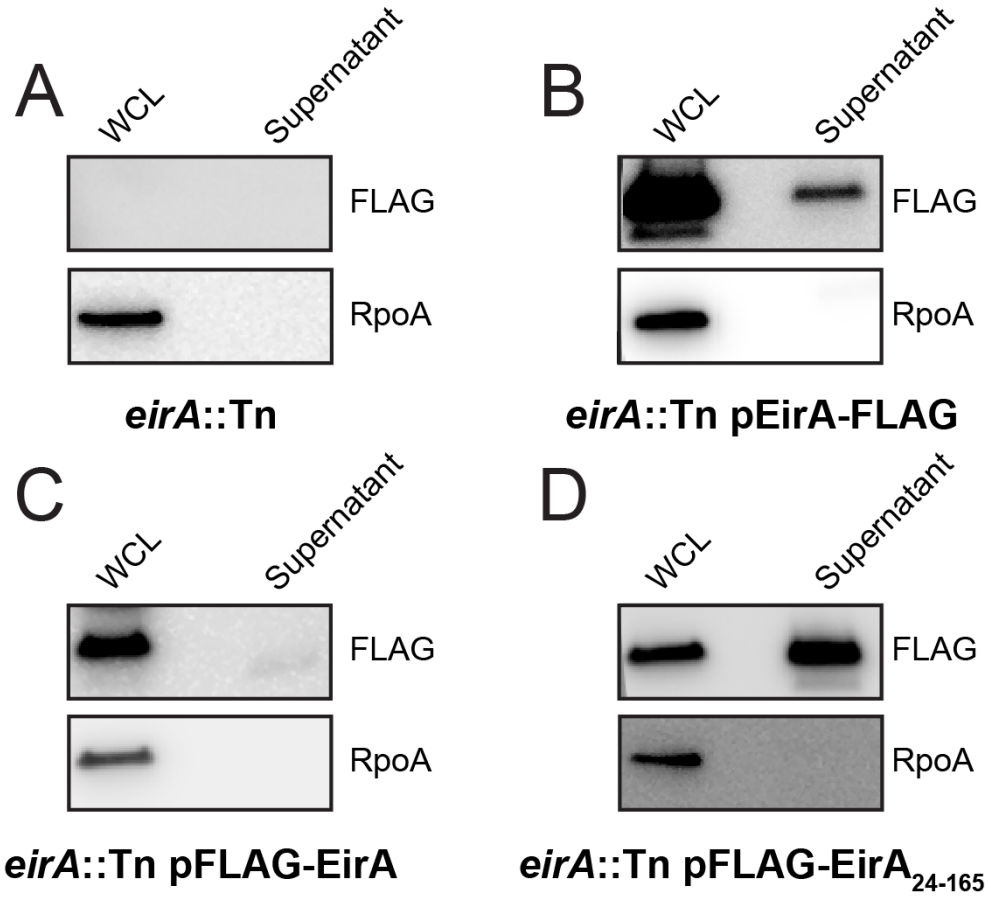

Figure 5.7. Functional EirA is predominantly retained within *C. burnetii* whole cell. Whole cell lysates (WCL) of *C. burnetii eirA*::Tn (A), *eirA*::Tn pEirA-FLAG (B), *eirA*::Tn pFLAG-EirA (C), and *eirA*::Tn pFLAG-EirA$_{24\text{-}165}$ (D) alongside TCA precipitated ACCM-2 media (supernatant) used to cultivate each respective strain were probed with anti-FLAG antibodies to determine EirA localisation. RpoA was used as a cytoplasmic loading control to ensure ACCM-2 culture media did not contain any *C. burnetii* contamination. Blots are representative of three independent biological replicates.

To address the potential loss of 3xFLAG tag from EirA, antibody against EirA was raised using recombinant MBP-EirA$_{24\text{-}165}$ (WEHI antibody facility) as outlined in section 2.10.2 (Figure 5.8). As anticipated, plasmid expression of EirA was confirmed to produce more EirA than what is found during native expression, as can be seen when comparing expression levels between *eirA*::Tn pFLAG-EirA and WT (Figure 5.8).

Comparison of EirA expression using EirA and FLAG antibody demonstrates that while 3xFLAG-EirA expression seems higher than 3xFLAG-EirA$_{24\text{-}165}$ using anti-EirA antibodies, the opposite is true when using anti-FLAG antibodies. This further supports the possibility that the 3xFLAG tag is cleaved in the *eirA*::Tn pFLAG-EirA strain, which is dependent on the N-terminal signal peptide that is not present in 3xFLAG-EirA$_{24\text{-}165}$.

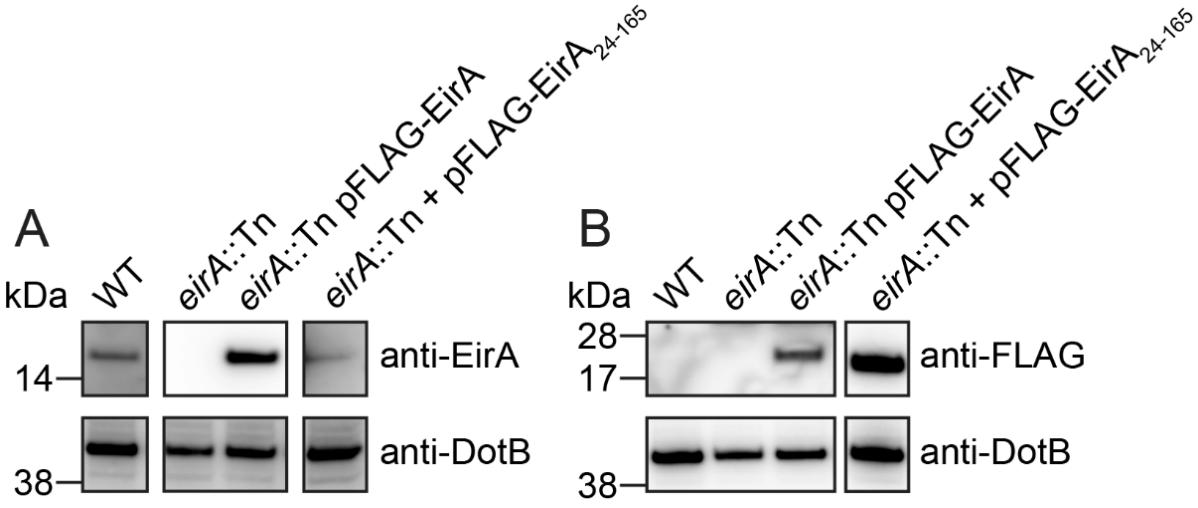

Figure 5.8. Western blot confirming specificity of anti-EirA antibody to EirA. Whole cell lysates of strains used for subcellular fractionations were probed with anti-EirA (A) or anti-FLAG (B). DotB was used as a cytoplasmic loading control. Blots were segmented

to account for different protein expression levels requiring different exposure times in each strain.

To further investigate the localisation of EirA within the bacterial cell, axenically grown *C. burnetii* WT, *eirA*::Tn, *eirA*::Tn pFLAG-EirA and *eirA*::Tn pFLAG-EirA$_{24\text{-}165}$ strains were fractionated and EirA subcellular localisation was monitored in each strain (Figure 5.9). Each isolated fraction was also probed with antibodies against the T4BSS outer membrane core complex protein IcmK (OM), periplasmic protein IcmX, inner membrane component IcmD (IM), and cytoplasmic ATPase DotB (Cyto) (183) to validate the fractionation process.

All forms of EirA, including truncated 3xFLAG-EirA$_{24\text{-}165}$, were detected in both the bacterial cytoplasm and the TX-100 soluble membrane fraction (referred to throughout as the inner membrane fraction). EirA in the inner membrane fraction consistently demonstrated slightly higher apparent molecular weight than the cytoplasmic band (Figure 5.9), suggesting that the inner membrane localised EirA may be modified.

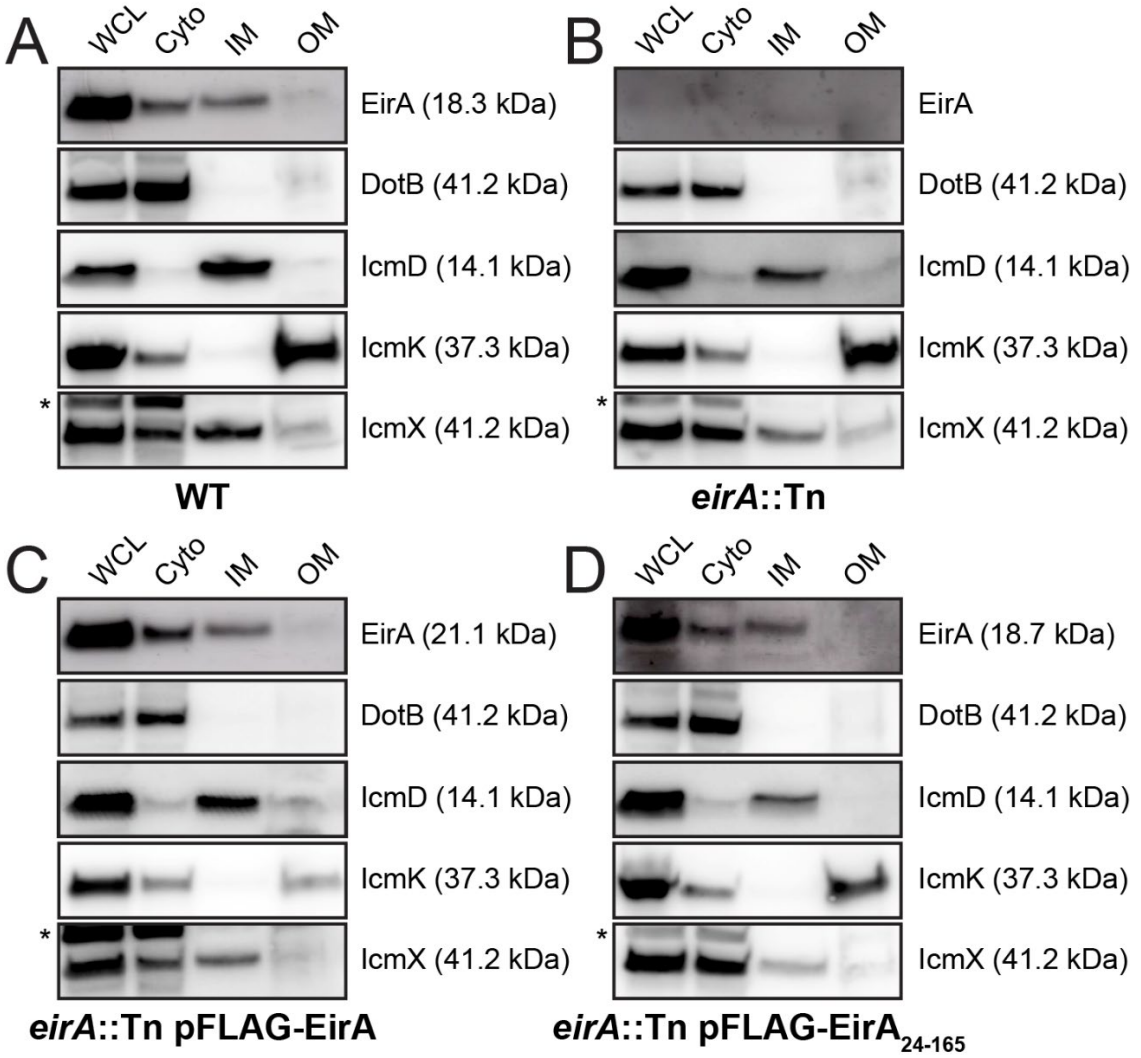

Figure 5.9. EirA localise to the bacterial cytoplasm and TX-100 soluble membrane fraction. Subcellular fractionations of *C. burnetii* WT (A), *eirA*::Tn (B), *eirA*::Tn pFLAG-EirA (C) and *eirA*::Tn pFLAG-EirA$_{24\text{-}165}$ (D) were performed to observe the subcellular localisation of EirA within the bacterial cell. DotB (cyto/cytoplasm), IcmK (TX-100 insoluble/OM/outer membrane), IcmD (TX-100 soluble/IM/inner membrane) and IcmX (periplasm) were used to denote specific subcellular localisations as well as whole cell lysate (WCL). Blots are representative of three independent biological replicates. * denotes non-specific bands.

5.2.5 EirA function does not appear to be related to tolerance of a high oxidative stress environment

C. burnetii must withstand the highly oxidative environment of the host phagolysosome in order to replicate. The *eirA*::Tn mutant appears unable to replicate within this environment, which suggests that the function of EirA may relate to tolerance of this harsh intracellular niche. In order to determine whether EirA expression leads to increased tolerance of oxidative stress, *E. coli* DH5α strains expressing 3xFLAG tagged EirA derivatives (Figure 5.10A) were exposed to hydrogen peroxide for 24 hours, and survival was compared to strains not expressing EirA. There were no significant differences to hydrogen peroxide tolerance across all strains (Figure 5.10B). This suggests that there are no observable advantages in *E. coli* strains to oxidative stress tolerance with EirA expression.

As hydrogen peroxide is unstable in the ACCM-2 medium, the peroxide experiments were conducted in *E. coli*. To test oxidative stress resistance in *C. burnetii*, varying concentrations of glutathione (GSH) was added to both *C. burnetii* WT and *eirA*::Tn during infection in HeLa cells, to determine whether the antioxidant could rescue replication of the mutant strain (184). Increasing concentrations of GSH caused host cell toxicity, leading to fewer numbers of HeLa cells remaining at 3 days post-infection (Figure 5.10C). There was no difference to intracellular replication in the *eirA*::Tn strain, even in the presence of GSH at physiological (10 mM) and higher concentrations (Figure 5.10C) (184), demonstrating that the intracellular replication defect observed in the absence of EirA is not rescuable with the addition of antioxidants.

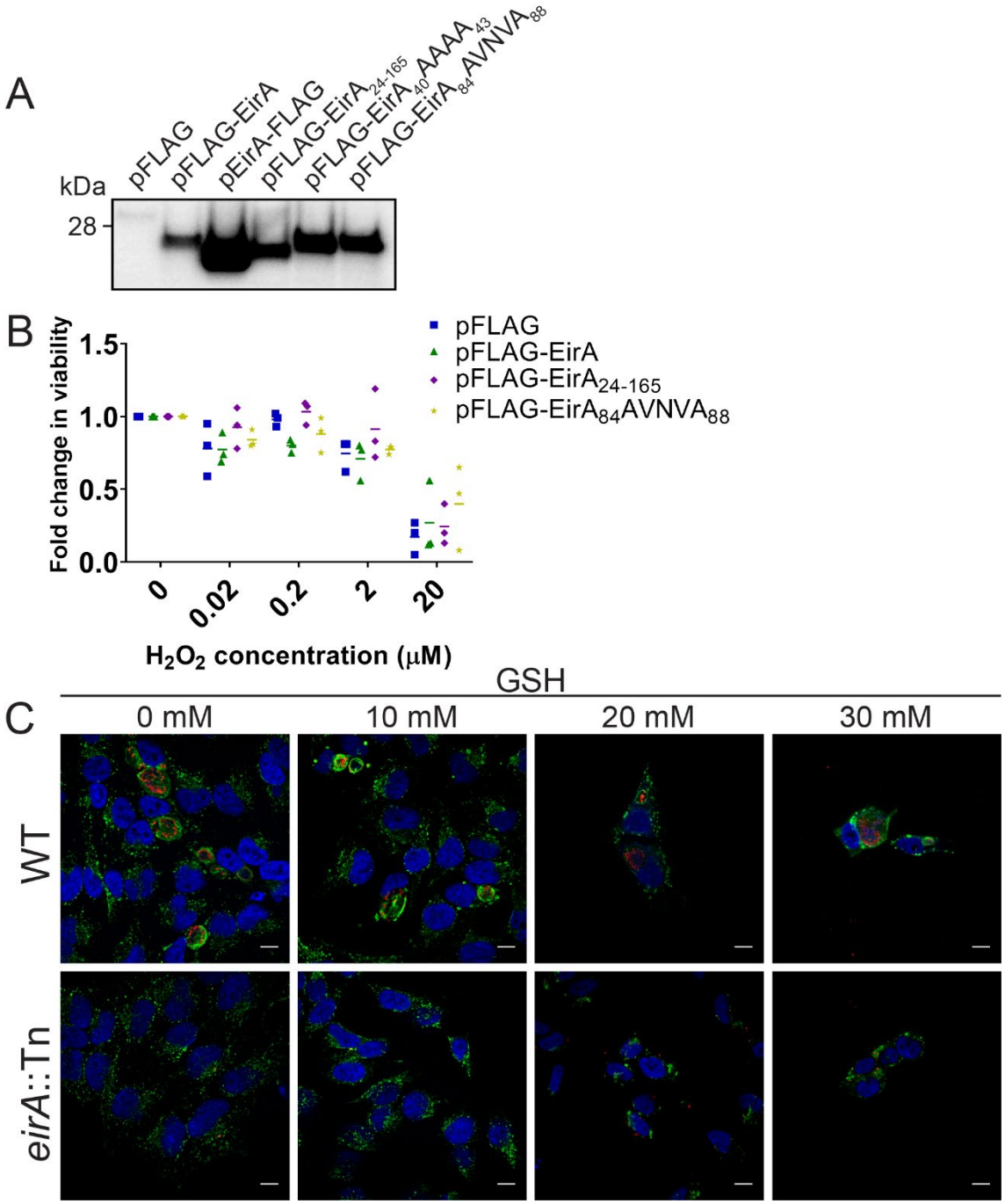

Figure 5.10. EirA function does not relate to oxidative stress tolerance. (A) Anti-FLAG western blot of *E. coli* strains expressing various versions of EirA. These strains were exposed to varying concentrations of hydrogen peroxide for 24 hours before bacterial colonies were counted (B). Fold change relative to before hydrogen peroxide exposure. (C) *C. burnetii* WT and *eirA*::Tn were exposed to varying concentrations of the antioxidant glutathione (GSH) during infection in HeLa cells. Images representative of

cells at 3 days post-infection and exposure to GSH. Cells stained with anti-LAMP-1 (green), anti-*C. burnetii* (red) and DAPI (blue). Scale bar = 10 μm.

5.2.6 EirA influences *C. burnetii* metabolism

EirA contains low homology to soluble transhydrogenases of *E. coli* between amino acids 24-96, and the conserved GXXXG motif within this region is required for EirA to facilitate intracellular replication of *C. burnetii* (Figure 5.2 and 5.3) (93, 126, 133, 137). In order to determine whether EirA has a significant effect on *C. burnetii* metabolism, polar metabolites were extracted from axenically cultivated *C. burnetii* WT and *eirA*::Tn and analysed by gas chromatography/mass spectrometry (GC/MS) and liquid chromatography/MS (LC/MS) as outlined in section 2.7 (Figure 5.11, Table 5.1 and 5.2, Appendix 2). Loss of EirA was associated with a significant increase in intracellular levels of NADH and decrease in NADP, consistent with a potential role for this protein in regulating the equilibrium between these essential cofactors. Given that these cofactors are utilised in both anabolic and catabolic processes, loss of EirA was also associated with global changes in many other metabolites, including most amino acids, and cell wall precursors (*meso*-2,6-diaminopimelate and LL-2,6-diaminopimelate) (Figure 5.11) (185). The decreased intermediates in the TCA cycle (malate and succinate) could reflect decreased oxidative phosphorylation and/or increased anaplerotic synthesis of non-essential amino acids such as aspartate and glutamate, which were both increased in abundance in the mutant (Figure 5.11).

Interestingly, overexpression of 3xFLAG-EirA in the *eirA*::Tn strain generated further global changes in intracellular metabolite levels, indicating a possible stress response. Fold change data comparing the *eirA*::Tn pFLAG-EirA strain to WT and *eirA*::Tn are presented in Table 5.3 and 5.4. Overall, these data strongly suggest that EirA influences bacterial cell metabolism, possibly by altering intracellular levels of NADH and NADP.

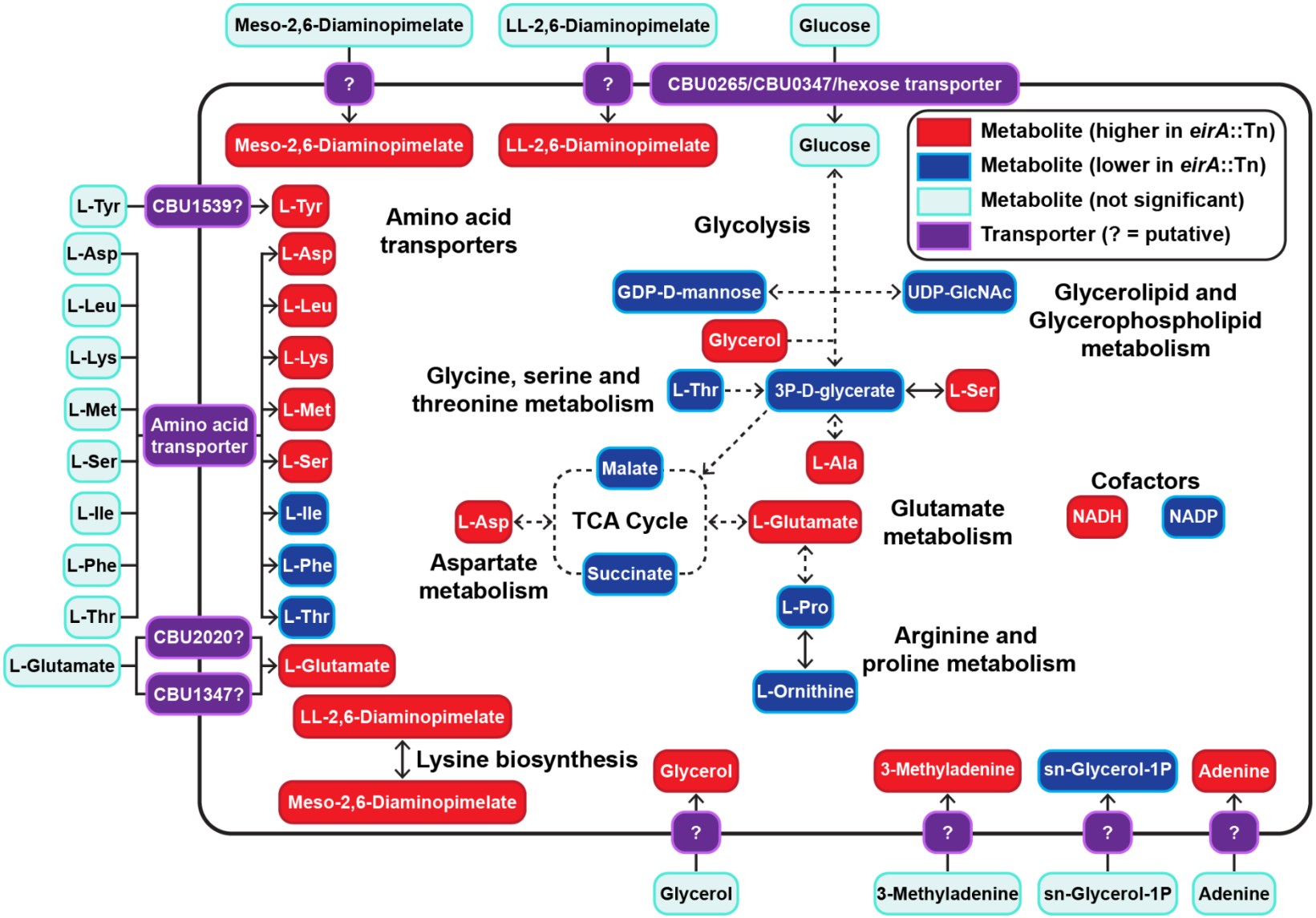
Meso-2,6-Diaminopimelate
LL-2,6-Diaminopimelate
Glucose
?
?
CBU0265/CBU0347/hexose transporter
Meso-2,6-Diaminopimelate
LL-2,6-Diaminopimelate
Glucose
Metabolite (higher in eirA::Tn)
Metabolite (lower in eirA::Tn)
Metabolite (not significant)
Transporter (? = putative)
L-Tyr
CBU1539?
L-Tyr
Amino acid transporters
Glycolysis
L-Asp
L-Leu
L-Lys
L-Met
L-Ser
L-Ile
L-Phe
L-Thr
Amino acid transporter
L-Asp
L-Leu
L-Lys
L-Met
L-Ser
L-Ile
L-Phe
L-Thr
GDP-D-mannose
UDP-GlcNAc
Glycerolipid and Glycerophospholipid metabolism
Glycerol
Glycine, serine and threonine metabolism
L-Thr
3P-D-glycerate
L-Ser
L-Ala
Malate
L-Asp
TCA Cycle
L-Glutamate
Glutamate metabolism
Cofactors
NADH
NADP
Aspartate metabolism
Succinate
L-Pro
Arginine and proline metabolism
L-Ornithine
CBU2020?
CBU1347?
L-Glutamate
L-Glutamate
LL-2,6-Diaminopimelate
Lysine biosynthesis
Meso-2,6-Diaminopimelate
Glycerol
3-Methyladenine
sn-Glycerol-1P
Adenine
?
?
?
?
Glycerol
3-Methyladenine
sn-Glycerol-1P
Adenine

Figure 5.11. Absence of EirA leads to accumulation of some amino acids and significantly lower glycolytic and TCA cycle activities. Metabolites detected on the GC/MS and/or LC/MS that were significantly different in abundance between *C. burnetii eirA*::Tn and WT. Red denotes metabolites which were significantly higher in abundance in *C. burnetii eirA*::Tn and blue denotes metabolites which were significantly lower in abundance in *C. burnetii eirA*::Tn. $p < 0.05$, BH-adjusted unpaired *t*-test. Pale blue denotes metabolites which were not significantly different. Purple denotes metabolite transporters, where '?' indicates those with putative functions. Dotted arrows indicate pathways which have been abbreviated. Metabolite abbreviations are listed in Appendix 2.

Table 5.1. Metabolites identified as significantly different in abundance between *C. burnetii eirA*::Tn and WT using GC/MS.

Metabolite	Fold change[A]	BH-adjusted *p*-value[B]
L-Pro	-1.33	1.52×10^{-5}
sn-Glycerol-1P	-0.94	6.97×10^{-4}
L-Ornithine	-0.82	2.95×10^{-3}
3P-D-glycerate	-0.68	1.20×10^{-2}
Succinate	-0.60	2.24×10^{-2}
L-Ile	-0.58	7.73×10^{-3}
L-Phe	-0.58	2.13×10^{-2}
Malate	-0.57	3.02×10^{-2}
L-Ala	0.54	2.37×10^{-2}
LL-2,6-Diaminopimelate	0.90	1.20×10^{-2}
L-Asp	**0.88**	**2.95×10^{-3}**
Adenine	4.44	5.93×10^{-5}
L-Glu	**4.66**	**1.73×10^{-4}**
Glycerol	4.66	3.57×10^{-2}

Metabolites in bold were detected in both GC/MS and LC/MS platforms. [A]Positive fold change value denotes metabolites with significantly high abundance, while negative fold change value denotes metabolites with significantly lower abundance in *C. burnetii eirA*::Tn samples. [B]Benjamini-Hochberg (BH).

Table 5.2. Metabolites identified as significantly different in abundance between *C. burnetii eirA*::Tn and WT using LC/MS.

Metabolite	Fold change[A]	BH-adjusted *p*-value[B]
NADP	-0.50	1.22×10^{-2}
UDP-GlcNAc	-0.37	1.41×10^{-2}
GDP-D-mannose	-0.32	1.55×10^{-2}
L-Tyr	0.24	1.19×10^{-2}
NADH	0.33	3.67×10^{-2}
L-Leu	0.38	2.42×10^{-2}
L-Met	0.43	1.04×10^{-3}
3'-Methyladenine	0.57	1.55×10^{-2}
L-Ser	0.59	1.60×10^{-3}
L-Asp	**0.62**	**3.56×10^{-3}**
L-Glu	**0.70**	**2.55×10^{-5}**
meso-2,6-Diaminopimelate	0.86	3.43×10^{-3}
L-Lys	1.04	9.28×10^{-3}

Metabolites in bold were detected in both GC/MS and LC/MS platforms. [A]Positive fold change value denotes metabolites with significantly high abundance, while negative fold change value denotes metabolites with significantly lower abundance in *C. burnetii eirA*::Tn samples. [B]Benjamini-Hochberg (BH).

Table 5.3. Metabolites identified as significantly different when comparing *eirA*::Tn pFLAG-EirA to WT.

Metabolite	Fold change[A]	BH-adjusted *p*-value[B]
R5P	-3.46	2.43×10^{-6}
Orotate	-3.29	1.29×10^{-5}
2'-Methylcitrate	-3.28	5.36×10^{-4}
Inosine	-3.09	9.18×10^{-6}
2-Deoxyribose-5P	-2.84	7.94×10^{-4}
Adenine	-2.40	6.62×10^{-6}
Biotin	-2.29	2.61×10^{-3}
L-Pro	-2.06	3.60×10^{-7}
UMP	-1.96	7.24×10^{-5}
Uridine	-1.94	9.86×10^{-4}
Uracil	-1.92	1.30×10^{-4}
Biopterin	-1.70	1.59×10^{-2}
G6P	-1.63	5.55×10^{-3}
F6P	-1.63	5.55×10^{-3}
D-Galactono-1,4-lactone	-1.61	1.90×10^{-2}
Xanthine	-1.29	2.43×10^{-6}
IMP	-1.25	8.29×10^{-6}
UDP-GlcNAc	-1.20	2.50×10^{-5}
GDP-D-mannose	-1.14	5.63×10^{-6}
dCMP	-1.11	6.81×10^{-3}
D-Glucono-1,4-lactone	-1.08	9.68×10^{-3}
AMP	-0.85	2.43×10^{-6}
dGMP	-0.85	2.43×10^{-6}
L-Val	-0.83	1.19×10^{-2}
D-Galactarate	-0.83	7.94×10^{-4}
L-Ornithine	-0.77	2.09×10^{-2}
L-Ile	-0.61	5.55×10^{-3}
GSH	-0.59	5.78×10^{-6}
D-Fructose	-0.56	9.02×10^{-3}
IDP	-0.54	2.30×10^{-3}
D-Gluconate	-0.46	1.63×10^{-3}
ADP	-0.46	5.36×10^{-4}
NADP	-0.46	5.55×10^{-3}

L-Tyr	0.16	1.76×10^{-2}
L-Cystathione	0.24	2.87×10^{-3}
NADH	0.45	3.78×10^{-3}
L-Citrulline	0.62	3.68×10^{-2}
L-Met	0.69	2.43×10^{-6}
L-Leu	0.78	2.88×10^{-4}
3'-Methyladenine	0.87	9.59×10^{-4}
L-Glu	1.08	2.43×10^{-6}
L-Ser	1.08	5.97×10^{-6}
L-Asp	1.22	4.02×10^{-5}
L-Arg	1.40	1.73×10^{-3}
L-Lys	1.50	1.43×10^{-4}
meso-2,6-Diaminopimelate	1.50	4.85×10^{-5}
dIMP	1.68	3.62×10^{-2}

[A]Positive fold change value denotes metabolites with significantly high abundance, while negative fold change value denotes metabolites with significantly lower abundance in *C. burnetii eirA*::Tn pFLAG-EirA samples. [B]Benjamini-Hochberg (BH).

Table 5.4. Metabolites identified as significantly different when comparing *eirA*::Tn pFLAG-EirA to *eirA*::Tn.

Metabolite	Fold change	BH-adjusted *p*-value
dIMP	-1.43	6.16×10^{-3}
L-Arg	-0.65	1.79×10^{-6}
meso-2,6-Diaminopimelate	-0.64	9.55×10^{-7}
L-Asp	-0.60	1.31×10^{-6}
L-Ser	-0.49	4.46×10^{-6}
L-Lys	-0.46	4.83×10^{-3}
L-Leu	-0.40	1.26×10^{-4}
L-Glu	-0.39	3.18×10^{-5}
GMP	-0.37	4.09×10^{-2}
Pthalate	-0.37	4.60×10^{-3}
L-Cysteate	-0.30	2.51×10^{-3}
3'-Methyladenine	-0.30	1.11×10^{-5}
N-Acetyl-L-Lysine	-0.29	1.27×10^{-3}
Oxalate	-0.29	1.27×10^{-3}
Succinate	-0.28	1.48×10^{-4}
Methylmalonate	-0.28	1.48×10^{-4}
L-Met	-0.26	3.38×10^{-3}
L-Thr	-0.23	6.36×10^{-3}
L-Citrulline	-0.18	1.42×10^{-2}
L-Cystathione	-0.18	3.70×10^{-3}

ADP	0.25	6.16×10^{-3}
L-Ile	0.28	8.54×10^{-3}
D-Mannitol	0.28	1.39×10^{-2}
IDP	0.38	7.75×10^{-3}
D-Sorbitol	0.43	3.14×10^{-2}
L-Val	0.51	5.69×10^{-4}
Homoserine	0.51	1.00×10^{-4}
GSH	0.52	3.18×10^{-5}
D-Galactarate	0.56	2.29×10^{-4}
D-Gluconate	0.59	3.34×10^{-4}
dGMP	0.64	2.49×10^{-3}
AMP	0.66	1.50×10^{-3}
L-Ornithine	0.67	2.11×10^{-4}
D-Fructose	0.77	2.29×10^{-4}
GDP-D-mannose	0.81	3.05×10^{-5}
UDP-GlcNAc	0.83	1.19×10^{-4}
D-Glucono-1,4-lactone	0.85	1.40×10^{-3}
IMP	1.02	1.48×10^{-4}
PEP	1.32	2.17×10^{-2}
dCMP	1.32	2.50×10^{-6}
Uracil	1.36	3.52×10^{-3}
UMP	1.46	4.15×10^{-5}
G6P	1.56	6.16×10^{-3}
F6P	1.56	6.16×10^{-3}
Biopterin	1.75	1.02×10^{-2}
L-Pro	1.92	2.48×10^{-7}
Adenine	2.34	2.50×10^{-6}
Uridine	2.35	2.35×10^{-4}
Biotin	2.66	2.04×10^{-3}
2-Deoxyribose-5P	2.68	5.69×10^{-4}
Orotate	2.70	1.30×10^{-4}
2'-Methylcitrate	2.78	1.48×10^{-4}
Inosine	3.22	2.48×10^{-7}
R5P	3.37	2.48×10^{-7}

[A]Positive fold change value denotes metabolites with significantly high abundance, while negative fold change value denotes metabolites with significantly lower abundance in *C. burnetii eirA*::Tn pFLAG-EirA samples. [B]Benjamini-Hochberg (BH).

5.2.7 EirA is not required for cell membrane integrity

The diamino acids *meso*-2,6-diaminopimelate and LL-2,6-diaminopimelate form part of the lysine biosynthesis pathway in *C. burnetii* (Appendix 3). However, these metabolites also serve as precursors for the bacterial peptidoglycan cell wall (185). During the conversion of UDP-MurNAc-dipeptide into UDP-MurNAc-tripeptide, the muramyl ligase MurE incorporate diamino acids in the growing UDP-MurNAc peptide chain (186, 187).

The accumulation of these metabolites in *C. burnetii eirA*::Tn indicated that EirA may indirectly or directly modulate metabolic pathways involved in cell wall biosynthesis. Such a role would also be consistent with partial localisation of EirA to the inner membrane of *C. burnetii*. Therefore, the impact of EirA on the susceptibility of *C. burnetii* to stressors of cell membrane integrity was investigated. Axenically grown *C. burnetii* WT, *eirA*::Tn, *eirA*::Tn pFLAG-EirA and *eirA*::Tn pFLAG-EirA$_{24\text{-}165}$ were treated with either ampicillin, a cell wall stressor, or polymyxin B, an outer membrane stressor, at varying concentrations at 4 days post-inoculation. Both before antibiotic treatment and at 24 hours post-antibiotic exposure, samples were harvested for genome equivalent quantification, and serial dilutions of *C. burnetii* were plated for colony forming unit quantification. No significant differences in antibiotic susceptibility were observed between the strains across all concentrations of antibiotics (Figure 5.12A-B). This may indicate that EirA does not have a functional role in cell membrane integrity. In support of this, transmission electron microscopy (TEM) images of *C. burnetii* WT, *eirA*::Tn and *eirA*::Tn pFLAG-EirA demonstrate no gross differences in bacterial morphology or cell membrane structure (Figure 5.12C). Despite observation of

significant differences in metabolite composition, these experiments could not demonstrate any EirA-dependent alterations to cell membrane integrity or bacterial morphology.

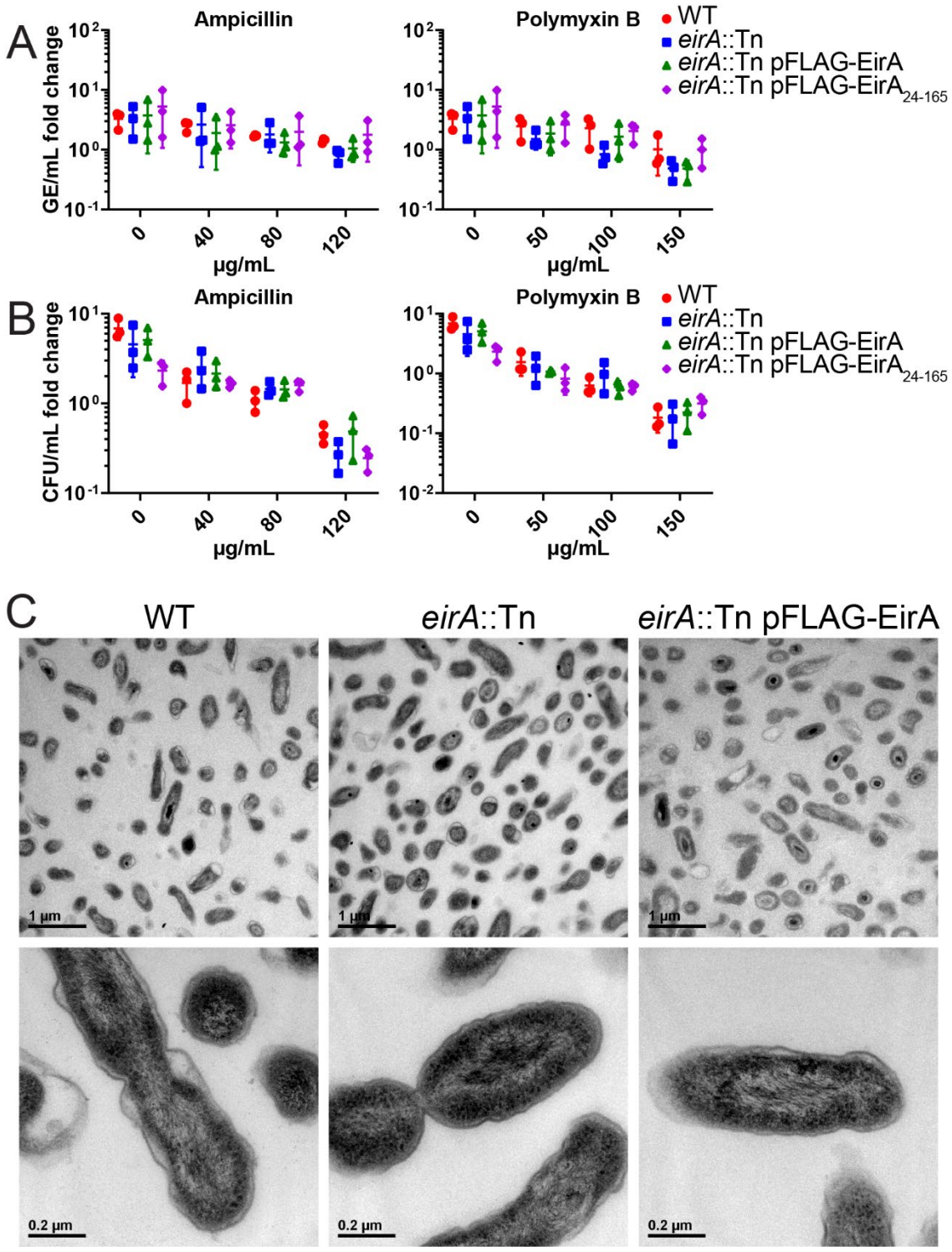

Figure 5.12. Absence of EirA does not impact susceptibility to cell membrane stressors or effect overall gross morphology of *C. burnetii*. *C. burnetii* WT, *eirA*::Tn, *eirA*::Tn pFLAG-EirA, *eirA*::Tn pFLAG-EirA$_{24\text{-}165}$ were exposed to varying concentrations of either ampicillin or polymyxin B at 4 days post-inoculation, and impact on bacterial viability was quantified at 24 hours post-treatment by genome

equivalents (GE) (A) and colony forming units (CFU)/mL (B). Fold change depicts bacterial numbers at 24 hours post-treatment, relative to numbers pre-treatment. In any one treatment group, no significant differences in GE and CFU were observed based on an unpaired student's *t*-test (C) *C. burnetii* WT, *eirA*::Tn and *eirA*::Tn pFLAG-EirA were grown for 6 days in ACCM-2 before being imaged using transmission electron microscopy (TEM). Scale bars for top panel = 1 μm and bottom panel = 0.2 μm. Images are representative of two technical replicates.

5.2.8 Translocation of effector proteins via the T4BSS is blocked in the absence of EirA

EirA is not a substrate of the T4BSS, as a β-lactamase (BlaM) EirA fusion protein was not translocated into the host cell cytosol during infection (76). Considering the inner membrane localisation of EirA, and the mutant phenotype mirroring that of a *dot/icm* mutation (107, 108), it was hypothesised that EirA may contribute to T4BSS function. In order to determine whether EirA is involved in T4BSS effector translocation, a BlaM translocation assay was performed using the characterised *C. burnetii* effector protein MceA. Expression of BlaM-MceA provides a robust reporter system which has been extensively used to monitor T4BSS activity in *C. burnetii* (70, 71, 76, 107, 120, 188). BlaM fusion protein translocation was determined by monitoring cleavage of the fluorescent BlaM substrate CCF2-AM and calculating the 450:520 nm fluorescence emission ratio 2 hours post-addition of CCF2-AM. HeLa cells were infected with either WT, WT pBlaM-MceA, *eirA*::Tn or *eirA*::Tn pBlaM-MceA, or a combination of these strains (Figure 5.13A-B). At both 48 and 72 hours post-infection, translocation of BlaM-MceA was observed in the WT pBlaM-MceA strain as expected (Figure 5.13A-B). However, even when replication was restored through coinfection with WT, the *eirA*::Tn pBlaM-MceA infected cells did not show any translocation of BlaM-MceA.

The requirement of EirA for T4BSS effector translocation was further confirmed using confocal immunofluorescence microscopy. *C. burnetii* expressing 3xFLAG-MceA shows distinct anti-FLAG signal at host mitochondria during infection (120), however this mitochondrial signal was not observed with *eirA*::Tn expressing 3xFLAG-MceA, even when co-infection with *C. burnetii* WT facilitated CCV formation (Figure 5.13C). Both

the BlaM reporter assay and immunofluorescence microscopy approaches employed here demonstrate that EirA is required for *C. burnetii* T4BSS effector translocation.

Given that the absence of EirA prevents T4BSS effector translocation, it is possible that EirA may have a functional role regulating the assembly of the T4BSS apparatus or expression levels. However, the subcellular fractionations performed here demonstrate no change in DotB, IcmD, IcmK and IcmX expression and localisation in the absence of functional EirA (Figure 5.9).

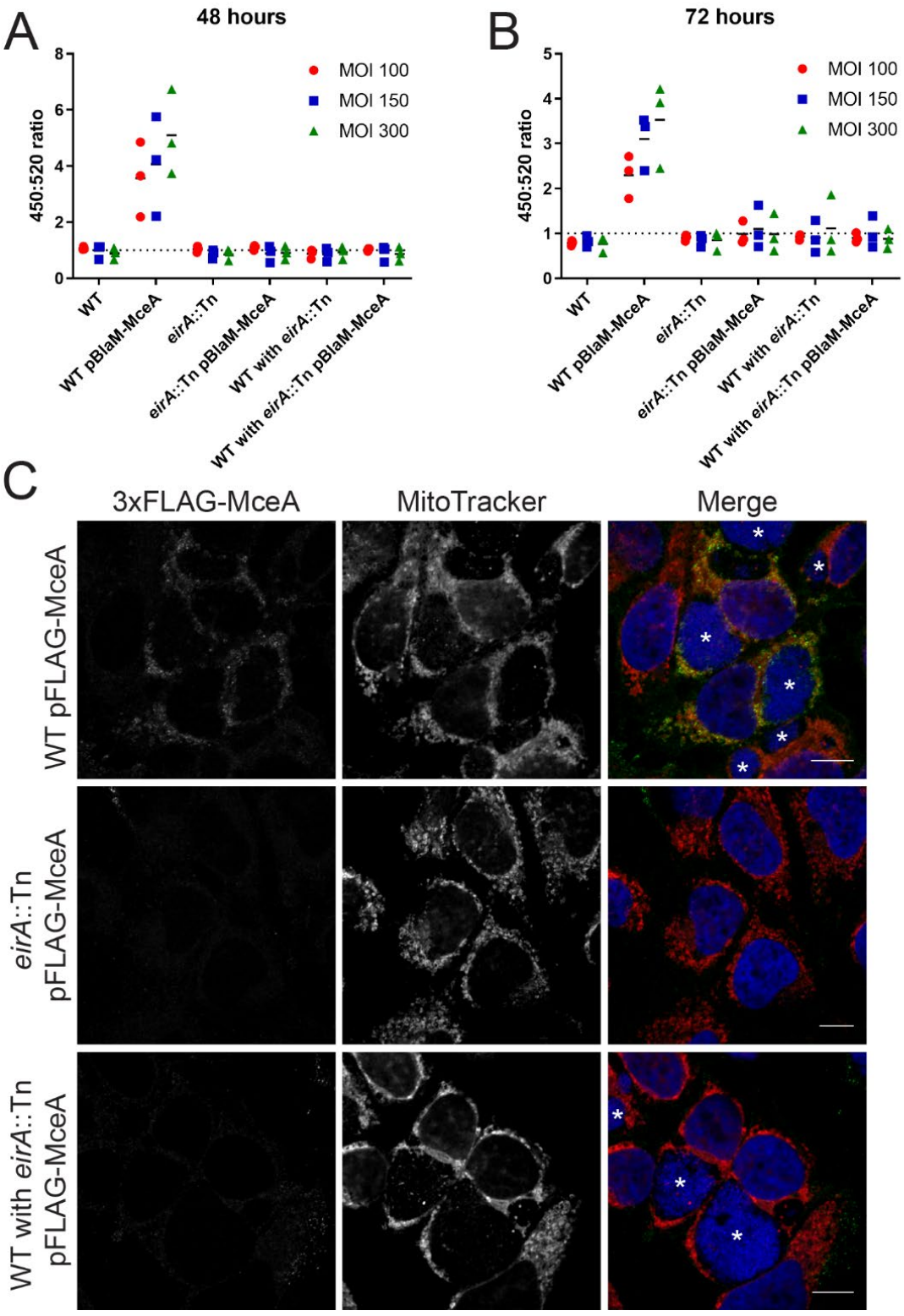

Figure 5.13. EirA is important for Dot/Icm Type IV secretion system effector translocation. Plasmids encoding transcriptionally fused β-lactamase (BlaM) and T4BSS effector MceA were introduced into *C. burnetii* WT and *eirA*::Tn. These strains, along

with *C. burnetii* WT and *eirA*::Tn, were used to infect HeLa CCL2 cells at an MOI of either 100 (red circles), 150 (blue squares) or 300 (green triangles), or a co-infection ratio of 1:1, 1:2 or 1:5 WT to *eirA*::Tn respectively, where two different strains were used. At either 48 hours (A) or 72 hours post-infection (B), the fluorescent β-lactamase substrate CCF2-AM was added to cells, and cleavage of substrate was determined by calculating the ratio of fluorescence at 450 nm to 520 nm, relative to uninfected cells, n = 3. (C) HeLa CCL2 cells were infected with *C. burnetii* strains expressing 3xFLAG-MceA, then fixed and stained at 3 days post-infection. Cells were stained with anti-FLAG (green), MitoTracker™ (red) and DAPI (blue). Images are representative of three independent biological replicates. Scale bar = 10 μm. Asterisks (*) indicate CCVs.

5.3 Discussion

The mechanisms used by the intracellular pathogenic bacteria *C. burnetii* to thrive and replicate within the normally hostile host phagolysosome are not fully understood. Previous studies have highlighted the role of *C. burnetii* lipopolysaccharide (LPS) as an important virulence factor, with avirulent phase II strains lacking mature LPS unable to infect humans or mice (55, 56). However, these strains are still able to establish and thrive within CCVs in tissue culture models of infection. The development of axenic culture conditions and tools for genetic manipulation has made it possible to identify other important proteinaceous *C. burnetii* virulence factors (175). Landmark mutational analyses have highlighted that the T4BSS is another major virulence determinant of *C. burnetii,* along with a subset of the effector proteins translocated by this system. Genetic disruption of T4BSS components result in total abolition of intracellular replication and virulence, which highlights the importance of this apparatus to *C. burnetii* (54, 107, 108). In this study, we have identified and characterised a novel virulence factor, EirA, and show that it is essential for intracellular replication and virulence.

The precise mechanism through which EirA facilitates *C. burnetii* virulence remains to be elucidated. Previous work using mass spectrometry has detected EirA in the culture media during axenic growth of *C. burnetii* (182). Presence of EirA in axenic media was confirmed using a C-terminal 3xFLAG tagged EirA expressed on an inducible *C. burnetii* vector (182). Given that EirA does not appear to be a T4BSS effector protein (76), this suggests that EirA is secreted out of the bacterial cell in a T4BSS independent manner. The probable mechanism for this secretion is via outer membrane vesicles, which were shown to be formed during both axenic and intracellular cultivation (182). However, data

presented in this study suggests that functional, full length EirA may be associated more with the bacterial cell, with localisation detected in the *C. burnetii* cytoplasm and inner membrane space. Further investigations are warranted to determine the true localisation of EirA, perhaps by using the anti-EirA antibody developed during this study.

This research has shown that the N-terminal 23 amino acids, encoding a putative signal peptide sequence, is required for EirA function within host cells. In addition, the conserved GXXXG motif within the area of homology to soluble transhydrogenases was also shown to be required for EirA function. It is interesting to note that while truncated EirA cannot restore WT level phenotypes, fractionation experiments demonstrate similar localisation to the bacterial cytoplasm and inner membrane. It was initially hypothesised that the signal peptide present in EirA would be responsible for trafficking of this protein into the extracellular environment via the Sec machinery (182). However, truncated EirA was found at a higher abundance in the ACCM-2 culture media when compared to full length EirA, demonstrating that this signal peptide is not required for secretion out of *C. burnetii*. Lack of the N-terminus may impact on the structure of EirA at the inner membrane or its capacity to interact with other bacterial factors. Interaction of EirA with other proteins may require the aforementioned GXXXG motif, as this motif is known to stabilise protein-protein interactions (138). The subcellular fractionation of *C. burnetii* also indicates that membrane associated EirA is potentially modified, independent of the N-terminus, appearing to be a slightly larger molecular weight than in the cytoplasmic fraction.

Absence of EirA is not lethal for *C. burnetii* during infection, as the bacteria are not cleared by the host cell and can be rescued through co-infection or super-infection at 5 days post initial infection with T4BSS competent *C. burnetii*. As mentioned earlier, this phenotype is identical to mutants of the T4BSS apparatus, such as *C. burnetii icmL*::Tn (107) and *icmD*::Tn (108). Viability of both mutants after infection have been demonstrated. The *icmL*::Tn mutant was able to be recovered in ACCM-2 media after 24, 72 and 120 hours post-infection of HeLa cells, with growth comparable to WT (107). The *icmD*::Tn mutant was also shown to maintain viability in host cells as replication could be restored 24 hours post-infection using an inducible complementation construct (108). Our similar findings again highlight the innate ability of *C. burnetii* to withstand the host phagolysosomal environment, independent of T4BSS activity and replication.

EirA partially localises to the inner membrane, and loss of this protein results in changes to the intracellular levels of cell wall intermediates. Therefore investigations were conducted to determine whether EirA has a direct role in cell wall biosynthesis. However, absence of EirA did not appear to affect cell membrane integrity in *C. burnetii*, as assessed by their sensitivity to antibiotics and TEM ultrastructure. The resolution that was used to examine the impact of EirA on the bacterial cell membrane may have been insufficient to observe more subtle contributions of EirA to the cell membrane. Therefore, observing bacterial membrane integrity or T4BSS assembly at higher resolutions may be of interest, for instance, through the use of cryogenic electron microscopy.

Both the β-lactamase translocation reporter assay and the immunofluorescence microscopy performed in this study show that absence of EirA disrupts T4BSS effector translocation. Even when replication was restored, the EirA mutants showed no T4BSS activity. This, together with the observation that the EirA mutant has an identical rescuable replication defect phenotype to T4BSS mutants, and the partial membrane localisation of EirA, led to the hypothesis that EirA contributes to *C. burnetii* T4BSS function. Given that *eirA* is not encoded within the T4BSS gene loci, and there are no EirA homologues encoded by *Legionella* species, which utilises a functionally analogous T4BSS (189), it is unlikely that EirA forms part of the T4BSS apparatus. EirA does not affect DotB, IcmD, IcmK and IcmX expression levels nor their subcellular localisation. However, it remains possible that EirA contributes to recruitment of other specific Dot/Icm components and/or assembly at the bacterial poles.

Recent studies in *Legionella pneumophila* have shown that this pathogen uses second messenger signalling to influence T4BSS effector translocation (113). *L. pneumophila* appears to regulate effector translocation using c-di-GMP signalling via a diguanylate cyclase enzyme. Mutants lacking this enzyme show delayed translocation of the *L. pneumophila* effector protein LepA, and transcriptomics suggests this enzyme has a post-transcriptional regulatory role for T4BSS effector translocation (113). *C. burnetii* lacks diguanylate cyclases but may have evolved similar post-translational regulatory mechanisms to temporally regulate effector translocation during infection. EirA contains a region with homology to soluble transhydrogenases, which interact with NAD(P) cofactors. Here we show that loss or overexpression of EirA results in reciprocal changes in the intracellular levels of key cofactors NADH and NADP, as well as global changes

in other metabolites. This suggests EirA may regulate multiple metabolic pathways, one or more of which may in turn regulate T4BSS assembly and function. However, given that the diguanylate cyclase mutant in *L. pneumophila* does not display an intracellular replication defect similar to what has been shown in the *eirA*::Tn mutant, EirA may function using other mechanisms to regulate T4BSS activity. This is likely, as there are no EirA homologues present in *L. pneumophila*, suggesting the T4BSS may be regulated differently between the two species. Future work could determine possible enzymatic activity of EirA and any protein interacting partners of EirA, which may help elucidate the mechanism through which EirA impacts T4BSS activity.

This chapter has characterised a novel and unique *C. burnetii* inner membrane protein, EirA, which is essential for intracellular replication and virulence. Further investigations are required to determine the biochemical mechanisms by which EirA facilitates virulence. However, data presented here indicates that EirA is a novel factor contributing to T4BSS function. Elucidating the mechanisms through which EirA exerts virulence capacity is important for understanding *C. burnetii* pathogenesis. Given the unique aspects of this protein, determining the function of EirA and subsequently developing the capacity to specifically inhibit EirA function may serve as an important and powerful therapeutic strategy.

Chapter 6

Perspective

Intracellular pathogenic bacteria have developed numerous mechanisms to survive within the host cell environment. Many avoid degradation by evading endosomal trafficking to the host lysosome. For instance, the human pathogen *Mycobacterium tuberculosis* inhibits endosomal maturation by preventing the acquisition of Rab7 GTPases to the *M. tuberculosis* containing phagosome (101, 190). *Legionella pneumophila*, the causative agent of Legionnaire's disease, uses the Dot/Icm type 4B secretion system to translocate a suite of effectors that promote fusion of the phagosome with host endoplasmic reticulum-derived vesicles to block endocytic maturation (191, 192). Other bacterial pathogens, such as *Listeria monocytogenes*, have developed mechanisms to evade the endosomal trafficking pathway by disrupting the vacuolar membrane, thus allowing replication within the host cytosol (193).

In stark contrast, *C. burnetii*, requires passive trafficking of the phagosome to the host lysosome, where inhibition of endosomal maturation is detrimental to bacterial replication (71). Trafficking of the pathogen-containing phagosome to the lysosomal environment triggers both the metabolic activation of the bacteria and the activation of the T4BSS (71, 114). This T4BSS, which translocates approximately 130 effector proteins into the host cell, is essential for intracellular replication (107, 108).

The requirement to replicate within a phagolysosome or lysosome-derived vacuole is not a unique feature to *C. burnetii*. Protozoan parasites of the *Leishmania* spp. also require this environment to replicate within the host cell (157). Genetically these species have little similarity with *C. burnetii*. However, it is presumed that *Leishmania* have also

developed unique mechanisms to withstand and/or manipulate the lysosomal environment to facilitate replication (157).

Despite occupying divergent intracellular niches, a common requirement for pathogens to thrive within the host cell is the capacity to acquire sufficient nutrients and utilise them efficiently. The intracellular environment is abundant in host metabolites (97). However, the availability of these metabolites may differ depending on the host cell type and intracellular compartment that the pathogen resides in. Thus, intracellular pathogens must adapt and utilise specific metabolic pathways, which may only be activated under certain conditions and environments. For instance, *Leishmania mexicana* are able to catabolise amino acids during replication, but will specifically reduce the uptake of glutamate during intracellular replication within phagolysosomes (90). Reducing glutamate uptake may prevent the accumulation of reactive oxygen species (ROS) via the TCA cycle, which is an important adaptation to the high oxidative stress environment of a host phagolysosome.

The research reported in this thesis has given insight into the metabolic pathways utilised by *C. burnetii*, both during axenic and intracellular replication. The initial aim of the study was to determine whether any novel, *C. burnetii*-specific metabolic pathways and/or enzymes were present, which may be essential for replication. This has the potential to reveal new therapeutic targets against *C. burnetii*. Data from the first chapter did not indicate that such pathways exist, instead demonstrating the surprising metabolic flexibility of *C. burnetii*. However, this research has given a unique insight into how *C. burnetii* metabolise various nutrient substrates. Genome annotation indicates that

C. burnetii do not have a mechanism to phosphorylate glucose to form G6P, as they lack the classical hexokinase or phosphotransferase system (PTS) required to undergo this process. Data from this thesis, as well as work published by another research group (98), have conclusively shown that *C. burnetii* are in fact capable of catabolising glucose via glycolysis, generating G6P and downstream metabolites. The exact mechanism/s involved in this process are yet to be elucidated but may reveal a novel approach for bacteria to phosphorylate glucose.

Techniques developed throughout these studies, including steady state profiling and ^{13}C-stable isotope labelling, have proved valuable in the study of *C. burnetii* metabolism. The steady state profiling methodology has provided a comprehensive dataset, which allowed the mapping of the *C. burnetii* metabolic pathway using a reference database.

Substrate utilisation in axenically grown *C. burnetii* has been shown previously (98), with data presented in this thesis showing consistency with this previous work. However, data presented in this thesis has given first insights into the metabolism of intracellular *C. burnetii*. Combined, the results indicate that *C. burnetii* have greater metabolic flexibility than previously thought, being able to catabolise both sugars and amino acids, with significant differences seen between cultivation methods and different replication stages. In addition, *C. burnetii* was shown to possess at least two glucose transporters, CBU0265 and CBU0347. [^{13}C]glucose labelling demonstrated that mutants lacking either of these proteins are attenuated for glucose uptake when compared to WT. Single mutants lacking either of these proteins did not show any attenuations in intracellular replication

or infection in the *G. mellonella* model. However, the extent to which glucose uptake affects intracellular replication and virulence of *C. burnetii* is not fully understood, and further investigations are warranted.

Combined, these results suggest that this pathogen has evolved mechanisms to scavenge all available nutrient sources within the intracellular niche, which may aid replication in a variety of cell types. Interestingly, comparison between the preliminary metabolite analysis in HeLa human epithelial cells and the comprehensive studies in THP-1 human monocytic cells indicated that overall substrate usage in these different cell types was comparable.

With insights into bacterial metabolism now established, future work may focus on how the host metabolism is altered during *C. burnetii* infection. Given that *C. burnetii* scavenges nutrients from the host cell, this may affect how the host itself metabolises nutrients.

A rapidly growing area of research is in the field of immunometabolism, where the host metabolic pathways have been shown to contribute significantly to the immune response (194). In macrophages, which *C. burnetii* have tropism for, central carbon metabolism has been shown to trigger a cascade of events which results in the production of nitric oxide, ROS production, interleukin production, and the pro-inflammatory response (194, 195).

It is likely that some of the T4BSS effector proteins translocated by the pathogen may aid in nutrient acquisition, whether it be through the homotypic fusion of vacuoles, or by altering the host metabolism to facilitate production of essential nutrients. For instance, the T4BSS effector protein CBU0513 appears to be a fructose 1,6-bisphosphatase (173). This effector may be translocated into the host cell cytosol to act on host-derived metabolites instead of those found in *C. burnetii*.

Immunogenic shifts in host metabolism may also be used to exploit the host cell to the pathogen's advantage. This has been demonstrated in the fungal pathogen *Candida albicans* during infection of macrophages. Glucose starvation in infected macrophages resulting from the Warburg effect (196) resulted in host cell death, allowing escape of *C. albicans* from their host (197). It would therefore be of interest to determine how the host cell metabolic landscape is altered during *C. burnetii* infection. This could potentially be explored using techniques established here, by isolating host cells and removing intact bacteria prior to metabolite extraction.

Research presented in this thesis has highlighted the importance of acquiring the appropriate metabolites required for the intracellular success of *C. burnetii*. Recent studies have identified *C. burnetii* specific proteins which are also required for intracellular pathogenesis.

Numerous studies have focused on the T4BSS and the effector repertoire of *C. burnetii*, which contribute to vital modulation of host processes to establish the replicative niche (67, 76, 77, 79, 107, 117, 173). Mutants of the T4BSS are unable to replicate intracellularly, which highlights the essentiality of this apparatus to *C. burnetii* pathogenesis (107, 108). Interestingly these mutant strains remain viable within the host cell, which suggests that there may be other factors that allow *C. burnetii* to survive within the intracellular environment.

This thesis has presented evidence that EirA is a unique proteinaceous virulence factor of *C. burnetii* that was shown to inhibit T4BSS effector translocation. Interestingly, the phenotype of the EirA deficient mutant is identical to mutants of the T4BSS, in that while they are unable to replicate, they are still viable within the host cell. How the absence of EirA inhibits the T4BSS, and the exact biochemical mechanisms which facilitate EirA function, remain to be elucidated.

Regulation of T4BSS activity involves numerous factors. At the transcriptional level, the PmrAB two-component system in *C. burnetii* is essential for the activation of the T4BSS, as mutants deficient in the PmrA response regulator were unable to translocate effector proteins and replicate intracellularly (110). Temporal regulation of the T4BSS and translocation of effector proteins via the IcmS chaperone has also been demonstrated (112). Mutants deficient in the IcmS chaperone were attenuated for intracellular replication, and demonstrated an altered set of translocated T4BSS effectors (112). Interestingly, while the translocation of a large number of effectors was inhibited in the

absence of IcmS, a subset of effectors demonstrate translocation only in the absence of IcmS (112). These findings indicate a post-translational regulatory mechanism that may aid the temporal control of effector translocation.

In addition, c-di-GMP signalling catalysed by the enzyme diguanylate cyclase was shown to regulate T4BSS translocation in *L. pneumophila* (113). While no homologous systems appear to exist in *C. burnetii, g*iven the homology of EirA to soluble transhydrogenases, and the metabolic profile shift observed in the absence of protein, EirA may provide a regulatory role for the T4BSS. Future investigations elucidating the mechanism of action of EirA may facilitate development of specific *C. burnetii* T4BSS inhibitors. Inhibitors for bacterial secretion systems have been developed for the type 3 secretion system (T3SS) (198). For instance, small molecule inhibitors have been developed to target various aspects of T3SS activity, including at the transcriptional and protein export level, against the human pathogen *Pseudomonas aeruginosa* (198). It is plausible to consider that T4BSS inhibitors developed against *C. burnetii* may be used both in a clinical setting, as well as for prophylactic treatment in animals exposed to *C. burnetii* in the environment.

In order to establish if EirA is an appropriate therapeutic target, it would be necessary to determine whether the data generated from this thesis could be recapitulated in the virulent, phase I form of *C. burnetii*. Both phase I and phase II *C. burnetii* replicate with similar kinetics in macrophages, and share the same endosomal/lysosomal markers on the CCV (57). However, phase II strains cannot cause disease in animals such as mice or humans, due to the truncated LPS (50, 51, 53). Regarding the metabolomics studies

conducted as part of this thesis, it would be of interest to determine whether virulent forms of *C. burnetii* share similar metabolic pathway usages as the phase II strains.

In exploring these various mechanisms used by *C. burnetii* to facilitate intracellular replication and infection, it is important to highlight the issues surrounding the overall disease caused by this pathogen. Q fever is currently not a well-known disease in the broader community (16). *C. burnetii* are environmentally hardy, have a low infectious dose, and are spread via aerosol transmission (12-15). Therefore, increased rates of extreme weather events exacerbated by climate change, such as drought and strong winds, could further the spread of *C. burnetii* and lead to increased rates of Q fever (27). This poses great risk to both human and animal health, as was demonstrated during the Netherlands Q fever outbreak between 2007-2010. This outbreak highlighted the significant impact a large-scale *C. burnetii* infection could cause to both agricultural industries and public health. A significant and ongoing repercussion from this outbreak is the reduced quality of life in patients (25, 26, 32). In addition, chronic Q fever has been detected in at-risk patients with pre-existing cardiac conditions, seven years after the initial outbreak, highlighting the ongoing risk to exposed individuals (199). Chronic Q fever is lethal without treatment. However, current treatment options are sub-optimal, in that doxycycline cannot be administered to pregnant individuals, and treatment of these chronic infections lead to issues with unwanted side effects and long term compliance issues (12, 35, 200). A commercial vaccine is available in Australia, particularly to at risk individuals (36, 37). However, the two-step screening process prior to administration of the vaccine is not ideal for use within a larger population (17). These issues highlight the need for a novel therapeutic target for *C. burnetii* infection.

Data obtained from this thesis has given insights into how different nutrient sources are metabolised by *C. burnetii*. Given intracellular bacteria seemed primed to catabolise glutamate over glucose, suggesting a reliance on amino acids during intracellular replication, it may be of interest to determine and functionally characterise amino acid transporters of *C. burnetii*. Studies on axenic *C. burnetii* have highlighted auxotrophies for a number of amino acids. Inhibition of nutrient uptake may be a novel therapeutic approach to treat Q fever infection, particularly during chronic infection. In addition, the likely existence of a unique mechanism to phosphorylate sugars may also provide a useful therapeutic target, as this is unlikely to be present in mammals. Inhibition of metabolic pathways as a novel therapeutic approach is an expanding field. Targeting bacteria specific metabolic enzymes in conjunction with traditional treatment options may provide a much-needed alternative in the efforts to prevent the current rise of antibiotic resistance. Folate biosynthesis pathways have already been targeted for antimicrobial drug development (201-203). In addition, the *M. tuberculosis* ATP synthase has been studied as a drug target for the treatment of tuberculosis (204-206).

This thesis has contributed to further understanding of the requirements for *C. burnetii* to replicate within the host phagolysosomal environment. Infection with *C. burnetii*, while not necessarily fatal, has the potential to develop into a debilitating and fatal chronic illness, which requires the establishment of novel therapeutic approaches. With increasing risk of Q fever outbreaks linked with the changing climate, it is of great importance to

identify novel mechanisms that allow *C. burnetii* to thrive within the host cell, which may in turn be exploited to prevent and/or treat infection.

Bibliography

1. Derrick EH. 1983. "Q" Fever, a New Fever Entity: Clinical Features, Diagnosis and Laboratory Investigation. Reviews of Infectious Diseases 5:790-800.
2. Burnet FM, Freeman M. 1983. Experimental Studies on the Virus of "Q" Fever. Reviews of Infectious Diseases 5:800-808.
3. Delsing CE, Warris A, Bleeker-Rovers CP. 2011. Q fever: still more queries than answers. Adv Exp Med Biol 719:133-43.
4. Davis GE, Cox HR, Parker RR, Dyer RE. 1938. A Filter-Passing Infectious Agent Isolated from Ticks. Public Health Reports (1896-1970) 53:2259-2282.
5. Philip CB. 1948. Comments on the Name of the Q Fever Organism. Public Health Reports (1896-1970) 63:58.
6. Cox HR. 1939. Studies of a Filter-Passing Infectious Agent Isolated from Ticks: V. Further Attempts to Cultivate in Cell-Free Media. Suggested Classification. Public Health Reports (1896-1970) 54:1822-1827.
7. Musso D, Broult J, Parola P, Raoult D, Fournier PE. 2014. Absence of antibodies to *Rickettsia* spp., *Bartonella* spp., *Ehrlichia* spp. and *Coxiella burnetii* in Tahiti, French Polynesia. BMC Infect Dis 14:255.
8. Sanchez J, Souriau A, Buendia AJ, Arricau-Bouvery N, Martinez CM, Salinas J, Rodolakis A, Navarro JA. 2006. Experimental *Coxiella burnetii* infection in pregnant goats: a histopathological and immunohistochemical study. J Comp Pathol 135:108-15.
9. Hatchette TF, Hudson RC, Schlech WF, Campbell NA, Hatchette JE, Ratnam S, Raoult D, Donovan C, Marrie TJ. 2001. Goat-associated Q fever: a new disease in Newfoundland. Emerg Infect Dis 7:413-9.

10. Rodolakis A, Berri M, Hechard C, Caudron C, Souriau A, Bodier CC, Blanchard B, Camuset P, Devillechaise P, Natorp JC, Vadet JP, Arricau-Bouvery N. 2007. Comparison of *Coxiella burnetii* shedding in milk of dairy bovine, caprine, and ovine herds. J Dairy Sci 90:5352-60.

11. Arricau Bouvery N, Souriau A, Lechopier P, Rodolakis A. 2003. Experimental *Coxiella burnetii* infection in pregnant goats: excretion routes. Vet Res 34:423-33.

12. Maurin M, Raoult D. 1999. Q fever. Clin Microbiol Rev 12:518-53.

13. Welsh HH, Lennette EH, Abinanti FR, Winn JF. 1958. Air-borne transmission of Q fever: the role of parturition in the generation of infective aerosols. Ann N Y Acad Sci 70:528-40.

14. Tissot-Dupont H, Torres S, Nezri M, Raoult D. 1999. Hyperendemic focus of Q fever related to sheep and wind. Am J Epidemiol 150:67-74.

15. Tigertt WD, Benenson AS, Gochenour WS. 1961. Airborne Q fever. Bacteriol Rev 25:285-93.

16. Eastwood K, Graves SR, Massey PD, Bosward K, van den Berg D, Hutchinson P. 2018. Q fever: A rural disease with potential urban consequences. Australian journal of general practice 47:5555-5555.

17. Gidding HF, Wallace C, Lawrence GL, McIntyre PB. 2009. Australia's national Q fever vaccination program. Vaccine 27:2037-41.

18. Madariaga MG, Rezai K, Trenholme GM, Weinstein RA. 2003. Q fever: a biological weapon in your backyard. Lancet Infect Dis 3:709-21.

19. Bjork A, Marsden-Haug N, Nett RJ, Kersh GJ, Nicholson W, Gibson D, Szymanski T, Emery M, Kohrs P, Woodhall D, Anderson AD. 2014. First

reported multistate human Q fever outbreak in the United States, 2011. Vector Borne Zoonotic Dis 14:111-7.

20. Bond KA, Vincent G, Wilks CR, Franklin L, Sutton B, Stenos J, Cowan R, Lim K, Athan E, Harris O, Macfarlane-Berry L, Segal Y, Firestone SM. 2016. One Health approach to controlling a Q fever outbreak on an Australian goat farm. Epidemiol Infect 144:1129-41.

21. Chmielewski T, Tylewska-Wierzbanowska S. 2013. Q fever outbreaks in Poland during 2005-2011. Med Sci Monit 19:1073-9.

22. van der Hoek W, Morroy G, Renders NH, Wever PC, Hermans MH, Leenders AC, Schneeberger PM. 2012. Epidemic Q fever in humans in the Netherlands. Adv Exp Med Biol 984:329-64.

23. Karagiannis I, Morroy G, Rietveld A, Horrevorts AM, Hamans M, Francken P, Schimmer B. 2007. Q fever outbreak in the Netherlands: a preliminary report. Euro Surveill 12:E070809 2.

24. Schneeberger PM, Wintenberger C, van der Hoek W, Stahl JP. 2014. Q fever in the Netherlands - 2007-2010: what we learned from the largest outbreak ever. Med Mal Infect 44:339-53.

25. van Asseldonk MA, Prins J, Bergevoet RH. 2013. Economic assessment of Q fever in the Netherlands. Prev Vet Med 112:27-34.

26. Kampschreur LM, Delsing CE, Groenwold RH, Wegdam-Blans MC, Bleeker-Rovers CP, de Jager-Leclercq MG, Hoepelman AI, van Kasteren ME, Buijs J, Renders NH, Nabuurs-Franssen MH, Oosterheert JJ, Wever PC. 2014. Chronic Q fever in the Netherlands 5 years after the start of the Q fever epidemic: results from the Dutch chronic Q fever database. J Clin Microbiol 52:1637-43.

27. Archibald J. 2019. Disease in the dust: experiences of Q fever during drought in Australia. Perspectives in public health 139:77-78.

28. Raoult D, Tissot-Dupont H, Foucault C, Gouvernet J, Fournier PE, Bernit E, Stein A, Nesri M, Harle JR, Weiller PJ. 2000. Q fever 1985-1998. Clinical and epidemiologic features of 1,383 infections. Medicine (Baltimore) 79:109-23.

29. Espejo E, Gil-Diaz A, Oteo JA, Castillo-Rueda R, Garcia-Alvarez L, Santana-Baez S, Bella F. 2014. Clinical presentation of acute Q fever in Spain: seasonal and geographical differences. Int J Infect Dis 26:162-4.

30. Tissot Dupont H, Raoult D, Brouqui P, Janbon F, Peyramond D, Weiller PJ, Chicheportiche C, Nezri M, Poirier R. 1992. Epidemiologic features and clinical presentation of acute Q fever in hospitalized patients: 323 French cases. Am J Med 93:427-34.

31. Heppell CW, Egan JR, Hall I. 2017. A human time dose response model for Q fever. Epidemics 21:30-38.

32. van Loenhout JA, Hautvast JL, Vercoulen JH, Akkermans RP, Wijkmans CJ, van der Velden K, Paget WJ. 2015. Q-fever patients suffer from impaired health status long after the acute phase of the illness: results from a 24-month cohort study. J Infect 70:237-46.

33. Anderson A, Bijlmer H, Fournier PE, Graves S, Hartzell J, Kersh GJ, Limonard G, Marrie TJ, Massung RF, McQuiston JH, Nicholson WL, Paddock CD, Sexton DJ. 2013. Diagnosis and management of Q fever--United States, 2013: recommendations from CDC and the Q Fever Working Group. MMWR Recomm Rep 62:1-30.

34. Wegdam-Blans MC, Kampschreur LM, Delsing CE, Bleeker-Rovers CP, Sprong T, van Kasteren ME, Notermans DW, Renders NH, Bijlmer HA, Lestrade PJ, Koopmans MP, Nabuurs-Franssen MH, Oosterheert JJ. 2012. Chronic Q fever: review of the literature and a proposal of new diagnostic criteria. J Infect 64:247-59.

35. Sobradillo V, Zalacain R, Capelastegui A, Uresandi F, Corral J. 1992. Antibiotic treatment in pneumonia due to Q fever. Thorax 47:276-8.

36. O'Neill TJ, Sargeant JM, Poljak Z. 2014. The effectiveness of *Coxiella burnetii* vaccines in occupationally exposed populations: a systematic review and meta-analysis. Zoonoses Public Health 61:81-96.

37. Kermode M, Yong K, Hurley S, Marmion B. 2003. An economic evaluation of increased uptake in Q fever vaccination among meat and agricultural industry workers following implementation of the National Q Fever Management Program. Aust N Z J Public Health 27:390-8.

38. Kersh GJ, Fitzpatrick KA, Self JS, Biggerstaff BJ, Massung RF. 2013. Long-Term immune responses to *Coxiella burnetii* after vaccination. Clin Vaccine Immunol 20:129-33.

39. Lackman DB, Bell EJ, Bell JF, Pickens EG. 1962. Intradermal sensitivity testing in man with a purified vaccine for Q fever. Am J Public Health Nations Health 52:87-93.

40. Bell JF, Luoto L, Casey M, Lackman DB. 1964. Serologic and skin-test response after Q Fever vaccination by the intracutaneous route. J Immunol 93:403-8.

41. Gilroy N, Formica N, Beers M, Egan A, Conaty S, Marmion B. 2001. Abattoir-associated Q fever: a Q fever outbreak during a Q fever vaccination program. Aust N Z J Public Health 25:362-7.

42. Arricau-Bouvery N, Souriau A, Bodier C, Dufour P, Rousset E, Rodolakis A. 2005. Effect of vaccination with phase I and phase II *Coxiella burnetii* vaccines in pregnant goats. Vaccine 23:4392-402.

43. de Cremoux R, Rousset E, Touratier A, Audusseau G, Nicollet P, Ribaud D, David V, Le Pape M. 2012. Assessment of vaccination by a phase I *Coxiella burnetii*-inactivated vaccine in goat herds in clinical Q fever situation. FEMS Immunol Med Microbiol 64:104-6.

44. Roest HI, Bossers A, van Zijderveld FG, Rebel JM. 2013. Clinical microbiology of *Coxiella burnetii* and relevant aspects for the diagnosis and control of the zoonotic disease Q fever. Vet Q 33:148-60.

45. Weisburg WG, Dobson ME, Samuel JE, Dasch GA, Mallavia LP, Baca O, Mandelco L, Sechrest JE, Weiss E, Woese CR. 1989. Phylogenetic diversity of the Rickettsiae. J Bacteriol 171:4202-6.

46. Roux V, Bergoin M, Lamaze N, Raoult D. 1997. Reassessment of the taxonomic position of *Rickettsiella grylli*. Int J Syst Bacteriol 47:1255-7.

47. Seshadri R, Paulsen IT, Eisen JA, Read TD, Nelson KE, Nelson WC, Ward NL, Tettelin H, Davidsen TM, Beanan MJ, Deboy RT, Daugherty SC, Brinkac LM, Madupu R, Dodson RJ, Khouri HM, Lee KH, Carty HA, Scanlan D, Heinzen RA, Thompson HA, Samuel JE, Fraser CM, Heidelberg JF. 2003. Complete genome sequence of the Q-fever pathogen *Coxiella burnetii*. Proc Natl Acad Sci U S A 100:5455-60.

48. Samuel JE, Frazier ME, Kahn ML, Thomashow LS, Mallavia LP. 1983. Isolation and characterization of a plasmid from phase I *Coxiella burnetii*. Infect Immun 41:488-93.

49. Maturana P, Graham JG, Sharma UM, Voth DE. 2013. Refining the plasmid-encoded type IV secretion system substrate repertoire of *Coxiella burnetii*. J Bacteriol 195:3269-76.

50. Beare PA, Unsworth N, Andoh M, Voth DE, Omsland A, Gilk SD, Williams KP, Sobral BW, Kupko JJ, 3rd, Porcella SF, Samuel JE, Heinzen RA. 2009. Comparative genomics reveal extensive transposon-mediated genomic plasticity and diversity among potential effector proteins within the genus *Coxiella*. Infect Immun 77:642-56.

51. Moos A, Hackstadt T. 1987. Comparative virulence of intra- and interstrain lipopolysaccharide variants of *Coxiella burnetii* in the guinea pig model. Infect Immun 55:1144-50.

52. Setiyono A, Ogawa M, Cai Y, Shiga S, Kishimoto T, Kurane I. 2005. New criteria for immunofluorescence assay for Q fever diagnosis in Japan. J Clin Microbiol 43:5555-9.

53. Stoker MG, Fiset P. 1956. Phase variation of the Nine Mile and other strains of *Rickettsia burnetii*. Can J Microbiol 2:310-21.

54. Norville IH, Hartley MG, Martinez E, Cantet F, Bonazzi M, Atkins TP. 2014. *Galleria mellonella* as an alternative model of *Coxiella burnetii* infection. Microbiology 160:1175-81.

55. Hoover TA, Culp DW, Vodkin MH, Williams JC, Thompson HA. 2002. Chromosomal DNA deletions explain phenotypic characteristics of two

antigenic variants, phase II and RSA 514 (crazy), of the *Coxiella burnetii* nine mile strain. Infect Immun 70:6726-33.

56. Beare PA, Jeffrey BM, Long CM, Martens CM, Heinzen RA. 2018. Genetic mechanisms of *Coxiella burnetii* lipopolysaccharide phase variation. PLoS Pathog 14:e1006922.

57. Howe D, Shannon JG, Winfree S, Dorward DW, Heinzen RA. 2010. *Coxiella burnetii* phase I and II variants replicate with similar kinetics in degradative phagolysosome-like compartments of human macrophages. Infect Immun 78:3465-74.

58. Heinzen RA, Hackstadt T, Samuel JE. 1999. Developmental biology of *Coxiella burnettii*. Trends Microbiol 7:149-54.

59. Heinzen RA, Hackstadt T. 1996. A developmental stage-specific histone H1 homolog of *Coxiella burnetii*. Journal of bacteriology 178:5049-5052.

60. Coleman SA, Fischer ER, Howe D, Mead DJ, Heinzen RA. 2004. Temporal analysis of *Coxiella burnetii* morphological differentiation. J Bacteriol 186:7344-52.

61. Heinzen RA, Howe D, Mallavia LP, Rockey DD, Hackstadt T. 1996. Developmentally regulated synthesis of an unusually small, basic peptide by *Coxiella burnetii*. Molecular microbiology 22:9-19.

62. Coleman SA, Fischer ER, Cockrell DC, Voth DE, Howe D, Mead DJ, Samuel JE, Heinzen RA. 2007. Proteome and antigen profiling of *Coxiella burnetii* developmental forms. Infection and immunity 75:290-298.

63. Sandoz KM, Popham DL, Beare PA, Sturdevant DE, Hansen B, Nair V, Heinzen RA. 2016. Transcriptional Profiling of *Coxiella burnetii* Reveals

Extensive Cell Wall Remodeling in the Small Cell Variant Developmental Form. PloS one 11:e0149957-e0149957.

64. Moormeier DE, Sandoz KM, Beare PA, Sturdevant DE, Nair V, Cockrell DC, Miller HE, Heinzen RA. 2019. *Coxiella burnetii* RpoS Regulates Genes Involved in Morphological Differentiation and Intracellular Growth. Journal of bacteriology 201:e00009-19.

65. Raoult D, Marrie T, Mege J. 2005. Natural history and pathophysiology of Q fever. Lancet Infect Dis 5:219-26.

66. Graham JG, MacDonald LJ, Hussain SK, Sharma UM, Kurten RC, Voth DE. 2013. Virulent *Coxiella burnetii* pathotypes productively infect primary human alveolar macrophages. Cell Microbiol 15:1012-25.

67. Martinez E, Cantet F, Fava L, Norville I, Bonazzi M. 2014. Identification of OmpA, a *Coxiella burnetii* protein involved in host cell invasion, by multi-phenotypic high-content screening. PLoS Pathog 10:e1004013.

68. Turco J, Thompson HA, Winkler HH. 1984. Interferon-gamma inhibits growth of *Coxiella burnetii* in mouse fibroblasts. Infection and immunity 45:781-783.

69. Beron W, Gutierrez MG, Rabinovitch M, Colombo MI. 2002. *Coxiella burnetii* localizes in a Rab7-labeled compartment with autophagic characteristics. Infect Immun 70:5816-21.

70. McDonough JA, Newton HJ, Klum S, Swiss R, Agaisse H, Roy CR. 2013. Host pathways important for *Coxiella burnetii* infection revealed by genome-wide RNA interference screening. MBio 4:e00606-12.

71. Newton HJ, McDonough JA, Roy CR. 2013. Effector protein translocation by the *Coxiella burnetii* Dot/Icm type IV secretion system requires endocytic maturation of the pathogen-occupied vacuole. PLoS One 8:e54566.

72. Hackstadt T, Williams JC. 1981. Biochemical stratagem for obligate parasitism of eukaryotic cells by *Coxiella burnetii*. Proc Natl Acad Sci U S A 78:3240-4.

73. Heinzen RA, Scidmore MA, Rockey DD, Hackstadt T. 1996. Differential interaction with endocytic and exocytic pathways distinguish parasitophorous vacuoles of *Coxiella burnetii* and *Chlamydia trachomatis*. Infect Immun 64:796-809.

74. Howe D, Melnicakova J, Barak I, Heinzen RA. 2003. Fusogenicity of the *Coxiella burnetii* parasitophorous vacuole. Ann N Y Acad Sci 990:556-62.

75. Veras PS, de Chastellier C, Moreau MF, Villiers V, Thibon M, Mattei D, Rabinovitch M. 1994. Fusion between large phagocytic vesicles: targeting of yeast and other particulates to phagolysosomes that shelter the bacterium *Coxiella burnetii* or the protozoan *Leishmania amazonensis* in Chinese hamster ovary cells. J Cell Sci 107 (Pt 11):3065-76.

76. Newton HJ, Kohler LJ, McDonough JA, Temoche-Diaz M, Crabill E, Hartland EL, Roy CR. 2014. A screen of *Coxiella burnetii* mutants reveals important roles for Dot/Icm effectors and host autophagy in vacuole biogenesis. PLoS Pathog 10:e1004286.

77. Kohler LJ, Reed Sh C, Sarraf SA, Arteaga DD, Newton HJ, Roy CR. 2016. Effector Protein Cig2 Decreases Host Tolerance of Infection by Directing Constitutive Fusion of Autophagosomes with the *Coxiella*-Containing Vacuole. MBio 7:e01127-16.

78. Latomanski EA, Newton HJ. 2018. Interaction between autophagic vesicles and the *Coxiella*-containing vacuole requires CLTC (clathrin heavy chain). Autophagy 14:1710-1725.

79. Latomanski EA, Newton P, Khoo CA, Newton HJ. 2016. The Effector Cig57 Hijacks FCHO-Mediated Vesicular Trafficking to Facilitate Intracellular Replication of *Coxiella burnetii*. PLoS Pathog 12:e1006101.

80. Larson CL, Beare PA, Howe D, Heinzen RA. 2013. *Coxiella burnetii* effector protein subverts clathrin-mediated vesicular trafficking for pathogen vacuole biogenesis. Proc Natl Acad Sci U S A 110:E4770-9.

81. Lamkanfi M, Dixit VM. 2010. Manipulation of host cell death pathways during microbial infections. Cell host & microbe 8:44-54.

82. Voth DE, Howe D, Heinzen RA. 2007. *Coxiella burnetii* inhibits apoptosis in human THP-1 cells and monkey primary alveolar macrophages. Infection and immunity 75:4263-4271.

83. Bitew MA, Hofmann J, De Souza DP, Wawegama NK, Newton HJ, Sansom FM. 2019. SdrA, an NADP(H)-regenerating enzyme, is crucial for *Coxiella burnetii* to resist oxidative stress and replicate intracellularly. Cellular microbiology doi:10.1111/cmi.13154:e13154-e13154.

84. Samanta D, Clemente TM, Schuler BE, Gilk SD. 2019. *Coxiella burnetii* Type 4B Secretion System-dependent manipulation of endolysosomal maturation is required for bacterial growth. PLoS Pathog 15:e1007855.

85. Omsland A, Beare PA, Hill J, Cockrell DC, Howe D, Hansen B, Samuel JE, Heinzen RA. 2011. Isolation from animal tissue and genetic transformation of

Coxiella burnetii are facilitated by an improved axenic growth medium. Appl Environ Microbiol 77:3720-5.

86. Vallejo Esquerra E, Yang H, Sanchez SE, Omsland A. 2017. Physicochemical and Nutritional Requirements for Axenic Replication Suggest Physiological Basis for *Coxiella burnetii* Niche Restriction. Front Cell Infect Microbiol 7:190.

87. Sanman LE, van der Linden WA, Verdoes M, Bogyo M. 2016. Bifunctional Probes of Cathepsin Protease Activity and pH Reveal Alterations in Endolysosomal pH during Bacterial Infection. Cell Chem Biol 23:793-804.

88. Winder CL, Dunn WB, Goodacre R. 2011. TARDIS-based microbial metabolomics: time and relative differences in systems. Trends Microbiol 19:315-22.

89. Drapal M, Perez-Fons L, Wheeler PR, Fraser PD. 2014. The application of metabolite profiling to *Mycobacterium* spp.: determination of metabolite changes associated with growth. J Microbiol Methods 106:23-32.

90. Saunders EC, Ng WW, Kloehn J, Chambers JM, Ng M, McConville MJ. 2014. Induction of a stringent metabolic response in intracellular stages of *Leishmania mexicana* leads to increased dependence on mitochondrial metabolism. PLoS Pathog 10:e1003888.

91. Masukagami Y, De Souza DP, Dayalan S, Bowen C, O'Callaghan S, Kouremenos K, Nijagal B, Tull D, Tivendale KA, Markham PF, McConville MJ, Browning GF, Sansom FM. 2017. Comparative Metabolomics of *Mycoplasma bovis* and *Mycoplasma gallisepticum* Reveals Fundamental Differences in Active Metabolic Pathways and Suggests Novel Gene Annotations. mSystems 2:e00055-17.

92. Masukagami Y, Nijagal B, Tseng CW, Dayalan S, Tivendale KA, Markham PF, Browning GF, Sansom FM. 2018. Metabolite profiling of *Mycoplasma gallisepticum* mutants, combined with bioinformatic analysis, can reveal the likely functions of virulence-associated genes. Vet Microbiol 223:160-167.

93. Sauer U, Canonaco F, Heri S, Perrenoud A, Fischer E. 2004. The soluble and membrane-bound transhydrogenases UdhA and PntAB have divergent functions in NADPH metabolism of *Escherichia coli*. J Biol Chem 279:6613-9.

94. Omsland A, Cockrell DC, Howe D, Fischer ER, Virtaneva K, Sturdevant DE, Porcella SF, Heinzen RA. 2009. Host cell-free growth of the Q fever bacterium *Coxiella burnetii*. Proc Natl Acad Sci U S A 106:4430-4.

95. Sandoz KM, Beare PA, Cockrell DC, Heinzen RA. 2016. Complementation of Arginine Auxotrophy for Genetic Transformation of *Coxiella burnetii* by Use of a Defined Axenic Medium. Appl Environ Microbiol 82:3042-51.

96. Kuley R, Bossers-deVries R, Smith HE, Smits MA, Roest HI, Bossers A. 2015. Major differential gene regulation in *Coxiella burnetii* between in vivo and in vitro cultivation models. BMC Genomics 16:953.

97. Abu-Remaileh M, Wyant GA, Kim C, Laqtom NN, Abbasi M, Chan SH, Freinkman E, Sabatini DM. 2017. Lysosomal metabolomics reveals V-ATPase- and mTOR-dependent regulation of amino acid efflux from lysosomes. Science 358:807-813.

98. Hauslein I, Cantet F, Reschke S, Chen F, Bonazzi M, Eisenreich W. 2017. Multiple Substrate Usage of *Coxiella burnetii* to Feed a Bipartite Metabolic Network. Front Cell Infect Microbiol 7:285.

99. Ray K, Marteyn B, Sansonetti PJ, Tang CM. 2009. Life on the inside: the intracellular lifestyle of cytosolic bacteria. Nat Rev Microbiol 7:333-40.

100. Roy CR, Berger KH, Isberg RR. 1998. *Legionella pneumophila* DotA protein is required for early phagosome trafficking decisions that occur within minutes of bacterial uptake. Mol Microbiol 28:663-74.

101. Clemens DL, Horwitz MA. 1995. Characterization of the *Mycobacterium tuberculosis* phagosome and evidence that phagosomal maturation is inhibited. J Exp Med 181:257-70.

102. Chandran Darbari V, Waksman G. 2015. Structural Biology of Bacterial Type IV Secretion Systems. Annu Rev Biochem 84:603-29.

103. Kubori T, Koike M, Bui XT, Higaki S, Aizawa S, Nagai H. 2014. Native structure of a type IV secretion system core complex essential for *Legionella* pathogenesis. Proc Natl Acad Sci U S A 111:11804-9.

104. Segal G, Purcell M, Shuman HA. 1998. Host cell killing and bacterial conjugation require overlapping sets of genes within a 22-kb region of the *Legionella pneumophila* genome. Proc Natl Acad Sci U S A 95:1669-74.

105. Vogel JP, Andrews HL, Wong SK, Isberg RR. 1998. Conjugative transfer by the virulence system of *Legionella pneumophila*. Science 279:873-6.

106. Zamboni DS, McGrath S, Rabinovitch M, Roy CR. 2003. *Coxiella burnetii* express type IV secretion system proteins that function similarly to components of the *Legionella pneumophila* Dot/Icm system. Mol Microbiol 49:965-76.

107. Carey KL, Newton HJ, Luhrmann A, Roy CR. 2011. The *Coxiella burnetii* Dot/Icm system delivers a unique repertoire of type IV effectors into host cells and is required for intracellular replication. PLoS Pathog 7:e1002056.

108. Beare PA, Gilk SD, Larson CL, Hill J, Stead CM, Omsland A, Cockrell DC, Howe D, Voth DE, Heinzen RA. 2011. Dot/Icm type IVB secretion system requirements for *Coxiella burnetii* growth in human macrophages. MBio 2:e00175-11.

109. Newton P, Thomas DR, Reed SCO, Lau N, Xu B, Ong SY, Pasricha S, Madhamshettiwar PB, Edgington-Mitchell LE, Simpson KJ, Roy CR, Newton HJ. 2020. Lysosomal degradation products induce *Coxiella burnetii* virulence. Proceedings of the National Academy of Sciences doi:10.1073/pnas.1921344117:201921344.

110. Beare PA, Sandoz KM, Larson CL, Howe D, Kronmiller B, Heinzen RA. 2014. Essential role for the response regulator PmrA in *Coxiella burnetii* type 4B secretion and colonization of mammalian host cells. J Bacteriol 196:1925-40.

111. Capra EJ, Laub MT. 2012. Evolution of two-component signal transduction systems. Annu Rev Microbiol 66:325-47.

112. Larson CL, Beare PA, Heinzen RA. 2019. Dependency of *Coxiella burnetii* Type 4B Secretion on the Chaperone IcmS. Journal of bacteriology 201:e00431-19.

113. Allombert J, Jaboulay C, Michard C, Andréa C, Charpentier X, Vianney A, Doublet P. 2019. Orchestrated delivery of *Legionella* effectors by the Icm/Dot secretion system. bioRxiv doi:10.1101/754762:754762.

114. Larson CL, Martinez E, Beare PA, Jeffrey B, Heinzen RA, Bonazzi M. 2016. Right on Q: genetics begin to unravel *Coxiella burnetii* host cell interactions. Future Microbiol 11:919-39.

115. Pan X, Luhrmann A, Satoh A, Laskowski-Arce MA, Roy CR. 2008. Ankyrin repeat proteins comprise a diverse family of bacterial type IV effectors. Science 320:1651-4.

116. Chen C, Banga S, Mertens K, Weber MM, Gorbaslieva I, Tan Y, Luo ZQ, Samuel JE. 2010. Large-scale identification and translocation of type IV secretion substrates by *Coxiella burnetii*. Proc Natl Acad Sci U S A 107:21755-60.

117. Weber MM, Chen C, Rowin K, Mertens K, Galvan G, Zhi H, Dealing CM, Roman VA, Banga S, Tan Y, Luo ZQ, Samuel JE. 2013. Identification of *Coxiella burnetii* type IV secretion substrates required for intracellular replication and *Coxiella*-containing vacuole formation. J Bacteriol 195:3914-24.

118. Luhrmann A, Nogueira CV, Carey KL, Roy CR. 2010. Inhibition of pathogen-induced apoptosis by a *Coxiella burnetii* type IV effector protein. Proc Natl Acad Sci U S A 107:18997-9001.

119. Klingenbeck L, Eckart RA, Berens C, Luhrmann A. 2013. The *Coxiella burnetii* type IV secretion system substrate CaeB inhibits intrinsic apoptosis at the mitochondrial level. Cell Microbiol 15:675-87.

120. Fielden LF, Moffatt JH, Kang Y, Baker MJ, Khoo CA, Roy CR, Stojanovski D, Newton HJ. 2017. A Farnesylated *Coxiella burnetii* Effector Forms a Multimeric Complex at the Mitochondrial Outer Membrane during Infection. Infect Immun 85:e01046-16.

121. Graham JG, Winchell CG, Sharma UM, Voth DE. 2015. Identification of ElpA, a *Coxiella burnetii* pathotype-specific Dot/Icm type IV secretion system substrate. Infect Immun 83:1190-8.

122. Weber MM, Faris R, McLachlan J, Tellez A, Wright WU, Galvan G, Luo Z-Q, Samuel JE. 2016. Modulation of the host transcriptome by *Coxiella burnetii* nuclear effector Cbu1314. Microbes and infection 18:336-345.

123. Martinez E, Allombert J, Cantet F, Lakhani A, Yandrapalli N, Neyret A, Norville IH, Favard C, Muriaux D, Bonazzi M. 2016. *Coxiella burnetii* effector CvpB modulates phosphoinositide metabolism for optimal vacuole development. Proc Natl Acad Sci U S A 113:E3260-9.

124. Dorer MS, Kirton D, Bader JS, Isberg RR. 2006. RNA interference analysis of *Legionella* in Drosophila cells: exploitation of early secretory apparatus dynamics. PLoS Pathog 2:e34.

125. Park JM, Ghosh S, O'Connor TJ. 2020. Combinatorial selection in amoebal hosts drives the evolution of the human pathogen *Legionella pneumophila*. Nature microbiology doi:10.1038/s41564-019-0663-7:10.1038/s41564-019-0663-7.

126. Altschul SF, Madden TL, Schaffer AA, Zhang J, Zhang Z, Miller W, Lipman DJ. 1997. Gapped BLAST and PSI-BLAST: a new generation of protein database search programs. Nucleic Acids Res 25:3389-402.

127. Arkblad EL, Tuck S, Pestov NB, Dmitriev RI, Kostina MB, Stenvall J, Tranberg M, Rydstrom J. 2005. A *Caenorhabditis elegans* mutant lacking functional nicotinamide nucleotide transhydrogenase displays increased sensitivity to oxidative stress. Free Radic Biol Med 38:1518-25.

128. Hatefi Y, Yamaguchi M. 1996. Nicotinamide nucleotide transhydrogenase: a model for utilization of substrate binding energy for proton translocation. Faseb j 10:444-52.

129. Jackson JB, Cotton NP, Williams R, Bizouarn T, Hutton MN, Sazanov LA, Thomas CM. 1993. Proton-translocating transhydrogenase in bacteria. Biochem Soc Trans 21:1010-3.

130. Karlsson J, Althage M, Rydstrom J. 2003. Roles of individual amino acids in helix 14 of the membrane domain of proton-translocating transhydrogenase from *Escherichia coli* as deduced from cysteine mutagenesis. Biochemistry 42:6575-81.

131. Jackson JB, Leung JH, Stout CD, Schurig-Briccio LA, Gennis RB. 2015. Review and Hypothesis. New insights into the reaction mechanism of transhydrogenase: Swivelling the dIII component may gate the proton channel. FEBS Lett 589:2027-33.

132. Meuller J, Rydstrom J. 1999. The membrane topology of proton-pumping *Escherichia coli* transhydrogenase determined by cysteine labeling. J Biol Chem 274:19072-80.

133. Boonstra B, French CE, Wainwright I, Bruce NC. 1999. The udhA gene of *Escherichia coli* encodes a soluble pyridine nucleotide transhydrogenase. J Bacteriol 181:1030-4.

134. French CE, Boonstra B, Bufton KA, Bruce NC. 1997. Cloning, sequence, and properties of the soluble pyridine nucleotide transhydrogenase of *Pseudomonas fluorescens*. J Bacteriol 179:2761-5.

135. Voordouw G, Veeger C, Van Breemen JF, Van Bruggen EF. 1979. Structure of pyridine nucleotide transhydrogenase from *Azotobacter vinelandii*. Eur J Biochem 98:447-54.

136. Voordouw G, van der Vies SM, Themmen AP. 1983. Why are two different types of pyridine nucleotide transhydrogenase found in living organisms? Eur J Biochem 131:527-33.

137. Cao Z, Song P, Xu Q, Su R, Zhu G. 2011. Overexpression and biochemical characterization of soluble pyridine nucleotide transhydrogenase from *Escherichia coli*. FEMS Microbiol Lett 320:9-14.

138. Kleiger G, Eisenberg D. 2002. GXXXG and GXXXA motifs stabilize FAD and NAD(P)-binding Rossmann folds through C(alpha)-H... O hydrogen bonds and van der waals interactions. J Mol Biol 323:69-76.

139. MacKenzie KR, Prestegard JH, Engelman DM. 1997. A transmembrane helix dimer: structure and implications. Science 276:131-3.

140. MacKenzie KR, Engelman DM. 1998. Structure-based prediction of the stability of transmembrane helix-helix interactions: the sequence dependence of glycophorin A dimerization. Proc Natl Acad Sci U S A 95:3583-90.

141. Walker IH, Hsieh PC, Riggs PD. 2010. Mutations in maltose-binding protein that alter affinity and solubility properties. Appl Microbiol Biotechnol 88:187-97.

142. Froger A, Hall JE. 2007. Transformation of plasmid DNA into *E. coli* using the heat shock method. Journal of visualized experiments : JoVE doi:10.3791/253:253-253.

143. Jaton K, Peter O, Raoult D, Tissot JD, Greub G. 2013. Development of a high throughput PCR to detect *Coxiella burnetii* and its application in a diagnostic laboratory over a 7-year period. New Microbes New Infect 1:6-12.

144. O'Callaghan S, De Souza DP, Isaac A, Wang Q, Hodkinson L, Olshansky M, Erwin T, Appelbe B, Tull DL, Roessner U, Bacic A, McConville MJ, Likic VA. 2012. PyMS: a Python toolkit for processing of gas chromatography-mass spectrometry (GC-MS) data. Application and comparative study of selected tools. BMC Bioinformatics 13:115.

145. Kowalski GM, De Souza DP, Burch ML, Hamley S, Kloehn J, Selathurai A, Tull D, O'Callaghan S, McConville MJ, Bruce CR. 2015. Application of dynamic metabolomics to examine *in vivo* skeletal muscle glucose metabolism in the chronically high-fat fed mouse. Biochem Biophys Res Commun 462:27-32.

146. Rohn H, Junker A, Hartmann A, Grafahrend-Belau E, Treutler H, Klapperstuck M, Czauderna T, Klukas C, Schreiber F. 2012. VANTED v2: a framework for systems biology applications. BMC Syst Biol 6:139.

147. Schindelin J, Arganda-Carreras I, Frise E, Kaynig V, Longair M, Pietzsch T, Preibisch S, Rueden C, Saalfeld S, Schmid B, Tinevez JY, White DJ, Hartenstein V, Eliceiri K, Tomancak P, Cardona A. 2012. Fiji: an open-source platform for biological-image analysis. Nat Methods 9:676-82.

148. Bowden SD, Rowley G, Hinton JCD, Thompson A. 2009. Glucose and glycolysis are required for the successful infection of macrophages and mice by *Salmonella enterica* serovar typhimurium. Infection and immunity 77:3117-3126.

149. Sumner LW, Amberg A, Barrett D, Beale MH, Beger R, Daykin CA, Fan TW, Fiehn O, Goodacre R, Griffin JL, Hankemeier T, Hardy N, Harnly J, Higashi R, Kopka J, Lane AN, Lindon JC, Marriott P, Nicholls AW, Reily MD, Thaden JJ,

Viant MR. 2007. Proposed minimum reporting standards for chemical analysis Chemical Analysis Working Group (CAWG) Metabolomics Standards Initiative (MSI). Metabolomics 3:211-221.

150. Schumann C, Michlmayr H, Del Hierro AM, Kulbe KD, Jiranek V, Eder R, Nguyen TH. 2013. Malolactic enzyme from *Oenococcus oeni*: heterologous expression in *Escherichia coli* and biochemical characterization. Bioengineered 4:147-52.

151. Bitew MA, Khoo CA, Neha N, De Souza DP, Tull D, Wawegama NK, Newton HJ, Sansom FM. 2018. De novo NAD synthesis is required for intracellular replication of *Coxiella burnetii*, the causative agent of the neglected zoonotic disease Q fever. J Biol Chem 293:18636-18645.

152. Dennis D, Kaplan NO. 1960. D- and L-lactic acid dehydrogenases in *Lactobacillus plantarum*. J Biol Chem 235:810-8.

153. Yamaguchi M. 1979. Studies on regulatory functions of malic enzymes. IV. Effects of sulfhydryl group modification on the catalytic function of NAD-linked malic enzyme from *Escherichia coli*. J Biochem 86:325-33.

154. Cordwell SJ, Basseal DJ, Pollack JD, Humphery-Smith I. 1997. Malate/lactate dehydrogenase in mollicutes: evidence for a multienzyme protein. Gene 195:113-120.

155. Masukagami Y, Tivendale KA, Browning GF, Sansom FM. 2018. Analysis of the *Mycoplasma bovis* lactate dehydrogenase reveals typical enzymatic activity despite the presence of an atypical catalytic site motif. Microbiology 164:186-193.

156. Billig S, Schneefeld M, Huber C, Grassl GA, Eisenreich W, Bange FC. 2017. Lactate oxidation facilitates growth of *Mycobacterium tuberculosis* in human macrophages. Sci Rep 7:6484.

157. Kaye P, Scott P. 2011. Leishmaniasis: complexity at the host-pathogen interface. Nat Rev Microbiol 9:604-15.

158. Naderer T, Heng J, Saunders EC, Kloehn J, Rupasinghe TW, Brown TJ, McConville MJ. 2015. Intracellular Survival of *Leishmania major* Depends on Uptake and Degradation of Extracellular Matrix Glycosaminoglycans by Macrophages. PLoS Pathog 11:e1005136.

159. Saunders EC, Naderer T, Chambers J, Landfear SM, McConville MJ. 2018. *Leishmania mexicana* can utilize amino acids as major carbon sources in macrophages but not in animal models. Mol Microbiol 108:143-158.

160. Singh R, Mailloux RJ, Puiseux-Dao S, Appanna VD. 2007. Oxidative stress evokes a metabolic adaptation that favors increased NADPH synthesis and decreased NADH production in *Pseudomonas fluorescens*. J Bacteriol 189:6665-75.

161. Henderson PJ, Maiden MC. 1990. Homologous sugar transport proteins in *Escherichia coli* and their relatives in both prokaryotes and eukaryotes. Philos Trans R Soc Lond B Biol Sci 326:391-410.

162. Kundig W, Ghosh S, Roseman S. 1964. Phosphate bound to histidine in a protein as an intermediate in a novel phospho-transferase system. Proc Natl Acad Sci U S A 52:1067-74.

163. Sun L, Zeng X, Yan C, Sun X, Gong X, Rao Y, Yan N. 2012. Crystal structure of a bacterial homologue of glucose transporters GLUT1-4. Nature 490:361-6.

164. Henderson PJ, Macpherson AJ. 1986. Assay, genetics, proteins, and reconstitution of proton-linked galactose, arabinose, and xylose transport systems of *Escherichia coli*. Methods Enzymol 125:387-429.

165. Bradley SA, Tinsley CR, Muiry JA, Henderson PJ. 1987. Proton-linked L-fucose transport in *Escherichia coli*. Biochem J 248:495-500.

166. Pickl A, Johnsen U, Schonheit P. 2012. Fructose degradation in the haloarchaeon *Haloferax volcanii* involves a bacterial type phosphoenolpyruvate-dependent phosphotransferase system, fructose-1-phosphate kinase, and class II fructose-1,6-bisphosphate aldolase. J Bacteriol 194:3088-97.

167. Cai L, Cai S, Zhao D, Wu J, Wang L, Liu X, Li M, Hou J, Zhou J, Liu J, Han J, Xiang H. 2014. Analysis of the transcriptional regulator GlpR, promoter elements, and posttranscriptional processing involved in fructose-induced activation of the phosphoenolpyruvate-dependent sugar phosphotransferase system in *Haloferax mediterranei*. Appl Environ Microbiol 80:1430-40.

168. Gunn FJ, Tate CG, Henderson PJ. 1994. Identification of a novel sugar-H+ symport protein, FucP, for transport of L-fucose into *Escherichia coli*. Mol Microbiol 12:799-809.

169. Spooner PJ, O'Reilly WJ, Homans SW, Rutherford NG, Henderson PJ, Watts A. 1998. Weak substrate binding to transport proteins studied by NMR. Biophys J 75:2794-800.

170. Krogh A, Larsson B, von Heijne G, Sonnhammer EL. 2001. Predicting transmembrane protein topology with a hidden Markov model: application to complete genomes. J Mol Biol 305:567-80.

171. Maiden MC, Davis EO, Baldwin SA, Moore DC, Henderson PJ. 1987. Mammalian and bacterial sugar transport proteins are homologous. Nature 325:641-3.

172. Sievers F, Wilm A, Dineen D, Gibson TJ, Karplus K, Li W, Lopez R, McWilliam H, Remmert M, Soding J, Thompson JD, Higgins DG. 2011. Fast, scalable generation of high-quality protein multiple sequence alignments using Clustal Omega. Mol Syst Biol 7:539.

173. Crabill E, Schofield WB, Newton HJ, Goodman AL, Roy CR. 2018. Dot/Icm-Translocated Proteins Important for Biogenesis of the *Coxiella burnetii*-Containing Vacuole Identified by Screening of an Effector Mutant Sublibrary. Infect Immun 86.

174. Viitanen P, Newman MJ, Foster DL, Wilson TH, Kaback HR. 1986. Purification, reconstitution, and characterization of the lac permease of *Escherichia coli*. Methods in enzymology 125:429-452.

175. Luhrmann A, Newton HJ, Bonazzi M. 2017. Beginning to Understand the Role of the Type IV Secretion System Effector Proteins in *Coxiella burnetii* Pathogenesis. Curr Top Microbiol Immunol 413:243-268.

176. Akporiaye ET, Rowatt JD, Aragon AA, Baca OG. 1983. Lysosomal response of a murine macrophage-like cell line persistently infected with *Coxiella burnetii*. Infect Immun 40:1155-62.

177. Mulye M, Samanta D, Winfree S, Heinzen RA, Gilk SD. 2017. Elevated Cholesterol in the *Coxiella burnetii* Intracellular Niche Is Bacteriolytic. MBio 8:e02313-16.

178. Mansilla Pareja ME, Bongiovanni A, Lafont F, Colombo MI. 2017. Alterations of the *Coxiella burnetii* Replicative Vacuole Membrane Integrity and Interplay with the Autophagy Pathway. Front Cell Infect Microbiol 7:112.

179. Hofmann K. 1993. TMBASE-A database of membrane spanning protein segments. Biol Chem Hoppe-Seyler 374:166.

180. Soding J, Biegert A, Lupas AN. 2005. The HHpred interactive server for protein homology detection and structure prediction. Nucleic Acids Res 33:W244-8.

181. Kuba M, Neha N, De Souza DP, Dayalan S, Newson JPM, Tull D, McConville MJ, Sansom FM, Newton HJ. 2019. *Coxiella burnetii* utilizes both glutamate and glucose during infection with glucose uptake mediated by multiple transporters. Biochem J 476:2851-2867.

182. Stead CM, Omsland A, Beare PA, Sandoz KM, Heinzen RA. 2013. Sec-mediated secretion by *Coxiella burnetii*. BMC Microbiol 13:222.

183. Vincent CD, Friedman JR, Jeong KC, Buford EC, Miller JL, Vogel JP. 2006. Identification of the core transmembrane complex of the *Legionella* Dot/Icm type IV secretion system. Mol Microbiol 62:1278-91.

184. Lushchak VI. 2012. Glutathione homeostasis and functions: potential targets for medical interventions. J Amino Acids 2012:736837.

185. Barreteau H, Kovač A, Boniface A, Sova M, Gobec S, Blanot D. 2008. Cytoplasmic steps of peptidoglycan biosynthesis. FEMS Microbiology Reviews 32:168-207.

186. Mengin-Lecreulx D, Michaud C, Richaud C, Blanot D, van Heijenoort J. 1988. Incorporation of LL-diaminopimelic acid into peptidoglycan of *Escherichia coli*

mutants lacking diaminopimelate epimerase encoded by dapF. Journal of bacteriology 170:2031-2039.

187. Michaud C, Mengin-Lecreulx D, van Heijenoort J, Blanot D. 1990. Over-production, purification and properties of the uridine-diphosphate-N-acetylmuramoyl-L-alanyl-D-glutamate: *meso*-2,6-diaminopimelate ligase from *Escherichia coli*. Eur J Biochem 194:853-61.

188. Newton P, Latomanski EA, Newton HJ. 2016. Applying Fluorescence Resonance Energy Transfer (FRET) to Examine Effector Translocation Efficiency by *Coxiella burnetii* during siRNA Silencing. Journal of visualized experiments : JoVE doi:10.3791/54210:54210.

189. Isaac DT, Isberg R. 2014. Master manipulators: an update on *Legionella pneumophila* Icm/Dot translocated substrates and their host targets. Future Microbiol 9:343-59.

190. Deretic V, Singh S, Master S, Harris J, Roberts E, Kyei G, Davis A, de Haro S, Naylor J, Lee H-H, Vergne I. 2006. *Mycobacterium tuberculosis* inhibition of phagolysosome biogenesis and autophagy as a host defence mechanism. Cellular microbiology 8:719-727.

191. Kagan JC, Roy CR. 2002. *Legionella* phagosomes intercept vesicular traffic from endoplasmic reticulum exit sites. Nature cell biology 4:945-954.

192. Coers J, Monahan C, Roy CR. 1999. Modulation of phagosome biogenesis by *Legionella pneumophila* creates an organelle permissive for intracellular growth. Nature cell biology 1:451-453.

193. Pizarro-Cerdá J, Cossart P. 2018. *Listeria monocytogenes*: cell biology of invasion and intracellular growth. Microbiology spectrum 6:10.1128/microbiolspec.GPP3-0013-2018.

194. Van den Bossche J, O'Neill LA, Menon D. 2017. Macrophage Immunometabolism: Where Are We (Going)? Trends Immunol 38:395-406.

195. Diskin C, Palsson-McDermott EM. 2018. Metabolic Modulation in Macrophage Effector Function. Front Immunol 9:270.

196. Zhu L, Zhao Q, Yang T, Ding W, Zhao Y. 2015. Cellular metabolism and macrophage functional polarization. International reviews of immunology 34:82-100.

197. Tucey TM, Verma J, Harrison PF, Snelgrove SL, Lo TL, Scherer AK, Barugahare AA, Powell DR, Wheeler RT, Hickey MJ, Beilharz TH, Naderer T, Traven A. 2018. Glucose Homeostasis Is Important for Immune Cell Viability during *Candida* Challenge and Host Survival of Systemic Fungal Infection. Cell metabolism 27:988-1006.e7.

198. Anantharajah A, Mingeot-Leclercq M-P, Van Bambeke F. 2016. Targeting the Type Three Secretion System in *Pseudomonas aeruginosa*. Trends in pharmacological sciences 37:734-749.

199. de Lange MMA, Scheepmaker A, van der Hoek W, Leclercq M, Schneeberger PM. 2019. Risk of chronic Q fever in patients with cardiac valvulopathy, seven years after a large epidemic in the Netherlands. PloS one 14:e0221247-e0221247.

200. Raoult D, Houpikian P, Tissot Dupont H, Riss JM, Arditi-Djiane J, Brouqui P. 1999. Treatment of Q fever endocarditis: comparison of 2 regimens containing doxycycline and ofloxacin or hydroxychloroquine. Arch Intern Med 159:167-73.

201. Bushby SR, Hitchings GH. 1968. Trimethoprim, a sulphonamide potentiator. British journal of pharmacology and chemotherapy 33:72-90.

202. Baccanari DP, Kuyper LF. 1993. Basis of selectivity of antibacterial diaminopyrimidines. Journal of chemotherapy (Florence, Italy) 5:393-399.

203. Kwon YK, Higgins MB, Rabinowitz JD. 2010. Antifolate-induced depletion of intracellular glycine and purines inhibits thymineless death in *E. coli*. ACS chemical biology 5:787-795.

204. Andries K, Verhasselt P, Guillemont J, Göhlmann HWH, Neefs J-M, Winkler H, Van Gestel J, Timmerman P, Zhu M, Lee E, Williams P, de Chaffoy D, Huitric E, Hoffner S, Cambau E, Truffot-Pernot C, Lounis N, Jarlier V. 2005. A diarylquinoline drug active on the ATP synthase of *Mycobacterium tuberculosis*. Science (New York, NY) 307:223-227.

205. Haagsma AC, Abdillahi-Ibrahim R, Wagner MJ, Krab K, Vergauwen K, Guillemont J, Andries K, Lill H, Koul A, Bald D. 2009. Selectivity of TMC207 towards mycobacterial ATP synthase compared with that towards the eukaryotic homologue. Antimicrobial agents and chemotherapy 53:1290-1292.

206. Koul A, Dendouga N, Vergauwen K, Molenberghs B, Vranckx L, Willebrords R, Ristic Z, Lill H, Dorange I, Guillemont J, Bald D, Andries K. 2007. Diarylquinolines target subunit c of mycobacterial ATP synthase. Nature chemical biology 3:323-324.

Appendices

Appendix 1. Recipes for media, reagents, buffers and *G. mellonella* food

Media and broth:

All media was obtained from the Media Preparation Unit (MPU) at the Peter Doherty Institute unless otherwise stated.

ACCM-2 (prepared by members of the Newton laboratory)**:**

RPMI 1640 with GlutaMAX	12.5% (v/v)
Citric acid (Chem Supply)	13.4 mM
Sodium citrate tribasic dihydrate (Chem Supply)	16.1 mM
Casamino acids (BD Biosciences)	2.5 mg/mL
L-cysteine (Sigma-Aldrich)	1.56 mM
Bacto^{TM} Neopeptone (BD Biosciences)	0.1 mg/mL
KH_2PO_4 (Sigma-Aldrich)	3.67 mM
$MgCl_2*6H_2O$ (Chem Supply)	0.980 mM
$CaCl_2*2H_2O$ (Sigma-Aldrich)	0.089 µM
$FeSO_4*7H_2O$ (Chem Supply)	0.010 µM
NaCl (Chem Supply)	124.5 mM
Methyl-β-cyclodextrin (Acros Organics)	1 mg/mL
Made to pH 4.75 and filter sterilised before use	

ACCM-D (prepared by members of the Newton laboratory)**:**

RPMI (-amino acids) (US Biologicals)	1 mg/mL
Citric acid	13.4 mM
Sodium citrate tribasic dihydrate	16.1 mM
Sodium phosphate dibasic (Sigma-Aldrich)	0.704 mM
KH_2PO_4	3.67 mM
$MgCl_2*6H_2O$	0.980 mM
$CaCl_2*7H_2O$	0.089 µM
$FeSO_4*7H_2O$	0.010 µM
NaCl	125.4 mM

Methyl-β-cyclodextrin	1 mg/mL
L-alanine (Sigma-Aldrich)	1.26 mM
L-arginine monohydrochloride (Sigma-Aldrich)	0.750 mM
L-asparagine (Sigma-Aldrich)	0.666 mM
L-aspartic acid (Sigma-Aldrich)	0.541 mM
L-cysteine hydrochloride monohydrate (Sigma-Aldrich)	1.56 mM
L-glutamine (Sigma-Aldrich)	2.44 mM
L-glutamic acid potassium salt (Sigma-Aldrich)	3.31 mM
Glycine (Sigma-Aldrich)	1.17 mM
L-histidine (Sigma-Aldrich)	0.354 mM
L-isoleucine (Sigma-Aldrich)	0.854 mM
L-leucine (Sigma-Aldrich)	1.76 mM
L-lysine monohydrochloride (Sigma-Aldrich)	1.43 mM
L-methionine (Sigma-Aldrich)	0.455 mM
L-phenylalanine (Sigma-Aldrich)	0.630 mM
L-proline (Sigma-Aldrich)	3.02 mM
L-serine (Sigma-Aldrich)	1.68 mM
L-threonine (Sigma-Aldrich)	1.02 mM
L-tryptophan (Sigma-Aldrich)	0.245 mM
L-tyrosine (Sigma-Aldrich)	0.602 mM
L-valine (Sigma-Aldrich)	1.37 mM
Made to pH 4.75 and filter sterilised before use	

Glycerol broth:

Glycerol	50%(v/v)
Heart infusion broth	(0.37% (w/v)
Sodium thioglycolate	(0.1%% (w/v)

LB Agar:

Agar	1.5% (w/v)
Tryptone	1% (w/v)

Yeast extract	0.5% (w/v)
NaCl	1% (w/v)

LB broth:

Tryptone	1% (w/v)
Yeast extract	0.5% (w/v)
NaCl	1% (w/v)

SOB:

Tryptone	2% (v/v)
Yeast extract	0.5% (w/v)
KCl	2.5 mM
NaCl	10 mM

SOC:

Glucose	20 mM
Tryptone	2% (v/v)
Yeast extract	0.5% (w/v)
KCl	2.5 mM
$MgCl_2$	10 mM
$MgSO_4$	10 mM
NaCl	10 mM

Reagents and buffers:

All reagents and buffers were made to volume with dH_2O unless otherwise stated.

Column buffer:

Tris-HCl (pH 7.5) (Chem Supply)	20 mM
NaCl	200 mM
EDTA (Chem Supply)	1 mM
Phenylmethanesulphonyl fluoride (PMSF) (Sigma-Aldrich)	20 μM

Dithiothreitol (DTT) (Astral)	1 mM

Coomassie brilliant blue stain:

Coomassie Brilliant blue G-250 powder (Amresco)	2.5 g
Methanol (Chem Supply)	40% (v/v)
Glacial acetic acid (UniVAR)	10% (v/v)

Filtered with Whatman No. 1 filter paper (Sigma-Aldrich) once made.

Destain for Coomassie:

Methanol	30% (v/v)
Glacial acetic acid	10% (v/v)

Lysis buffer:

Tris-HCl (pH 7.6)	50 mM
EDTA	1 mM
Glycerol	10%
cOmplete, EDTA-free protease inhibitor cocktail tablet (Sigma-Aldrich)	1 tablet

PBS (made by MPU)**:**

KCl	2.7 mM
KH_2PO_4	1.8 mM
Na_2HPO_4	10 mM
NaCl	2.7 mM

SDS lysis buffer

SDS (Amresco)	4%

Tris-HCl (p**2x SDS loading dye** (pH 6.8) (made to volume with Milli-Q H_2O)**:**

Tris	125.5 mM
Glycerol	20% (v/v)
SDS	2% (w/v)
β-mercaptoethanol (Sigma-Aldrich)	2% (v/v)

Bromophenol blue (Bio-Rad)	0.001% (w/v)

Solubilisation buffer:

Tris-HCl (pH 7.6)	50 mM
$MgCl2*6H_2O$	200 mM
TX-100 (Sigma-Aldrich)	1%

50x TAE buffer:

Tris	0.2 M
EDTA	0.05 M
Glacial acetic acid	17.5% (v/v)

TBS/TBST:

Tris-HCl (pH 8.0)	200 mM
NaCl	150 mM
Tween-20 (for TBST) (Sigma-Aldrich)	0.1% (v/v)

Transformation buffer:

KCl (Amresco)	250 mM
CaCl2*2H2O (Sigma-Aldrich)	15 mM
PIPES (Sigma-Aldrich)	10 mM
Made to pH 6.7	
$MnCl_2*4H_2O$	55 mM
Filter sterilised	

***G. mellonella* food recipe**

Per Jar:

Weet-Bix™ (Sanitarium Health and Wellbeing)	1 block
Wheat bran (Kellogg's®)	10 g
Stabilised wheat germ (Coles)	5 g
Milk powder (Coles)	5 g

Methyl 4-hydroxybenzoate (Sigma-Aldrich)	0.3 g
Honey (Coles)	20 g
Raw honeycomb (Land of Soy and Honey)	3 cm^3

All ingredients except the raw honeycomb was crushed and mixed by hand. Food was placed in jars until depth reached ~2 cm. Cube of raw honeycomb was placed on top of the food mixture in the centre of the jar.

Appendix 2. Metabolite abbreviations.

Abbreviation	Metabolite
P	Phosphate
1P	1-phosphate
2P	2-phosphate
3P	3-phosphate
4P	4-phosphate
5P	5-phosphate
6P	6-phosphate
G6P	D-Glucose 6-phoshate
F6P	D-Fructose 6-phosphate
FBP	D-Fructose 1,6-bisphosphate
PEP	Phophoenolpyruvate
TPP	Thiamin diphosphate
ThPP	Thiamin diphosphate
R5P	D-Ribose 5-phosphate
PRPP	5-phospho-D-ribose 1-diphosphate
M1P	D-Mannose 1-phosphate
M6P	D-Mannose 6-phosphate
UMP	Uridine 5'-monophosphate
UDP	Uridine 5'-diphosphate
UTP	Uridine 5'-triphosphate
CMP	Cytidine 5’-monophosphate
CDP	Cytidine 5’-diphosphate
CTP	Cytidine 5’-triphosphate
dCMP	Deoxycytidine 5’-monophosphate
dCDP	Deoxycytidine 5’-diphosphate
dCTP	Deoxycytidine 5’-triphosphate
dUMP	Deoxyuridine 5'-monophosphate
dUDP	Deoxyuridine 5'-diphosphate
dUTP	Deoxyuridine 5'-triphosphate
dTMP	Deoxythymidine 5’-monophosphate
dTDP	Deoxythymidine 5’-diphosphate
hm5dCDP	2’-Deoxy-5-hydroxymethylcytidine-5’-diphosphate
hm5dCTP	2’-Deoxy-5-hydroxymethylcytidine-5’-triphosphate
GAR	5’-Phosphoribosylgycinamide
FGAR	5’-Phosphoribosyl-N-formylglycinamide
FGAM	5'-Phosphoribosylformylglycinamidine
AIR	Aminoimidazole ribotide
AppppA	P1,P4-Bis(5'-adenosyl)tetraphosphate
AMP	Adenosine 5'-monophosphate
ADP	Adenosine 5'-diphosphate
ATP	Adenosine 5'-triphosphate
IMP	Inosine 5’-monophosphate
IDP	Inosine 5’-diphosphate
ITP	Inosine 5’-triphosphate

XMP	Xanthosine 5'-monophosphate
XTP	Xanthosine 5'-triphosphate
GMP	Guanosine 5’-monophosphate
GDP	Guanosine 5’-diphosphate
GTP	Guanosine 5’-triphosphate
dAMP	Deoxydenosine 5'-monophosphate
dADP	Deoxyadenosine 5'-diphosphate
dIMP	Deoxyinosine 5’-monophosphate
dIDP	Deoxyinosine 5’-diphosphate
dITP	Deoxyinosine 5’-triphosphate
dGMP	Deoxyguanosine 5’-monophosphate
dGDP	Deoxyguanosine 5’-diphosphate
dGTP	Deoxyguanosine 5’-triphosphate
FAICAR	5'-Phosphoribosyl-5-formamido-4-imidazolecarboxamide
AICAR	5'-Phosphoribosyl-5-amino-4-imidazolecarboxamide
SAICAR	5'-Phosphoribosyl-4-(N-succinocarboxamide)-5-aminoimidazole
CAIR	1-(5-Phospho-D-ribosyl)-5-amino-4-imidazolecarboxylate
ppGpp	Guanosine 3',5'-bis(diphosphate)
pppGpp	Guanosine 3'-diphosphate 5'-triphosphate
L-Ala	L-Alanine
L-Asp	L-Aspartate
L-Asn	L-Asparagine
L-Cys	L-Cysteine
L-Glu	L-Glutamine
L-His	L-Histidine
L-Ile	L-Isoleucine
L-Leu	L-Leucine
L-Met	L-Methionine
L-Phe	L-Phenylalanine
L-Pro	L-Proline
L-Ser	L-Serine
L-Thr	L-Threonine
L-Trp	L-Tryptophan
L-Tyr	L-Tyrosine
L-Val	L-Valine
β-Ala	Beta-Alanine
HTPA	(2S,4S)-4-Hydroxy-2,3,4,5-tetrahydrodipicolinate
Gly	Glycine
Cys-Gly	L-Cysteinylglycine
GSH	Glutathione
MurNAc	N-Acetylmuramate
GlcNAc	N-Acetyl-D-glucosamine
GlcNAcA	N-Acetyl-D-glucosaminuronate
GlcN	D-Glucosamine
Glc	D-Glucose
GlcA	D-Glucuronate

Gal	D-Galactose
GalA	D-Galacturonate
GalNAc	N-Acetyl-D-galactosamine
GalNAcA	N-Acetyl-D-galactosaminuronate
ManNAc	N-Acetyl-D-mannosamine
FMN	Riboflavin-5-phosphate
FAD	Flavin adenine dinucleotide
DHF	Dihydrofolate
THF	Tetrahydrofolate
GSA	Glutamate-1-semialdehyde
ALA	5-Aminolevulinate
PBG	Porphobilinogen

Appendix 3. Complete metabolic pathway map of *C. burnetii.*

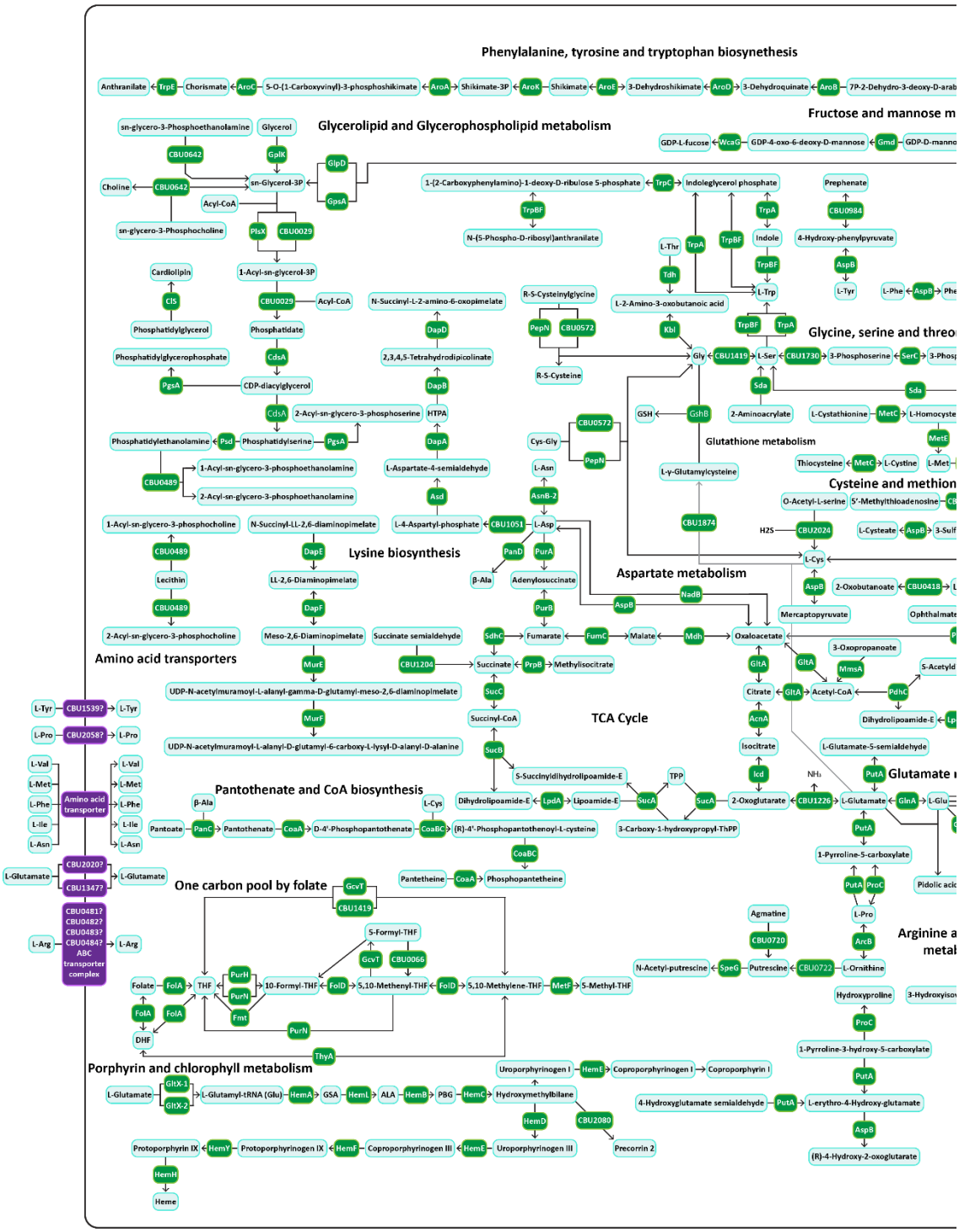

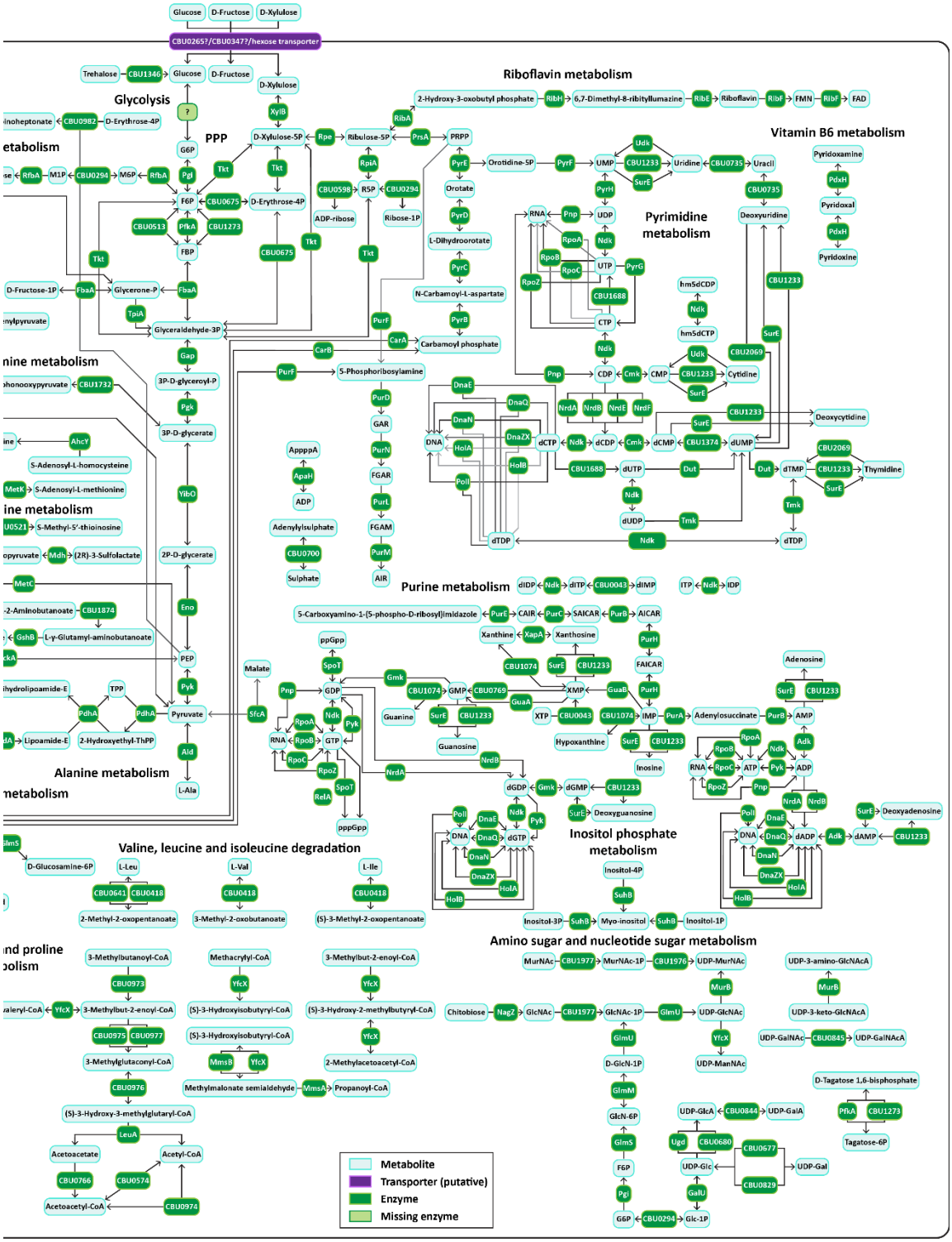
Glycolysis
PPP
Riboflavin metabolism
Vitamin B6 metabolism
Pyrimidine metabolism
Purine metabolism
Alanine metabolism
Valine, leucine and isoleucine degradation
Inositol phosphate metabolism
Amino sugar and nucleotide sugar metabolism
Metabolite
Transporter (putative)
Enzyme
Missing enzyme

Pale blue boxes indicate metabolites. Dark green boxes indicate existing enzymes while pale green boxes indicate missing enzymes based on genome annotation data in KEGG. Purple denotes putative transporters. Metabolite abbreviations are listed in Appendix 2.